SF 298 MASTER COPY KEEP THIS COPY FOR REPRODUCTION PURPOSES

REPORT DOCUMENTATION PAGE

Form Approved
OMB NO. 0704-0188

1. AGENCY USE ONLY *(Leave blank)*	2. REPORT DATE September 1997	3. REPORT TYPE AND DATES COVERED Final

4. TITLE AND SUBTITLE

Synthesis of Solidification Structure in Undercooled Liquids

5. FUNDING NUMBERS

DAAH04-93-G-0296

6. AUTHOR(S)

J.H. Perepezko

7. PERFORMING ORGANIZATION NAMES(S) AND ADDRESS(ES)

University of Wisconsin - Madison
Dept. of Materials Science and Engineering
1509 University Ave.
Madison, WI 53706

8. PERFORMING ORGANIZATION REPORT NUMBER

9. SPONSORING / MONITORING AGENCY NAME(S) AND ADDRESS(ES)

U.S. Army Research Office
P.O. Box 12211
Research Triangle Park, NC 27709-2211

10. SPONSORING / MONITORING AGENCY REPORT NUMBER

ARO 31042.12-MS

11. SUPPLEMENTARY NOTES

The views, opinions and/or findings contained in this report are those of the author(s) and should not be construed as an official Department of the Army position, policy or decision, unless so designated by other documentation.

12a. DISTRIBUTION / AVAILABILITY STATEMENT

Approved for public release: distribution unlimited.

12 b. DISTRIBUTION CODE

13. ABSTRACT *(Maximum 200 words)*

At high undercooling, the solidification of alloys can result in the suppression of the usual crystallization reactions and in the formation of nonequilibrium phases with distinct and novel microstructures. When a liquid is subdivided into a fine droplet dispersion in order to isolate nucleation catalysis, substantial undercooling may be observed before the onset of solidification, as demonstrated by the current work. An improved droplet technique has been applied to investigate the phase selection kinetics, nucleation catalysis reactions and thermal history that control microstructural evolution during solidification of highly undercooled melts. New developments involving droplet population and single droplet experiments in the application of nucleation catalysis to control undercooling have been used to identify specific active nucleants. In studies on Al-base alloys, an enhanced control and reproducibility of fine scale microstructure formation processes has been achieved in elevated temperature alloys and the new class of amorphous Al alloys. A continuing development of droplet methods to treat copper alloys and cast iron has been pursued along with the application of particle incorporated droplets to examine composite solidification processing. Throughout the experimental work, attention will is given to the evaluation of the relevant metastable phase equilibria and reaction kinetics which are quite useful for the interpretation of solidification microstructure and in the identification of alloy design strategies. In addition, processing models have been developed further with the aim to formulate microstructure maps for high undercooling solidification in order to guide the control of microstructure synthesis. An assessment of the undercooling and thermal history of the solidification products is provided by calorimetric measurements, controlled upquenching, and x-ray diffraction. Phase identification and microstructural characteristics which are essential for the proper interpretation of undercooling and solidification behavior are studied by optical and electron metallography including TEM and Auger surface analysis on selected samples, quantitative image analysis and x-ray diffraction methods. The basic information that droplet studies yield also has a broad application to many aspects of solidification processing. The results allow for a quantitative assessment of the undercooling of liquid alloys, the stability of solidification structures, an improved comprehension of the reaction path followed during alloy solidification including the influence of competing metastable phase and glass formation reactions and contribute to an improved understanding and modeling of microstructure evolution during RSP and other processing such as spray deposition, surface melting and composite fabrication.

14. SUBJECT TERMS

solidification, undercooling, nonequilibrium phases, Aluminum alloys, amorphous metal alloys, nanocrystals, novel microstructures,

15. NUMBER IF PAGES 88

16. PRICE CODE

17. SECURITY CLASSIFICATION OR REPORT	18. SECURITY CLASSIFICATION OF THIS PAGE	19. SECURITY CLASSIFICATION OF ABSTRACT	20. LIMITATION OF ABSTRACT
UNCLASSIFIED	UNCLASSIFIED	UNCLASSIFIED	UL

Table of Contents

LIST OF FIGURES

LIST OF TABLES

ABSTRACT

The undercooling of liquid metals is a fairly common observation, but the amount of undercooling is limited usually by the action of heterogeneous catalysts. When a liquid is subdivided into a fine droplet dispersion in order to isolate nucleation catalysis, substantial undercooling may be observed before the onset of solidification, as demonstrated by the current work. At high undercooling, the solidification of alloys can result in the suppression of the usual crystallization reactions and in the formation of nonequilibrium phases with distinct and novel microstructures. A continuing course of investigation is proposed for an experimental study and process modeling of alloy solidification at high undercooling. The study will employ an improved droplet technique to investigate the phase selection kinetics, nucleation catalysis reactions and thermal history that control microstructural evolution during solidification of highly undercooled melts. New developments in the application of nucleation catalysis to control undercooling will be pursued to identify specific active nucleants. In selected cases a detailed kinetics evaluation involving droplet population and single droplet experiments will be pursued to quantify the effects of catalysis on nucleation. Further studies on Al-base alloys will be directed towards an enhanced control and reproducibility of fine scale microstructure formation processes in elevated temperature alloys and the new class of amorphous Al alloys. A continuing development of droplet methods to treat copper alloys and cast iron is also planned along with the application of particle incorporated droplets to examine composite solidification processing. Throughout the experimental work, attention will be given to the evaluation of the relevant metastable phase equilibria and reaction kinetics which are quite useful for the interpretation of solidification microstructure and in the identification of alloy design strategies. In addition, a further development of processing models is intended with an aim to the formulation of microstructure maps for high undercooling solidification in order to guide in the control of microstructure synthesis.

The undercooling behavior of droplet samples will be determined by differential thermal analysis. An assessment of the stability and thermal history of the solidification products will be provided by calorimetric measurements, controlled upquenching, and x-ray diffraction. Phase identification and microstructural characteristics are essential for the proper interpretation of undercooling and solidification behavior and will be studied by optical and electron metallography

including TEM and Auger surface analysis on selected samples, quantitative image analysis and x-ray diffraction methods.

The basic information that droplet studies yield also has a broad application to many aspects of solidification processing. The results of the proposed study will allow for a quantitative assessment of the undercooling of liquid alloys, the stability of solidification structures, an improved comprehension of the reaction path followed during alloy solidification including the influence of competing metastable phase and glass formation reactions and contribute to an improved understanding and modeling of microstructure evolution during RSP and other processing such as spray deposition, surface melting and composite fabrication.

INTRODUCTION

The undercooling of liquid metals below their equilibrium melting point is a common occurrence in solidification. Throughout the analysis of solidification processing, the conditions of nucleation and liquid undercooling behavior have been recognized for the strong influence that they can exert on the initial stage of solidification structure formation. Moreover, undercooling phenomenon are recognized as being of central importance in the nucleation of equilibrium and non-equilibrium crystalline phases and in the formation of amorphous phases. At the same time, in theoretical and applied crystal growth work the amount of liquid undercooling is regarded as one of the critical parameters in determining the path of morphological evolution and the final solidification structure.

Although undercooling effects can be observed during the slow cooling of a liquid metal, most often, before an appreciable undercooling can develop, crystallization initiates at some heterogeneous catalytic site [64CHA]. In practice, nucleation catalysts may be activated by any of a number of different types of sites in contact with the liquid including impurity aggregates, foreign inclusions and container walls. However, a number of experimental approaches have been developed which are effective in extending the range of observable undercooling and in permitting the examination of the rapid crystallization that develops following nucleation at high undercooling.

One of the highlights in the development of novel microstructures by advanced solidification processing methods is the common occurrence of various metastable structural

states. Whether these structures represent ultrafine grain sizes, supersaturated compositions of equilibrium phases or non-equilibrium phase structures, their development has expanded significantly the range of microstructural options that are available for the synthesis of new materials and the attainment of new levels of performance. Along with the development of new microstructural options and solidification processing technologies, it has become apparent that a number of the existing models for the analysis of solidification and microstructure evolution must be modified and extended in order to treat the new domains of processing and kinetic conditions that are now accessible. In these efforts the important role of melt undercooling has been recognized repeatedly as a common underlying link between advanced processing methods and the development of novel solidification structures.

Although a given novel microstructure may be synthesized through a variety of seemingly different processing routes, there is a common underlying thermodynamic criterion that is always applicable [94PER]. Through the various stages of a processing operation the initial state of the reacting material must be energized to an elevated free energy configuration which represents a partially relaxed state. In the case of solidification processing operations, the energized state is achieved by cooling the liquid into the undercooled domain. While this viewpoint is widely acknowledged and frequently used to account for metastable structure synthesis, the application is usually developed in a qualitative manner. For the most part this is due to the difficulty in accessing the undercooled state in a manner which allows for the measurement of the relevant thermodynamic properties. In fact, most of the thermodynamic measurements pertaining to metastable solidification reactions have been obtained from droplet samples which can exhibit a deep undercooling during slow cooling [80PERa, 79PER, 82PERa, 80PERb]. The commonly used rapid quench methods do not permit reliable thermodynamic measurements in general.

The establishment of melt undercooling as a key variable in microstructural development provides an important link between rapid quenching studies and undercooling research. Indeed, in many respects undercooling is a more fundamental parameter than cooling rate. In most work on RSP, cooling rate is used as a convenient process variable. However, in solidification studies on undercooled samples, it has been demonstrated that undercooling can be treated in a meaningful way as a process variable [80PERa, 82PERa, 83RIC, 82COO]. Moreover, not only can the high solidification velocities encountered during RSP be understood in terms of high levels of interfacial undercooling, but also the development of metastable phases can be analyzed in a direct manner in terms of undercooling. The examination of RSP only in terms of cooling rate does not allow for this broad range of structure and kinetics analysis. Accordingly, examination of

solidification in undercooled liquids can contribute to the basic understanding necessary for a successful microstructure control and alloy design in the optimization of processing treatments.

As a result of numerous studies on the rapid solidification of liquids it has become clear that the processing conditions play a major role in determining the selection of specific solidification phases and microstructural morphologies. Indeed, the rich variety of solidification microstructures that is accessible by RSP represents an important strength of the approach. At the same time, the flexibility in microstructure selection represents a key challenge to implementing a coherent guide to the control of processing that will permit an optimization of alloy design and processing in order to achieve a given structure. During the current work progress has been achieved in developing the desired alloy design and processing guide based upon advances in the fundamental understanding of some of the intrinsic sample characteristics and extrinsic factors involved in melt processing that control structure selection and development. Much of the current effort has focused upon melt undercooling as the key process variable, but new insight has also been developed on the role of external cooling rate and the interaction between cooling rate and undercooling in microstructure formation.

An effective experimental approach that may be applied successfully to yield large undercoolings before the initiation of solidification involves the slow cooling from the melt of a dispersion of stabilized fine droplets [80PERa, 50TUR]. An important advantage of the droplet method is the capability to determine both the undercooling to the start of solidification and the nucleation kinetics. In addition, the high liquid undercooling that is possible in droplet samples has been found to result in conditions favorable for the formation of metastable solid structures during a slow cooling which are similar to those produced during rapid quenching treatments. Beyond these kinetic features, the use of droplet samples allows for the structural characterization of the solidification product phases and the microstructural morphology and for the measurement of the properties of the metastable undercooled liquid state [84PERa]. With the advent of improved sample preparation and more extensive structural determinations, the droplet method has provided also a basis for the judgment of the phase selection nucleation kinetics that govern structure development during rapid solidification processing [82PERa, 84PERb]. Moreover, this information represents a background that is needed in order to develop a new alloy design strategy to optimize the desirable microstructural features of RSP treatment.

As part of the investigation of melt processing, progress has been made in the analysis and interpretation of metastable phase formation. The application of metastable phase diagrams and T_0 constructions are now recognized as valuable aids in such an analysis. Further work on analytical treatments based upon physical models of heat flow and nucleation and growth kinetics

has also been advanced to allow for the development of an understanding of the competitive solidification kinetics that controls the formation and evolution of metastable phases and novel microstructures. New capabilities for experiment and analysis have also been established in the examination of controlled nucleation catalysis, thermal stability of metastable structures, the influence of composite reinforcement particles to modify the solidification pathway and the development of solidification microstructural maps.

While progress has been made, there are still important challenges to understanding that remain to be addressed in the solidification of highly undercooled liquids. For example, the reliable prediction of nucleation control of structure selection is an open issue, but there are developments in experiment and analysis that offer promise for new predictive capability. Although the experience in rapid solidification has increased, it is certainly not a mature area. New advances in structure development and modeling analysis continue to be made. Some developments represent totally new observations and others represent a better understanding of reported behavior. Beyond the potential for innovative applications, rapid solidification has provided an experimental vehicle and a stimulus that has pushed the limits of the basic understanding of structure development and has motivated major efforts to extend current analysis and modeling capability. These developments have a wide impact on a range of processing applications including spray deposition, surface melting, soldering , joining and composite fabrication

I. BACKGROUND

I.A Development of Undercooling

I.A.1 Droplet-emulsion Undercooling Technique

A large continuous sample of liquid metal contains a variety of catalytic nucleation centers which acts to preclude the attainment of high levels of undercooling prior to solidification. Since crystallization will be catalyzed by the most potent nucleation site present, a means of circumventing the effect of catalytic sites such as oxides or container walls is necessary in order to observe extensive undercooling. Following from this basis, an effective approach to obtain large undercoolings is to disperse the bulk liquid into a collection of fine droplets which effectively isolates potent nucleation sites into a small fraction of the droplet population. As shown in Fig. 1 the effect of these catalytic sites will then be restricted to the few drops in which they are located. The high purity liquid sample is dispersed within a suitable carrier fluid, and droplet independence is maintained by the formation of thin, inert surface coatings which are not catalytic to

crystallization. When a sample of liquid metal in the form of a stabilized droplet emulsion is cooled, those droplets containing potent nucleants will freeze at low undercoolings, but the majority will not freeze until reaching the maximum nucleation undercooling level which can range from 0.3 to 0.4 T_m [84PERb].

In considering the droplet approach to undercooling, a distinction should be made between the several modifications of this technique which have been employed by a number of investigators in the past as illustrated in Fig. 1. For example, in the droplet substrate method [50TUR], a small sample of liquid metal is placed on an inert glass substrate in a chamber with an inert reducing atmosphere. With this approach, the onset of solidification is determined by visual observation of the change in surface reflectivity of a metal droplet which is about 50-100 μm in diameter. In the entrained droplet technique [50WAN], a bulk alloy sample is equilibrated in a liquid-solid two-phase field with the temperature and alloy composition selected so that only a small fraction of the volume will be liquid. Since the liquid phase is in contact with the primary solid solution, which is a potential heterogeneous nucleant, the undercooling achieved with this sample configuration would be expected to be smaller than that attained using techniques in which the liquid is not in contact with an active catalyst. In addition, several other procedures have been developed for generating liquid metal droplet dispersions which exhibit a propensity for substantial undercooling. These droplet forming techniques include exploding wires [75MEY], shotting [56CEC] and the containerless solidification in drop tubes [80LAC]. While the majority of droplet undercooling schemes have a provision for some method of temperature measurement, the undercooling tendency of liquid metal droplets in most atomization methods is usually judged from microstructural observations. Moreover, it is clear that atomization of liquids is a commercial RSP method which incorporates an effective nucleant isolation operation as well as rapid quenching.

Another approach for bulk samples uses the removal of active nucleation sites from the melt to achieve high levels of undercooling. The removal of catalysts is usually accomplished by physical separation of the sites from the liquid or by chemical treatment which acts to incorporate or deactivate possible catalytic sites in the presence of a chemical containment layer. These approaches include the containment of a liquid sample in an inorganic glass [66KAT, 67KAT] as well as the levitation of a bulk melt using induction [64SHI] and have demonstrated that in some cases, large levels of undercooling (of the order of 0.2 T_m) may be achieved. The layer of glass encasing the melt is believed to promote undercooling not only by isolating the liquid from catalytic sites present on the crucible walls, but also by a possible scavenging action of nucleation centers that may be distributed within the volume of the melt.

In principle, the droplet emulsion technique (DET) of sample preparation appears to offer a relatively simple means of isolating internal catalysts which tend to promote nucleation of the solid at low levels of undercooling below T_m. In fact, samples of liquid metal in the form of droplet emulsions have yielded undercooling results which exceed the values reported by any other undercooling method (such as the droplet substrate or encased melt techniques) by a large margin [84PERb]. In practice, the effectiveness of the dispersion operation appears to be limited by the nature of the surface film and the droplet supporting medium. It appears clear that the liquid metal-substrate (i.e. coating) interaction is important in determining the level of undercooling observed prior to nucleation [80PERa, 82PERa, 76PAU]. Similarly, a variety of possible surface films consisting of different metal oxides, sulfides, and salts may be formed on liquid droplets, but the selection of a suitable film that is inert in catalyzing nucleation is quite difficult as is the selection of a suitable inert, stable carrier fluid. In general it is desirable that the liquid wet the coating more effectively than the solid so that amorphous coatings appear to be preferable. At the same time the coating/carrier fluid surface energy must be low to allow for a high degree of dispersion that is necessary for effective emulsification. However, there is at present, no set of well established guidelines to follow in selecting a satisfactory inert coating film for a particular metal or alloy. Nevertheless, the acquired experience in applying the droplet emulsion technique has indicated that film coatings can be generated on a variety of different metal surfaces which permit the attainment of the largest reported maximum undercooling limits [82PERa, 84PERb].

Furthermore, the experience gained from earlier work on relatively low melting point metals (Tm < 500°C) using organic carrier fluids has permitted the extension of the droplet emulsion technique to high melting point metals [83RIC, 85PER]. With the current experience it is now possible to prepare droplet emulsion samples in molten salt fluids from alloys with melting points up to 1100°C (including Cu-based alloys) which exhibit large undercooling values. In a related development a method of preparing samples of droplet dispersions encased in a glass slag has been established as a suitable approach to the study of ferrous alloys such as cast iron. A further extension of the droplet technique now allows for direct measurement of the effect of cooling rate on the undercooling potential of the liquid for cooling rates approaching 10^3°C/sec. In addition during the current program advances in droplet sample preparation have established the capability to examine composite droplet samples containing solid particles-liquid metal mixtures. Such samples are produced by either in-situ particle formation in emulsified droplets or by dispersing a bulk melt containing incorporated particles. This development represents a major advance in the application of droplet samples to study melt-particle interactions that govern the kinetics during solidification processing of metal matrix composites and is a good example of the

versatility of droplet samples in studying solidification processing. On the basis of the experience of continued development of the droplet emulsion technique both in terms of achieving increasing undercooling limit values and in terms of extending the upper working temperature and the range of alloys that can be examined, it is expected that further developments and improvements in undercooling capability and in the variety of alloys and composites that can be studied will be made during the proposed program.

I.A.2 Undercooling Development During RSP Methods

Since undercooling has been identified as a key factor in solidification structure development it is useful to consider how undercooling can occur during rapid quenching treatments. For example during the rapid freezing of melt streams, as in melt spinning as shown in Fig. 2, undercooled conditions will develop if the liquid exists for some time or distance in contact with the wheel without nucleation. This will develop if the thermal front associated with heat extraction moves more rapidly than the actual crystallization front. Alternately, during surface melting with a rapidly moving or pulsed heat source, an undercooled melt zone can develop in front of the resolidification interface if the rate of growth of the unmelted substrate is insufficient to keep pace with the rate of heat extraction to the substrate. The development of metastable crystalline phases, as well as amorphous products, during both melt spinning and surface melting operations is clear evidence for the existence of an undercooled alloy melt[86PER].

I.B Competitive Phase Selection Kinetics

Some further characteristics related to the development of a highly undercooled solidification microstructure in terms of stable equilibrium phases or metastable phases depends on the relative nucleation and growth kinetics of the competing structures that are illustrated schematically in Fig. 3 [93BOE]. The thermodynamic relationships for the molar free energy G of a material as a liquid, stable phase α and metastable phase β are given in Fig. 3a. In Fig. 3b a function describing the nucleation barrier, ΔG^* is shown to illustrate the role of competitive nucleation. Similarly, in Fig. 3c the relative growth kinetics for stable and metastable phases are illustrated. It is clear that the thermodynamic undercooling to yield temperatures below the melting point of the metastable phase is only a minimum necessary condition for its development. In order to dominate the microstructure, the metastable phase must form at a larger undercooling than the minimum in order to allow it to have faster nucleation and growth kinetics than the competing stable phase.

For the most part, crystal nucleation in a undercooled liquid is controlled by

heterogeneous nucleation sites [93BOE, 84PERb]. The analysis of competitive nucleation requires a consideration also of the potency and density of nucleation sites. This is illustrated schematically in Fig. 4 which depicts competitive nucleation of stable and metastable phases on a variety of heterogeneous nucleation sites. For example, transformation curves B, C, and D represent different heterogeneous nucleation conditions for an equilibrium phase and would tend to $T_r = T/T_m = 1$ at a long time. Transformation curve A represents the nucleation catalysis of a metastable phase with the melting phase T'_m and would tend to $T_r < 1$ at long time. Initially, if two catalysts of different site densities and potencies for nucleation of a given phase (B and C) are present, the undercooling limit at T_{rl} is determined by catalyst C at a cooling rate $\dot{T}_1$. At a cooling rate $\dot{T}_2$ however, the undercooling increases circumventing the catalytic effect of C, but maintaining the same product structure. When two different phase structures are in kinetic competition, the relative magnitude of the representative ΔG^* values becomes the most dominant kinetic factor. This is reflected in the breadth of the transformation curves for the different phases which is proportional to $(\Delta G^*)^{-1}$. For example, transformation curve A is broader than that for B, but the noses of the two diagrams have been placed at the same position. Under these conditions at high and increasing cooling rate, formation of the equilibrium phase is bypassed by nucleation of the metastable phase. Alternatively, if ΔG^* for A is higher than that for B, the equilibrium phase can nucleate at all cooling rates. It is also possible for the nucleation of the equilibrium phase to be favored by increasing cooling rate when the nucleation site density for the equilibrium phase (curve D) is greater than that for the metastable phase (curve A). In this case, an increase of cooling rate from $\dot{T}_1$ to $\dot{T}_2$ can result in a decreasing yield of metastable product until all nucleation is bypassed and a liquid reaches the glass transition. Certainly attention to catalyst potency and size distribution can be as important as cooling rate in optimizing the result of a high undercooling solidification treatment,[84PERb, 92PER, 90FEC].

I.C Product Structure of Metastability

At high undercooling levels microstructures consisting of supersaturated solid solutions, metastable intermediate phases or amorphous structures become product structure options. Consequently, it is useful to consider some of the ways in which relative phase stability may be judged in order to select the most suitable systems for a give category of metastable phase formation. A first level of such information is the melting temperature of a metastable phase which identifies the range of possible formation from the melt. In alloys it is also important to identify the T_0 temperature which represents the upper limit of formation of a solid by partitionless solidification, [93BOE]. With this information the plots shown in Fig. 3 may be constructed in a more quantitative matter for specific systems and metastable phases of interest.

For a pure component that exhibits an allotropic transformation between the low temperature β phase and high temperature α phase, the melting of β at T_m^β lies between the melting of α at T_m^α and the allotropic transformation at $T_{\alpha/\beta}$. When specific heat corrections are neglected,

$$T_m^\beta = [\Delta S_{\alpha/\beta} T_{\alpha/\beta} + \Delta S_m^\alpha T_m^\alpha]/[\Delta S_{\alpha/\beta} + \Delta S_m^\alpha] \quad (1)$$

where $\Delta S_{\alpha/\beta}$ is the entropy change for the allotropic transition and ΔS_m^α is the entropy of melting of the α phase, [83PER]. For many pure components, allotropic transitions are not observed. In these cases the thermodynamic analysis of the phase equilibria permits estimates of the component lattice stabilities as documented by the extensive work of Kaufman and Bernstein, [70KAU]. With the first level of assessment it is possible to identify candidate systems in which alternate metastable crystal structures may be produced at high undercooling. For example, if an undercooling level about 0.3 T_m below the stable phase melting point is used as the basis for evaluation, then alloys based on Be, Co, Cu, Fe, Mg, Ni, Ti, Zn and Zr are likely candidates for the formation of one or more alternate crystal structures [93BOE]. However, Al, Cr and Nb based alloys will not be good candidates. Instead as experience shows the latter systems are candidates for the development of supersaturated solid solutions [82JON].

I.D Thermal History Behavior

Understanding microstructural evolution during rapid solidification of an undercooled melt requires a consideration of the effects of recalescence which results from the rapid release of the latent heat of fusion. For an undercooled liquid droplet (which can be assumed to represent an adiabatic system [82LEV]) the maximum temperature reached during recalescence, T_R^{max}, is governed by thermodynamic considerations: the latent heat of fusion, the specific heat of the sample, and the degree of undercooling prior to the onset of crystallization. For a binary alloy, if the undercooling is large enough so that T_R^{max} is less than the T_0 temperature, the liquid is said to be hypercooled, and the entire droplet may solidify in a partitionless manner. However, since the hypercooling condition is not frequently achieved (even for the high liquid undercooling levels attained with the DET), the solidification of undercooled melts will usually involve a stage which occurs once T_R exceeds T_S during which the growth rate of the solid is much slower. That portion of the droplet which freezes during this stage of solidification can exhibit a segregated solidification pattern as opposed to the compositionally homogeneous solid which forms prior to recalescence above T_S.

A schematic representation of recalescence behavior is shown in Fig. 5 for an alloy of

composition C_0. This representation assumes solidification by slow cooling in an adiabatic system. The liquid of composition C_0 is slow cooled along path 1, and upon reaching point 2 at a temperature $T_N > T_N^{hyp}$ the undercooled liquid begins to solidify forming solid of composition C_0. As solidification is occurring heat is released sufficient to reheat the sample (along path 3) until a maximum temperature T_R^{max} is reached, at which point cooling of the sample continues since the sample is in a surrounding environment at a temperature of T_N (due to adiabatic assumption, environment is not allowed to change temperature as a result of recalescence). Cooling of the sample from T_R^{max} results in the solidification of the remaining liquid fraction of the droplet according to the usual alloy solidification pathway [66BRO]. The result will be solute partitioning in that portion of the droplet solidified after T_R^{max}, with compositions of liquid and solid in equilibrium at the interface varying, respectively, along the liquidus and solidus curves from T_R^{max} to $T_S(C_0)$ (path 4). Thus the post-solidification droplet would be expected to consist of an initial fraction solid of uniform composition and the remainder of the droplet with a segregated structure (possibly dendritic) resulting from solute partitioning along paths 3 and 4 in Fig. 5. As the droplet recalesces above T_S, the C_0 solid which formed during the initial stage of solidification becomes metastable with respect to formation of a two-phase mixture of solid + liquid with compositions given by the equilibrium phase boundaries. Therefore, once T_R exceeds T_S, an important factor controlling T_R^{max} is the kinetic stability of the C_0 solid with respect to melting. For this reason, the melting behavior of an initially homogeneous solid solution alloy during continuous heating was examined as a function of upquenching rate. The metastable melting behavior has been demonstrated for Sn-Bi alloys which were carefully prepared as homogeneous tin-rich solid solutions prior to continuous heating at different rates [75MEY].

For composite droplets containing a reinforcement particle-liquid mixture it is important to inquire if the presence of the particle can influence the thermal history behavior as outlined in Fig. 5. The direct analysis of the thermal history of a composite droplet initiating solidification from an undercooled condition does not appear to be available, but some general features may be identified for comparison with the pure liquid droplet model. With the provision that adiabatic conditions are maintained [82LEV], it appears that an incorporated particle that is wetted by the liquid can act as an internal heat sink with an initial temperature at T_N. Of course, the undercooled liquid metal would represent the major internal heat sink since it is the majority phase and has a thermal diffusivity that is about one order of magnitude greater than that for the oxide and carbide particles used for reinforcements [80GEI].

While a detailed heat flow analysis is necessary for a complete assessment, it appears that

if there is time for heat to flow into the particle, then the thermal history and microstructural development will be influenced. In this case it also seem likely that non-Newtonian conditions (i.e. development of thermal gradients) will pertain and complicate the heat flow analysis [50TUR]. However, some qualitative inferences may be drawn with regard to the behavior shown in Fig. 5. During path 3 as the temperature is increasing heat flow into the particle can act to reduce the maximum recalescence temperature, T_R^{max}. Similarly, during path 4 where external cooling becomes important the internal particle can assist the cooling process down to T_N and expedite final solidification. Both of these effects due to internal particles should yield a microstructural refinement compared to the freezing of a pure liquid droplet, but other effects may develop due to enhanced heat flow.

The influence of post solidification solid state transformation can be illustrated clearly by considering the microstructure development in undercooled Fe-Ni alloys, [92THO]. Over the range from Fe-10 wt.% Ni-Fe-30 wt.% Ni large millimeter drops were determined to undercool about 160°C during processing in a drop tube apparatus [92THO]. At this level of undercooling competitive nucleation and growth of either a stable FCC, γ phase or a metastable BCC, δ phase is possible. With the metastable path two options are available, either retention of the BCC phase or transformation in the solid state to the FCC phase which upon further cooling will form martensite. Clearly the selection of the final transformation structure is also a function of the solid state kinetics. With sufficiently rapid cooling in the solid state, which is promoted by a fine sample size, retention of the BCC phase is possible. However, in large samples with slow solid state cooling, the BCC phase can still develop during solidification but must be studied closely to determine the final pathway based upon the characteristics of the transformation structure. By examining the microstructural development in samples covering 7 orders of magnitude in sample volume, a clear trend has been defined as indicated in Fig. 6 to mark the operation of different solidification and solid state transformation reactions on a microstructural map. In fact, the boundary separating the BCC phase retention and decomposition in Fig. 6 is rate limited by solid state nucleation of the FCC phase from the BCC solidification product. Further analysis indicates that the BCC product nucleates from the melt once sufficient undercooling is available to place the melt below the metastable BCC phase boundary.

Thermal analysis of fine powder samples produced using the DET has proven to be a very effective method for analyzing microstructure development and metastable phase equilibria and for evaluating possible reaction pathways leading to the formation of metastable phases during solidification [82PERa]. The incorporation of interrupted thermal cycling and upquenching treatments has provided further insight into the thermal history governing microstructure

formation. With these capabilities a systematic evaluation of the thermal history associated with the solidification of composite droplets is now possible.

I.E Dispersed Particle Catalysis

In almost all solidification processes, the crystallization of a bulk liquid volume occurs through favorable interaction between the melt and internal or residual catalysts which act as heterogeneous nuclei. The heterogeneous sites can be melt impurities or other external catalysts inherent to most casting processes. To a large extent the heterogeneous sites ultimately control the initial solidification structure type, size scale, and spatial distribution of product phases.

Effects induced from heterogeneous nucleation catalysis also exert a strong influence on the resultant grain size, phase morphology and compositional homogeneity as well. In order to modify and refine the as-cast solidification microstructure, it is common practice to intentionally inoculate a melt with particle catalysts that surpass the catalytic activity of other less potent heterogeneous nuclei in contact with the bulk liquid. By using this inoculation procedure, the added catalysts can promote the nucleation of a refined primary phase, alternative product phase morphologies, or the formation of fine equiaxed as-cast grain structures with enhanced mechanical properties.

There is a wide commercial application of cast alloy treatments that modify the initial solidification characteristics to provide a means for effective control of grain size and morphology. Examples include the addition of ferrosilicon to cast iron in order to promote the nucleation of graphite; Zr or C can be added to refine Mg alloys; P is introduced to Al-Si alloys to refine the primary Si phase size; As or Te can be added to Pb alloys; and Ti is added to Zn based systems. Other additives, such as Na in Al-Si alloys, are used to modify the growth morphology. In addition there is also a wide body of experience on the grain refinement of Al based alloys by Al-Ti and Al-Ti-B melt additions [51CIB, 51CRO, 70DAV, 76JON, 70MAR, 75MAX, 82PERb, 82ARN, 87GUZ, 72CIS, 83MON, 85GRA, 86KIR].

While the success of inoculation procedures are clearly established, the actual performance of inoculant additions in practice exhibits a fair amount of variability. For example, Al-Ti and Al-Ti-B master alloy additions that refine Al alloys are relatively complex and minor changes in the manufacturing process used to prepare them can result in significant differences in their effectiveness [87GUZ, 75COR, 80CYN]. Moreover, even though there is a broad data base of literature concerning grain refinement processing, an understanding of the actual mechanism(s) by which grain refining agents operate in a melt still remains uncertain.

The basic requirements for an effective nucleating agent can be assessed from consideration of nucleation theory [52TUR, 68CRO, 79HEL]. In order to promote the formation of crystals on an intended nucleant, the interface between the nucleant and the liquid should be of higher energy than that between the nucleant and the solid. This condition is maximized by providing nucleant-solid crystallographic relationships that result in low disregistry orientations between the respective lattices. In fact, the potency of a given catalyst is believed to be increased for decreasing values of relative lattice disregistry with the crystalline phase, and results in solidification at lower levels of undercooling. However, under conditions of poor crystallographic fit, a reduction in interfacial energy may occur through chemical interaction [52TUR], electronic interaction [69TIL], or the formation of interfacial compounds and adsorbed reaction layers that are experimentally associated with much larger levels of undercooling [50WAN, 68CRO, 85HOF]. In addition to the basic requirement of lattice stability, to insure effective catalysis of solid, the melt should tend to wet the surface of the nucleant. Improved mutual wetting characteristics are generally associated with a decrease in substrate-liquid interfacial tension and can be affected by parameters such as substrate surface roughness [61SUN, 77JAC, 73WOO], substrate porosity [68SAM], temperature [70RHE, 66YAS], and adsorption phenomena induced by increased chemical affinity at the interface [54HUM] or impurity effects in the liquid and surrounding atmosphere [68NAI, 83NAI, 83NAG].

As an additional prerequisite for inoculant particles used as grain refining agents, the onset of solidification should not be followed by a rapid crystal growth, to allow the full effect of the potential nucleants to be realized. In alloys the growth restriction may be achieved as a consequence of solute redistribution during freezing which allows for nucleants dispersed throughout the melt to become effective and favors an equiaxed grain structure [70DAV, 75MAR, 52CIB].

Within these general requirements, a number of compounds appear to act as effective catalysts for the nucleation of Al with disregistry values below 10% and nucleation undercoolings of less than ~5°C [70MAR, 82ARN, 72CIS, 83KOB]. However, the exact identities of the active nucleants have not been established by direct observation, but rather the operative nucleants have been inferred from thermal and structural results obtained from standard bulk refinement tests.

The issue of specific nucleant identity is crucial when it is considered that in commercial melts, a broad spectrum of catalysts exists that may operate singly or together to yield crystallization events. The presence of uncontrolled nucleation sites can yield irreproducible catalysis results that are related to the sample environment and the population of internal particles which may be comprised of several different structural types with variable sizes, size distributions,

and surface conditions. For example, in Al castings containing refining agents which approach ideal effectiveness, the number of grains in a casting should approach the total number of inoculant particles added to a melt. However, from actual ingot grain density measurements in Al alloy castings containing inoculant additives, a grain density corresponding to only 1-2% inoculant particle effectiveness is usually observed [87GUZ]. Also, it appears that small amounts of V, Cr, and Zr can act to poison catalytic particle surfaces [76JON, 87GUZ, 80JON].

Since the nucleation and growth characteristics of grain refinement indicate a sharp selection of particles in terms of refinement effectiveness, it is important to investigate and identify the parameters that influence the catalysis of grains and the specific physical mechanisms that govern heterogeneous nucleation processes. With bulk melts and uncontrolled sample environments, it is not clear that such a study can be accomplished in a reliable manner.

However, by using the DET to produce droplet emulsions containing incorporated particle catalysts, residual catalytic interaction between intended nucleation sites and residual sites present in bulk samples and their environments are eliminated. In addition, the ability to produce changes in droplet coating chemistries allows for the assessment of secondary interaction between the particle catalysts and the applied droplet surface coatings. Analysis of secondary interaction allows for the assessment of the true catalytic potencies of intended inoculants by using differential thermal analysis (DTA) [88HOFa]. Moreover, because inoculant particles are isolated into individual droplets within an emulsion sample, the DET has been used to produce powders of commercial Al master alloy grain refiners. DET processing of master alloys results in the incorporation of effective and ineffective catalyst particles within discrete droplets [89HOF]. This technique used in conjunction with analytical x-ray and microbeam studies has allowed for the subsequent identification of chemical and morphological differences between the catalytically potent and ineffective particle species for the first time in commercial grain refiners [88HOFb] and is suitable for other studies of particle catalysis.

An important example of another dispersed particle system that has become accessible to experimental study with droplet samples in the current program is represented by the class of metal matrix composites. While there are numerous techniques for producing composites, solidification processes have attracted considerable attention because of their flexibility, speed and relative economy. With solidification processing of composites containing either continuous or discontinuous reinforcements, the interactions between the melt and the reinforcement are key factors in determining microstructural evolution. These interactions include the effects of reinforcement wetting by the melt [84KRI], chemical reactions at interfaces [92MOR] and the influence of reinforcements on the solidification reactions and matrix microstructure.

It is clear from the reported studies on bulk samples [84KRI, 92MOR] that matrix solidification behavior in composites can not be simply taken as identical to that of the unreinforced matrix. Even for reinforcements that are chemically inert with the matrix there is evidence that the wetting behavior and the geometrical physical constraints associated with a reinforcement array have a significant impact on microstructure development on a local (i.e. inter-reinforcement) size scale in terms of coarsening and microsegregation behavior [92MOR]. Of course, with chemically reactive systems the melt-reinforcement interaction plays an additional role in modifying the wetting behavior, phase distribution and even the solidification pathway for the matrix [87LAU]. With bulk samples, local nonuniformity of interaction and extraneous effects can yield microstructural variations and complicate the examination and separate study of the melt-reinforcement interactions.

An effective approach to investigate composite solidification involves the isolation of reinforcement particle-liquid mixtures into droplets in order to exclude the extraneous effects encountered in bulk sample. At the same time since the size of droplets is about the same as the reinforcement particle spacing, droplet samples can simulate the effects of geometrical constraint on solidification morphology. Moreover, the advantage of examining the behavior of a large number of droplets in an emulsion sample under common test conditions will provide statistically significant results on the different types of melt-particle interactions by monitoring nucleation undercooling levels and examining the solidification microstructure. With this strategy it will be possible to study the controlling interactions affecting wetting and matrix solidification under the influence of various reinforcement particle phases for a variety of processing methods ranging form bulk liquid solidification to spray deposition.

Based upon the results generated from the nucleation catalysis studies which rely upon the DET as an initial processing step, future work using these procedures should provide additional insight into mechanisms which influence heterogeneous nucleation. It is anticipated that this insight will aid not only in the assessment of existing inoculation agents and the development of more efficient catalyst particles, but also provide useful information for the evaluation of interfacial reactions during melt processing of metal matrix composites.

I.F Nucleation Controlled Solidification Kinetics

Throughout the analysis of solidification it is commonly recognized that nucleation kinetics are an important part of the initial stage of a reaction [89KUR, 74FLE]. However, the effects of nucleation reactions can be masked by other competing processes so that special care is required to isolate nucleation events. One possible approach to examining nucleation control to

identify regimes or processing conditions where growth kinetics are not the dominant factor. At the same time the microstructural transitions usually observed are relatively sharp and occur over rather restricted range of conditions. Outside of the transition regimes kinetic competition is often overwhelmingly biased towards one path so that only the dominant structure is observed in the final product. As a result it is not possible to know with confidence beforehand all of the participants in the kinetic competition to provide a basis for analysis [94GRE]. Moreover, there are possibilities for modification of the microstructure as a result of subsequent solid state reactions which must be considered before analyzing the true solidification reactions [92THO]. In spite of these qualifications experience has demonstrated the operation of several general regimes where nucleation controlled reactions can be identified as a dominant feature in the overall microstructural evolution. These regimes can be illustrated with selected examples and a consideration of the classical nucleation kinetics model.

In the classical model the most likely nucleation process is that involving a heterogeneous nucleation due to some catalytic surface. An expression for the heterogeneous nucleation rate taking into account the potency of catalysts is given by following [88PERb]:

$$J_{net} = (D_L / a_o^2)\left(\frac{2\pi r^{*2}(1-\cos\theta)}{a_o^2}\right) C_a \exp\left[-\frac{\Delta G^* f(\theta)}{kT}\right] \qquad (2)$$

where the contact angle function is given by

$$f(\theta) = 0.25\,(2-3\cos\theta+\cos^3\theta) \qquad (3)$$

and D_L = liquid diffusivity, a_o = jump distance, $r^* = -2\gamma_{LS}/\Delta G_v$

σ_{SL} = solid-liquid interface energy, ΔG_v is free energy change for solidification, $\cos\theta = (\sigma_{nl} - \sigma_{ns})/\sigma_{LS}$, σ_{ne} = nucleant-liquid interface energy, σ_{ns} = nucleant-solid interface energy, C_a = nucleation site density~ 10^{20} m^{-3}, $\Delta G^* = 16\pi\,\sigma_{SL}^3 / \Delta G_v^2$ and kT has the usual meaning.

Based upon experience there appear to be at least five separate general conditions that can be identified for nucleation controlled solidification kinetics as listed in Table 1.

Table 1

Undercooling Level	Nucleant Potency	Growth Rate
Low	High	Slow
High	Low	Slow

High	High	Rapid
High	High	Limited
High	Restricted	Rapid

In all cases the emergence of nucleation control is dependent on the potency and density of heterogeneous sites.

I.F.1 Low Undercooling - Active Nucleants - Slow Growth

Low undercooling implies that the nucleation temperature is nearly equal to the equilibrium transformation temperature so the driving free energy for reactions is also limited. From Eq. 1 an appreciable nucleation rate requires a high site density and a low contact angle, i.e. high potency. However, the nucleation rate is usually still relatively low. It is important that the growth rate be limited in order to observe the full effect of nucleation. This is a classical description for a highly effective grain refining operation [75MAX].

I.F.2 High Undercooling - Low Potency Nucleants - Slow Growth

Upon initial consideration the description of high undercooling associated with low potency nucleants and relatively sluggish growth appears to be the same as that for formation of an alloy glass [69TUR, 82BOE]. This is certainly true and at sufficient undercooling which is promoted strongly by a limited supply of relatively low potency nucleants, the slow growth that can develop into a highly viscous liquid allows for good glass forming ability. However, the same description also applies to other conditions, especially those involving a phase selection between stable and metastable phases. For example, consider the conditions illustrated in Fig. 7 where the relatively stability of the σ and α phases in an equiatomic Fe-V alloy is defined [87PERa, 88FOL]. If a sample of single phase σ is pulse melted as in a laser annealing treatment, the moving liquid-solid interface assumes a temperature near T_m^{σ} which is 55°C below T_m^{α}. Whether the subsequent resolidification upon removal of heat is limited by heat flow or more severally restricted by interface kinetics, there will be a liquid zone ahead of the growing σ phase that is undercooled with respect to the α phase [87PERa]. Nucleation of α during the resolidification process is an indication of nucleation control and a departure from the usual epitaxial resolidification found in surface melting reactions.

This behavior may be generalized as illustrated in Fig. 8. The usual conditions for regrowth of an existing substrate phase are shown in Fig. 8a. When conditions exist to limit the regrowth of substrate and provide time before complete freezing from the development of a

second phase (in this case β in Fig. 8b, c) the situation may be described as heteroepitaxy and there may exist a preferred orientation between the two phases. The conditions to allow for this to occur usually involve the release of latent heat by the substrate phase which limits its growth and allows for the second phase to develop. An intermediate or transition state may also be envisioned in which the competition between regrowth of the substrate and nucleation on the moving solid-liquid interface of another phase are of comparable kinetic rates so that a mixed microstructure composed of substrate regrowth segments and nucleated second phase segments can develop as labeledengulfment in Fig. 8b.

I.F.3 High Undercooling - Active Nucleants - Rapid Growth

The operation of a transition regime between substrate regrowth and heteroepitaxy indicated in Fig. 8b will also be expected to occur in the conditions of high undercooling with active nucleants where nucleation of the β phase occurs at the γ/liquid interface and is followed by relatively rapid growth of both γ and β phases. Alternatively, there can be a separate nucleation for each of the two-phases that need not develop during the regrowth process so that no orientation relationship develops between the two phases. The conditions which allow for this occurrence are illustrated in Fig. 9 for Ni-V alloys [93ALL]. In a region between 47 and 52 at%V a two phase duplex microstructure develops consisting of FCC and BCC grains having the same composition as each other and as the original liquid. The duplex microstructure requires the simultaneous development of relatively large undercooling so that the liquid is below the T_0 curves for both α/liquid and β/liquid and a high density of nucleation sites for both phases as well as the rapid growth.

I.F.4 High Undercooling - Active Nucleants - Growth Limitation

In alloy systems that experience significant undercooling while still far removed from the glass transition, it is the growth kinetics of the nuclei which determine the impact of the nucleant population. In pure metals growth kinetics dominate and do not allow for alternate grain formation ahead of a moving liquid-solid interface, but in certain alloy solidification reactions such as those represented by eutectics there is a limit to the growth rate [82BOE] which allows time for nucleation to occur ahead of the interface. A good example is illustrated in Fig. 10 for an Al-26 wt% Si alloy that was given a surface melting treatment which forced the resolidification velocity to be in access of 8 mm/sec which corresponds to the maximum growth rate for the imposed processing conditions [92PIE]. Further increases in resolidification rate allow for the development of a zone ahead of the moving interface with sufficient undercooling to activate internal nucleants and provide for formation of Si particles and associated eutectic units. With

continued increase in resolidification velocity more undercooling develops and a higher density of sites become active so that in a case of Al-Si alloys, the Si particle density increases with increasing beam speed [96GRE]. This is a characteristic signature of nucleation controlled solidification kinetics.

I.F.5 High Undercooling - Restricted Nucleants - Rapid Growth

In the cases considered so far the processing conditions promoting the onset of nucleation control have involved rapid cooling of the melt. This is not a general requirement for the production of highly undercooled liquids. The attainment of high liquid undercooling in the presence of nucleant distribution requires only that the influence of the nucleants be isolated in some way. With rapid quenching, the isolation is effective by limiting the time available for transformation and hence the volume of liquid that can be transformed by each nucleation site. While this approach is effective it does not allow for the separate study of the liquid or the detailed study of isothermal solidification kinetics.

An effective approach to nucleant isolation is based on the spatial isolation of nucleants by the dispersal of the liquid into separate independent volume elements or droplets. In order for the isolation to be effective the internal nucleants should have discrete well separated potencies and a numerical population that can be approached by the number of droplets [84PERb]. Additionally, physical droplet independence must be produced while minimizing new surface catalytic effects.

The effectiveness of nucleant isolation by liquid dispersal into droplets is demonstrated in Fig. 11. With decreasing droplet size there is a clear trend with the development of large undercoolings in additional crystallization exotherms [87PERc]. Since the magnitude of a given exotherm is proportional to the fraction of the sample containing a given nucleant, it is clear that increased dispersal reduces the number of droplets which contain a given nucleant. With droplet size reduction below about 4 microns there are only slight changes in the undercooling behavior apparent for Sn droplets. The type of behavior illustrated is consistent with the random distribution nucleants and from a Poisson distribution analysis of nucleant concentration, it is estimated that on the order of 10^{13} m^{-3} of internal nucleants may be present in the sample such as that shown in Fig. 11. Even at high dispersal the limitation on undercooling appears to be associated with heterogeneous nucleation at the liquid droplet coating interface. However, for the most part experience has shown that droplet dispersal is an effective procedure for achieving high undercooling in the presence of a limited active nucleant population. Under these conditions, nucleation is the rate limiting step in the overall solidification process and the resulting crystal growth into a highly undercooled liquid is rapid.

I.G Design of High Temperature Al Alloys

As a result of an extended effort in a number of laboratories a new generation of advanced high temperature-high strength Al alloys has evolved through the direct application of RSP. Many of the important highlights of this effort have been discussed in a rather thorough overview [92LAV]. Among these developments several alloy classes have been shown to be suitable for temperatures up to about 325°C including Al-Fe-Ce[81SAU], Al-Fe-Mo[86LAN], Al-Fe-V-Si[86SKI] and Al-V-Zr[86ZEN]. In all cases alloying additions yield intermetallic phase dispersoids (both stable and metastable) that display very low solubility in Al. The strengthening dispersoid phases are present in fairly large volume fraction (i.e. 20-30%) as a direct result of RSP to form a supersaturated solid solution or to use the liquid phase to solutionize the solute and allow dispersoid formation to initiate on a fine scale during solidification. From this base of experience, it is now recognized that in order to maintain a high volume fraction of fine scale particles in an Al matrix at relatively high temperature, it is essential to apply an alloy design that minimizes the effects of coarsening on the particle size distribution.

The essential features of the design strategy may be illustrated by examining the LSW [61LIF, 61WAG] model for volume diffusion controlled coarsening where the average particle size $\bar{d}$ varies with time, t, as

$$\bar{d}^3 - \bar{d}_0^3 = \frac{A\gamma_{\alpha/\beta} D_B C_B \bar{V}_B^2 t}{kT} \qquad (4)$$

where $\bar{d}_0$ is the initial size, A is a constant, $\gamma_{\alpha/\beta}$ is the particle matrix interfacial energy, C_B is the solubility in the matrix, $\bar{V}_B$ is the partial molar volume of solute B and kT has the usual meaning. Therefore, for a volume diffusion controlled process the effect of coarsening is minimized by reducing the ($\gamma_{\alpha/\beta} D_B C_B$) product to as low a value as possible. For the most promising high temperature Al alloys, C_B is at very low levels (< 0.03 at% Y and typically < 1 at% for transition metals) and the D_B values for transition metal [76MON] and rare earth [88ANG] solutes are also small (between $10^{-13\text{-}16}$ cm^2/sec at 700 K) so that much attention has been focused on $\gamma_{\alpha/\beta}$. Indeed in several detailed studies of the relative coarsening behavior a clear and consistent trend has emerged [85ANG]. The lowest coarsening rates are associated with intermetallic particle dispersions which may be expected to have the lowest values of $\gamma_{\alpha/\beta}$ based upon a low lattice misfit between the particle and Al

Based upon the current experience it appears that the lowest coarsening rate is achieved with particles that have an $L1_2$ structure and low misfit with Al. In addition a comparable

coarsening behavior or somewhat slower coarsening is reported in Al-Fe-V-Si alloys where the dispersoids are based on $Al_{13}(Fe,V)_3Si$ and $Al_{12}(Fe,V)_3Si_2$ complex silicides which also may have a low interfacial energy with Al. It is interesting in retrospect to note that the finding of an $L1_2$ dispersoid phase in Al as a favorable alloy design is analogous to the combination of $Ni_3Al(L1_2)$ in Ni which is the foundation of Ni-base superalloys. In Al-Zr, Al-Ti, and Al-Zr-V where the attributes of $L1_2$ particles were established initially, processing limitations restricted the maximum volume fractions to under 5%. While the processing limitations were not quantified it seems clear that these systems exhibit peritectic reactions with steeply rising liquidus temperatures. To increase the level of supersaturation to achieve high volume fractions of dispersoid phase requires an increasing liquid undercooling. Moreover, due to recalescence effects, attempts to increase the supersaturation level may yield non-uniform solidification microstructures. In order to address the solidification processing limitations it is useful to consider another class of solute addition based on rare earth metals that develops an $L1_2$ structure, but also exhibits a eutectic reaction with Al. In this case, of course, liquidus temperatures exhibit a shallow decline until hypereutectic compositions are reached so that high levels of supersaturation are facilitated. At the same time it is important to define the extent of the coupled zone, where cooperative eutectic growth develops, especially for hypereutectic compositions to which the coupled zone may be displaced [74BUR]. In addition, for hypereutectic compositions other intriguing possibilities exist for novel control of the solidification microstructure that warrant investigation. For example, for an $L1_2$ Al_3RE (RE≡Rare Earth) phase with low misfit with Al, the particles may be expected to promote efficient grain refinement. This has been demonstrated with Al_3Sc, but unfortunately Sc is quite expensive.

There have been some studies investigating a substitute for Sc. It has been reported the most likely substitute of Sc would be elements that are similar, like Y and the Lanthanide or rare earth elements[88SAW]. A different study on rapidly solidified ribbons of Al-Er, Al-Nd, and Al-Gd indicated that the Al-RE systems offer good dispersion strengthened alloys for potential use at high temperatures, based on microhardness and microstructure [86ELI]. In this case, at high undercooling a high density of fine Al_3RE particles can develop as a primary phase with each particle promoting the nucleation of Al during further cooling and effectively modifying the development of a cellular/dendritic structure that is usually observed in systems where the intermetallic particle lattice is not closely matched to Al.

I.H Design of High Strength Al Alloys

Although the previously discussed Al alloys have attractive mechanical properties, recently

reported Al-rich amorphous alloys exhibit superior strengths [88INO]. Aluminum and a combination of transition and rare earth element additions [95YAV, 93NAK, 88HE, 88SHI] has yielded microstructures of Al nanocrystals in an amorphous matrix with nanocrystal volume fractions approaching 20% [90KIM]. It has been reported that Al nanocrystal dispersions can enhance the fracture strength to 1300-1500 MPa with several percent strain [88HE, 91KIM].

The reported properties are strongly related to the size, and density of the Al nanocrystals. In the Al-Y-Ni system a microstructure consisting of small 3-5nm Al nanocrystals with a volume fraction around 20% exhibits the highest fracture strengths in as-solidified amorphous ribbon [94KIM]. Similar results are seen for other Al-RE-TM systems. The two-phase microstructure, of amorphous and nanocrystalline Al is achieved by decreasing the cooling rate to slightly lower than the critical cooling rate to form completely amorphous alloys. A schematic TTT diagram shown in Fig. 12 illustrates the two different solidification pathways.

Annealing of the completely amorphous alloy can also be used to form the two phase amorphous and Al nanocrystalline microstructure. The resulting microstructure is very sensitive to annealing temperature and time. In addition, the nucleation site density plays an important role in the limitation of the growth of the nanocrystalline Al [96FOLb]. However, it is not clear if the high nucleation site density (up to 10^{23} m^{-3}) is due to quenched-in nuclei or develops during annealing of the as-solidified amorphous structure. Some reports suggest that the high strengths exhibited by the amorphous and nanocrystalline Al is due to the lack of defects in the Al nanocrystals [96INO]. Initiation of defects requires higher energy and result in an overall higher tensile strength.

Recently, there have been reports of another new class of high strength Al alloys that are similar to the amorphous and nanocrystalline Al alloys [96INO]. The new class of high strength Al alloys are nearly 95 at % Al with additions of various transition metals (TM) and very small rare-earth (RE) additions (1-2 at % RE). Rapid solidification of these alloys forms a two-phase mixture of a nanoscale icosohedral phase surrounded by an Al matrix. The icosohedral phase is reported to have a high thermal stability and bulk alloys can be made by extruding atomized powders in the temperature range of 300-400°C. The bulk alloys exhibit strengths as high as 1350 MPa and can have elongation's up to 22%. From the graph shown in Figure 13 it is evident that the tensile strengths combined with elongation's of the new class of high strength Al alloys are superior to the conventional Al-based alloys. In addition these alloys exhibit excellent high elevated temperature strength compared to conventional alloys (200MPa at 300°C).

Even though these alloys are very promising in terms of elevated temperature stability and

mechanical properties information about the kinetics of formation, and decomposition of the phases in this system is limited. For example, the icosohedral phase has been reported to exhibit high temperature stability, but thermal analysis traces have not been reported. In addition, mechanisms for the limited growth of the icosohedral phase have not been presented or proposed. Experiments that provide useful kinetic parameters would improve the understanding of useful lifetimes and useful operating temperatures for different processing conditions and provide a basis for a fundamental analysis and understanding of the reaction pathway and kinetics. Moreover, these investigations would provide guidance and insight into the design of other possible systems with similar or improved properties.

II. RESEARCH ACCOMPLISHMENTS OF THE CURRENT PROGRAM

During the current program, research has been focused upon metastable phase formation and the controlling phase selection reactions, the evolution of solidification microstructure under the combined influence of undercooling, heterogeneous nucleation sites, recalescence and external cooling and several aspects of undercooled alloy solidification and product structure stability. The experimental approach that has been applied to carry out these studies is based principally on the droplet emulsion technique. With this method, samples may be produced which exhibit large undercoolings prior to solidification during slow cooling (10-30°C/min) and which may be maintained in the metastable undercooled state for extended high periods without the intervention of crystallization. In addition, to make contact with other common RSP methods, additional studies of splat quenched and melt spun samples were compared to the results of droplet experiments.

At deep undercoolings equilibrium crystallization reactions may be bypassed and metastable solid phases can be produced during freezing. With thermal analysis and x-ray diffraction experiments it has been possible to examine the undercooling conditions for metastable phase formation and to elucidate the kinetic competition during crystallization. Often the microstructural morphology and the structure of the product phases that solidify from the melt have features which are distinct to high undercooling solidification. Several examples of fine-scale eutectics, multizone structures and ultra fine dispersoids as well as uniform supersaturated solid solutions and amorphous phase products have been identified in droplet samples.

For selected reactions it has been possible to identify the solidification path for crystallization from the undercooled liquid state. With samples containing known nucleation catalysts, thermal analysis and x-ray diffraction study have been used to identify a path for the generation of supersaturated solid solutions and metastable intermediate phases. Based on these

findings it has been possible to develop a framework for describing the reaction paths followed during high undercooling solidification in terms of metastable phase diagram constructions. Indeed droplet samples offer a useful method of probing and measuring different portions of metastable phase diagrams. Moreover, with some solidification structures other forms of microstructure selection maps have been defined in terms of solidification kinetics parameters.

In a complementary examination, the use of droplet samples with controlled undercooling levels and known nucleation catalysts has permitted the documentation of new features governing heterogeneous nucleation [92PER]. For example, it is often considered that the lattice disregistery in a heteroepitaxy relationship between catalysts surface and the nucleus is the key to controlling heterogeneous nucleation at least at low undercooling. However, at high undercooling there is now clear evidence that a chemical interaction at the catalysts surface is important in establishing catalytic potency. Some of the implications of chemically controlled catalysis for wetting behavior during soldering and solidification processing of composites have been explored in an initial study. The complexity of the chemical interactions observed has further motivated the development of new types of droplet sample analysis for heterogeneous nucleation.

Several new applications and analysis methods involving droplet samples have also been advanced during a current research. A new perspective on rate effects has been established to allow for the measurement of nucleation undercooling temperatures at cooling rates approaching 10^3°C/sec. These results have been coupled with a nucleation kinetics model and measured thermodynamic properties to provide the quantitative assessment of the measurement requirements for reliable analysis of nucleation rates. Indeed, with this approach the establishment of bounds of uncertainty of certain kinetic parameters has been implemented for the first time to allow for an assessment of the uncertainties with the usual nucleation kinetics calculation methods.

Several advances in experimental capability have been established during the current work. A new type of droplet experiment focused on the repeated undercooling and nucleation behavior of a single droplet has been implemented. In this approach statistically significant data is obtained by using multiple cycles of melting and nucleation as opposed to the usual approach of using a large number of droplets in a single thermal cycle. As a result, a new method of evaluating nucleation rates will be available for future studies. In addition, with the continuing efforts to develop the droplet method to extend the use to high temperatures it has been possible to establish a method for preparing droplet dispersions of ferrous alloys where the droplets are encased in a glass slag. Also, emulsification procedures have been extended so that now copper alloys can be produced as droplet emulsion samples using high melting point salts as a carrier

medium. Lastly, the droplet technique has been modified to allow for analysis of the catalytic potency of various compounds for nucleation of a metallic phase through the incorporation of ceramic particles into the droplets during emulsification. This technique had been used to evaluate the effectiveness of Al grain refining master alloys and has been extended to permit the examination of reinforcement particle/melt interactions that influence the solidification processing of metal-matrix composites.

In the following sections a description is given of the results of the current areas of study. When these findings are viewed together, several new features of the solidification of highly undercooled alloys can be identified from the droplet studies. The significance and implications of these observations are discussed in terms of the factors determining the rate of solidification, the phase selection process for the solidification products and the microstructural evolution. A consideration of the results is of value not only in demonstrating the unique potential of the droplet technique, but also in providing the necessary background for the further development and application of the droplet method to study the solidification of undercooled liquid alloys.

II.A Undercooling Behavior of Pure Metals

The droplet emulsion technique has proved to be a very effective means of attaining high levels of liquid undercooling. Present experience with the droplet method has identified a number of processing parameters that are likely to govern the optimization of undercooling in powder samples [89PER]. These processing variables include droplet size refinement, sample purity, droplet surface coating, uniformity of coating, cooling rate and melt superheat as well as alloy composition and applied pressure. Although the influence of these processing variables has been demonstrated with droplet experiments, the results are general and are expected to apply to other processing methods where direct measurement and control of solidification is more difficult.

The effect of the various processing parameters on the undercooling response is summarized in Table 2. Even when these processing conditions are satisfied to produce maximum undercooling, experience suggests that solidification is still initiated by a heterogeneous nucleation site associated with the sample surface [87PERb].

Table 2

Parameter	Undercooling Response	Remarks
Droplet Size	Increased ΔT with size refinement at constant T	Nucleant isolation follows Poisson statistics
Droplet Coating	Function of coating structure and chemistry; major effect in limiting ΔT	Most effective coating is catalytically inert
Cooling Rate	ΔT generally increases with increasing T	Changing T can alter the nucleation kinetics
Melt Superheat	System specific	Appears to be related to coating catalysis
Composition	T_n follows trend of T_L	Melt purity not usually critical
Pressure	T_n parallels melting curve trend	Change in response can signal alternate phase formation

Therefore, it appears that close attention to the nature of the powder surface coating is of prime importance in achieving reproducible, large undercooling values in fine powders. The maximum undercooling limits for several pure metals measured using thermal analysis are listed in Table 3.

Table 3

Element	Previous Studies			Current Studies	
	ΔT (°C)	$\Delta T/T_m$	Reference	ΔT (°C)	$\Delta T/T_m$
Al	130	0.14	Turnbull and Cech (1950)	175	0.19
Sb	135	0.15	Turnbull and Cech (1950)	210	0.23
Bi	90	0.16	Turnbull and Cech (1950)	227	0.41
Cd	-	-		110	0.19
Ga	150	0.50	Bosio et al. (1966)	174	0.58
In	-	-		110	0.26
Pb	80	0.13	Turnbull and Cech (1950)	153	0.26
Hg	80	0.34	Turnbull (1952)	88	0.38
Te	-	-		236	0.32
Sn	117	0.23	Pound and LaMer (1952)	191	0.38

Based upon the comparison presented in Table 3, current studies have demonstrated clearly that the previous maximum undercooling values actually correspond to heterogeneous nucleation conditions. Indeed, the present findings emphasize that further nucleation kinetics studies are necessary before a complete characterization of the revised undercooling limits in terms of heterogeneous or homogeneous kinetics is possible.

II.A.1 Recent Advances in Undercooling Studies

As part of a continuing effort to extend the range of application of the droplet method and the versatility of its application to new areas of study two significant advances have been achieved in the current work. The first development relates to the capability to explore the statistical nature of nucleation with a diagnostic based upon the observation of single droplet solidification behavior. The second innovation deals with the development of new capability to study high temperature alloys including ferrous systems such as cast iron.

II.A.2 Nucleation Behavior in Undercooled Aluminum

One of the inherent attributes of the droplet method is the statistical significance of the observations from a single DTA run due to the fact that the thermogram displays behavior from a large number ($>10^5$ drops per sample). Of course, to achieve this result it is necessary to sacrifice the specific information on the behavior of each single drop in an averaging process. With this method it is still possible to detect behavior representing deviations from the average, but only if sufficiently, large numbers of drops in the sample show the deviation. In order to explore the specific behavior from an individual drop in more detail it is necessary to study single droplet undercooling and nucleation behavior. However, to obtain information that is also statistically significant, it is necessary to conduct many trials of the single drop behavior. This requires high detection sensitivity in DTA and also a sample which is robust under repeated thermal cycling.

Single droplet experiments can now be conducted on aluminum by incorporating a programmed thermal schedule and a PC-based data acquisition system. A typical thermal cycle is displayed in Fig. 14 and the resulting data for 845 thermal cycles is displayed in Fig. 15. It is apparent from the data in Fig. 15 that after some initial variability in nucleation temperature behavior over the first 150 cycles nucleation occurs in a band with a width of approximately 4°C for the remaining cycles. With the display shown in Fig. 15 it is possible to establish that there is no correlation between the individual data points and indeed that the sample obeys all the conditions required for a Poisson process. This is further illustrated by the results in Fig. 16 which show the distribution of nucleation events versus undercooling. For the solidification of a droplet sample, the rate can be expressed as shown in Eq. 5 and Eq. 6.

$$\frac{dN}{dT} = -N\lambda(t) \tag{5}$$

$$N(t) = N_0 \, exp\left[-\int_0^t \lambda(t')dt'\right] \tag{6}$$

Since the process under observation is not isothermal, but occurs during continuous cooling this represents what is termed a nonhomogeneous Poisson process. From the data in Fig. 16 and the known thermal history and sample volume for the 80 micron droplet, it is possible to deduce the nucleation rate as a function of undercooling for quantitative comparison to theory. This is illustrated in Fig. 17. This work is currently ongoing and the analysis is being extended to include the effect of incorporated nucleants but the results and further application are clear.

It is useful to note that in several ways the single drop and droplet population samples offer similar capabilities, but there also important distinguishing features. For a given nucleation mode, both sample types allow for measurement of the nucleation rate over a narrow range of crystallization. When different catalytic sites appear in separate droplets, the action of various sites may be difficult to resolve in a droplet population sample, particularly when the potencies are similar. The single drop method provides an alternate route for probing regions of overlapping potency, but of course, at the expense of multiple measurements. This new capability should be extremely valuable in examining the effect of incorporated reinforcement particles on the undercooling and solidification behavior that is important in composite processing.

II.A.3 Droplet Production for High Melting Point Materials

The droplet technique has found most use in low melting point systems where oil based carrier fluids can be used for emulsification and has been extended to include a variety of aluminum alloys by the use of molten salt as a carrier fluid. These limitations indicate that the production of droplet samples from metals and alloys with melting points above about 1000°C is difficult. This limitation has been addressed in the current work and two methods of overcoming it in selected cases have been developed as described below.

In terms of undercooled liquid solidification the class of materials represented by cast iron is by far one of the most important. Bulk castings often show some tens of degrees of undercooling, however, there is relatively little understood about nucleation [68HIL, 68LUX]. Yet nucleation controls graphite morphology and the eutectic type which has a significant impact on the applications and properties of cast irons. One of the main factors to consider in attempting to clarify the nucleation behavior is the fact that even in the undercooled state the initiation of freezing in cast iron is clearly influenced by various constituents that are normally present in the melt including the inclusions and various mold particulates. With this in mind there is an appeal in applying the droplet technique in order to isolate the separate influence of these various unknown nucleants on the undercooling behavior and to attempt to achieve nucleant-free droplets to examine the intrinsic undercooling response in cast irons of commercial purity.

In order to develop an appropriate droplet method there are two main issues that are necessary to address including the high melting temperature of cast iron and the need to provide some means of environmental protection against oxidation, decarburization and/or desiliconization in fine droplets. A resolution of these challenges has been achieved based upon the use of a SiO_2-Al_2O_3-CaO slag which provides a neutral environment for the melting and undercooling of fine droplets and also serves to prevent the agglomeration of droplets. The principle of the method is represented schematically in Fig. 18. In the approach, a slag which has a high melting point has been selected to keep the droplets independent. At first, a mixture of metal flakes produced by melt spinning in order to maintain the composition uniform and slag powders are prepared in a Al_2O_3 crucible. As a mixture is heated up it melts with the metal flakes melting first and than slag powder. Once both the metal and slag are molten the mixture is cooled through a temperature below the melting point of the slag so that the droplets can remain separate in the solidified slag. In this state the molten droplets form spheres and provide for nucleant isolation with droplet independence so that further DTA analysis of the undercooling and nucleation response may be carried out at standard cooling rates.

As indicated phase diagram in Fig. 19 both hypoeutectic and hypereutectic alloys consisting of Fe-(2.85-4.14) wt%C-(1.82-1.91) wt%Si were examined. Based upon liquidus temperature measurements of the droplets and microprobe analysis no significant changes in the carbon and silicon contents were observed after droplet production and subsequent DTA examination. With the selected compositions, two main types of thermal cycles were examined including cooling from above the liquidus which is denoted as the homogeneous cycle and cooling from the temperature between the eutectic and liquidus which is denoted as the heterogeneous cycle (Fig. 20). In the first case the undercooling pure liquid droplets is examined while in the second case a primary phase of either austenite for hypoeutectic compositions or graphite hypereutectic compositions is examined in terms of its influence on the undercooling and nucleation of the coexisting liquid. With this approach only a limited quantity of droplet sample may be produced which is insulated from the DTA detection system by the glass slag resulting in a diminished thermal signal. However, a careful study of the thermograms allows for the identification of nucleation events from droplet samples as distinguished from those of the slag and any solid state reactions. This is illustrated in Fig. 21. The maximum undercoolings with reference to the liquidus are 600°C for 2.85 wt % C, 500°C for 3.45 wt % C and 200°C for 4.15 wt % C. It is interesting to note that the reduced undercooling levels approach 0.475 for the 2.85 wt%C alloy. These studies are currently ongoing and a rich variety of very interesting solidification microstructures has been detected. As an example in Fig. 22 an interior section of a droplet containing primary austenite as a nucleant for the liquid is illustrated. In this case very

large undercooling was obtained of almost 430°C below the eutectic which demonstrates clearly that in the absence of extraneous nucleants, primary austenite is a rather poor nucleant for both graphite and Fe_3C. On the other hand, other measurements indicate that primary graphite is very catalytic for the formation of austenite at an undercooling of only 20°C below the eutectic. Other interesting effects have been detected including the development of metastable solid phases including ternary iron silicon carbon compounds. Clearly further work on the undercooling behavior and structural evolution in droplet samples is warranted to build on the very promising initial studies. Moreover, this effort has established that droplet samples may be produced and examined effectively in very high temperature systems which include not only ferrous systems but also Ni-base alloys.

In another effort it has been possible to produce high temperature emulsions based on high temperature $BaCl_2$ salt mixtures and the recently constructed high temperature emulsion furnace. The new salt combinations and high temperature emulsion furnace extend the maximum temperature capability of the droplet emulsion technique to 1500°C. In addition, a modified droplet emulsion technique has been identified to produce fine droplets of copper based alloys. The new technique uses a high temperature carrier salt, such as $BaCl_2$, and a small amount of surfactant salt that is added just before the emulsification process. This technique has produced fine droplets of a copper based alloy, shown in Fig. 23, which also exhibited very large undercoolings as illustrated in Fig. 24.

II.B Recent High Temperature, High Tensile Strength Al-rich Glasses

A similar influence of powder processing parameters has also been found to prevail in the treatment of Al-rich alloys as well. The solidification microstructure that develops in Al alloys has been documented to be related closely to the initial level of undercooling at the onset of solidification [85BOE, 86PER]. Of course, with alloy solidification the available pathways for freezing from an undercooled state involve a variety of options. In this case, the microstructural and thermal history capabilities that can be applied in the controlled solidification of powder samples produced from the DET are of particular assistance in identifying the operative pathway under a given set of processing conditions. A number of the RSP pathway options can be analyzed by examining the solidification of droplet samples in several Al alloy systems, some of which offer useful potential fordispersoid formation.

Through the control of melt undercooling in Al alloy droplet emulsions, highly dispersed phase mixtures have been produced in several alloys through various phase separation reactions, fine scale eutectic growth, precipitation of phases from supersaturated solid solutions, and from

the decomposition of metastable phases [88PERa]. In addition, the microstructural morphologies that develop during the solidification of the undercooled Al alloy droplets under slow cooling conditions are also comparable to the structures that evolve during the rapid quenching of atomized powders. Therefore, the information obtained from the alternative solidification pathways and the current experience with Al alloy droplets has allowed for favorable microstructures to be developed and can be used as a basis for effective RSP alloy design.

As part of a continuing study of Al alloy systems that offer the potential for the development of large volume fractions of fine dispersoid phases with high temperature stability the current focus has been directed towards Al-rich Al-Y-Transition Metal (TM) alloys. The Al-RE-TM alloys have tensile strengths that are comparable to steel and have a lower density than ferrous or titanium alloys. Using powder metallurgy extrusion techniques, near net shape products are possible. In order to tailor the microstructure and related properties a clear understanding of the fundamental properties of these Al-rich amorphous alloys is needed. Extensive work has been reported regarding the compositions and systems that form Al-rich glasses, but these reports provide limited insight into why the Al-RE-TM alloys are relatively easy glass formers, or why these alloys have such relatively high glass transitions [88INO, 93NAK]. In addition, it has been reported that the presence of the Al-nanocrystals increases the tensile strengths observed, but the main variables that affect the formation of the strengthening nanocrystals upon solidification have been limited to wheel speed and alloy composition. Since, the amorphous alloys can decompose to form many different microstructures, an understanding of the reaction kinetics and pathways for microstructure evolution from the initial as-solidified amorphous state is needed.

Before droplet studies were carried out, experiments that reproduce and define solidification products and pathways were performed. Rapidly solidified ribbon was made by melt-spinning selected Al-Y-Fe alloys. Initial TEM and XRD results (Fig. 25) indicate that the Al-7Y-5Fe as-solidified ribbon is predominately amorphous and the Al-5Y-5Fe alloy (Fig. 26) is a two phase mixture of amorphous and nanocrystalline Al. Additional alloys were made to characterize the Al-rich portion of the Al-Y-Fe phase diagram, because there is a very limited amount of information in the literature concerning the equilibrium phase equilibria. The equilibrium phase diagram, along with providing valuable phase equilibria, can also provide insight into the glass-forming behavior of the Al-rich ternary alloys. For example, many glass forming alloy systems exhibit deep eutectics. Associated with the deep eutectic are plunging T_0 curves shown in Fig. 27. In such systems the Tg can be reached with moderate undercoolings and a glass is formed. The equilibrium liquidus of the Al-rich portion of the Al-Y-Fe system has been

mapped out with the use of differential thermal analysis (DTA) shown in Fig. 28. The liquidus does not show any evidence of a ternary eutectic or plunging liquidus in the range of glass forming alloys. Moreover, the undercooling levels attained for the bulk alloys were comparable to other non-glass forming alloys.

With the liquidus information and the DET, droplets were made of each selected bulk alloy used to map out the equilibrium phase diagram. These droplets showed increased undercooling over the bulk alloys, but not enough to form amorphous droplets during slow cooling. The use of a water quenching apparatus to increase the cooling rate to 500°C/sec resulted in similar microstructures observed in droplets that were thermally cycled in the DTA. Therefore, higher undercoolings or faster cooling rates are needed to form amorphous droplets. These results seem to indicate that the Al-Y-Fe and possibly other Al-RE-TM systems do not fit the reported "rules" of that are usually applied to easy glass formers [91BEC]. In addition, since amorphous material was formed during melt-spinning and not in slow cooled droplets, cooling rate appears to be an important factor in the operative kinetics. This motivated an examination of the crystallization behavior to gain understanding of the competitive kinetics that influence the undercooling response.

Recent calorimetric analysis of nanocrystal development during devitrification has provided new insight into the understanding of primary crystallization reactions, including the application of devitrification reactions to form nanometer size dispersions of second phase. A DSC heating trace of melt-spun Al-7 Y-5 Fe is shown in Fig. 29 for the entire course of crystallization. The first observable crystallization reaction has an onset at about 276°C; the peak is distinctly asymmetric with a tail at high temperatures. The separation between the first observable peak and the onset of the succeeding crystallization involving intermetallic phases is more than 75°C. The DSC heating trace of melt-spun Al-8 Sm shown in Fig. 30 contains the same characteristic peaks. From this work and previous reports, XRD and TEM analysis indicates that the as-solidified melt-spun ribbon appears to be amorphous [96FOLa, 94BAT]. Moreover, heating beyond the first observable peak in Al-rich glass forming alloys results in primary crystallization of essentially pure Al [96FOLa, 94BAT]. Isothermal DSC scans were conducted in the range 235-280°C to examine the details of the kinetics. A typical trace (Fig. 31) consists of an instrumental transient at early times followed by a flat baseline. TEM micrographs of the sample isothermally held at 245°C for 10 minutes (Fig. 32a) indicate development of approximately 10^{21} m^{-3} nearly-spherical Al nanocrystals of 22 nm average diameter. The size distribution after this treatment was narrow, with >80% of the particles between 18 and 26 nm. TEM analysis of the sample held isothermally at 245°C for 100 minutes (figure 32b) indicates that the nanocrystals grew further developed a

non-spherical shape, but the number density was still about 10^{21} m^{-3}. However, for samples isothermally held above 270°C for 10 minutes (figure 33) the nanocrystals developed a highly dense dispersion (10^{22}-10^{23} m^{-3}). The change in density suggests a change in kinetic behavior.

From the results presented, the DSC and TEM observations appear to be in conflict. The isothermal DSC traces below 270°C as well as the continuous heating trace baseline below the first crystallization onset at 276°C exhibit no evidence of a reaction, while the TEM micrographs of the samples held isothermally at 245°C for 10 minutes shows a dispersion of Al nanocrystals that was not present in the as-solidified sample. This apparent discrepancy may be resolved through an analysis of the heat evolution rate during primary crystallization.

For identical spherical particles growing by diffusion control into a supersaturated matrix, the heat evolution rate, $\dot{Q}$, is

$$\dot{Q} \equiv dQ/dt = N_V V \cdot \Delta H_v \cdot 4\pi R^2 \, dR/dt \qquad (7)$$

where N_v is the particle density, V is the sample volume, ΔH_v is the enthalpy change per unit volume, and R is the particle radius. For diffusion kinetics, $R = S\sqrt{Dt}$ and the growth rate, dR/dt, is given by $(S/2)\sqrt{D/t}$, where S is a constant on the order unity [50FRA]. Substitution of these expressions into equation (4) yields

$$\dot{Q} = N_V V \cdot \Delta H_v \cdot 2\pi S^3 \sqrt{D^3 t} \qquad (8)$$

A thermodynamic model of the phase equilibria at 280°C [96ALL] indicates that the Al nanocrystals are in equilibrium with the amorphous phase of composition Al-11 Y-7 Fe, which changes little over the temperature range of interest. The enthalpy change for the formation of nanocrystalline Al from the bulk composition Al-7 Y-5 Fe is $\Delta H_v \approx -2.8 \times 10^8$ J/m^3 [96ALL]. Based on field ion microscopy (FIM) measurements [95HON], yttrium is taken to be the slow diffuser. Iron is assumed to diffuse rapidly and to adjust its composition in the amorphous matrix as a concentration gradient of yttrium evolves; this analysis treats the diffusion-field impingement of yttrium as the limiting factor innanocrystal growth.

An estimate of the volume diffusion coefficient of yttrium in the amorphous matrix at 245°C was based on the observed particle size and the Frank analysis [50FRA]. An as-solidified sample and a sample analyzed after 30 seconds at 245°C did not show any particles. The average diameter after the 10 minute treatment was 22 ± 5 nm; thus assuming zero initial particle size, $D \approx 9 \times 10^{-20}$ m^2/s. Assuming an initial particle diameter of 5 nm, which is well within the TEM

resolution limit, has little effect on the estimated value of D. The expected heat evolution rate from the primary crystallization reaction was calculated from equation (7) for several different conditions with constant $N_v=10^{21}$ m^{-3} (table 4).

Table 4

D [m^2/s]	$\dot{Q}$ (10 sec)	$\dot{Q}$ (100 sec)	$\dot{Q}$ (1000 sec)
10^{-19}	-1.8×10^{-3}	-5.7×10^{-3}	-1.8×10^{-2}
10^{-18}	-0.057	-0.18	-
10^{-17}	-1.8	-	-

Therefore, for $D\approx10^{-19}$ m^2/s, the level of heat output is nearly undetectable in the DSC, which requires a signal on the order of 0.1 mW or greater. Unless the value of D were at least two orders of magnitude larger than the estimate (i.e., about 10^{-17} m^2/s), the signal will be close to the noise level of the DSC. In the isothermal traces, the large initial instrument transient further obscures observation of the reaction. Indeed, some reports have confused the transient signal with a monotonically decreasing signal, leading to the incorrect conclusion that grain growth of fine crystallites is occurring.

For completeness the potential should be considered for a large nucleation time lag; this effect would produce most of the nuclei near the end of the isothermal hold and would result in an estimate of D that is much too low. The time lag may be expressed to within an order of magnitude by $\tau\approx4(r^*)^2/\pi^2D$ [83KEL], where r^* is the radius of a critical nucleus. With $r^*\approx0.7$ nm and a lower bound estimate of $D\approx9\times10^{-20}$ m^2/s, $\tau\approx2$ seconds and therefore nucleation is at steady state during the isothermal treatments; note that higher estimates of D would result in a smaller value of τ and a more rapid approach to steady state kinetics. Since the nanocrystal size distribution remained narrow after the 245°C treatments, it is likely that early saturation of heterogeneous sites occurred and few nanocrystals nucleated during the isothermal treatments below 270°C; thus the assumption that all of the particles started growing at nearly the same time is reasonable.

The observance of the distinctive peak in the continuous heating trace and the increase in observed nanocrystal site density indicates a change in kinetic behavior. The increase in site density from about 10^{21} to 10^{22}-10^{23} m^{-3} and nanocrystal growth are consistent with an increase in diffusivity above the glass transition. However, the Al nanocrystal growth is still inhibited due to solute diffusion-field impingement, which becomes the rate-limiting factor in the growth kinetics for high particle densities (10^{22}-10^{23} m^{-3}) or for long holding times at the low particle densities

observed at lower temperatures (T<270°C). For a more complete analysis, Ham has developed an expression for time-dependent particle growth under the condition of diffusion-field impingement [58HAM]. The application of this analysis in combination with equation (7) yields an expression for the expected $\dot{Q}(t)$. This approach, together with an increase in N_v from 10^{21} to 10^{22} m^{-3} and D from $9x10^{-20}$ to $6x10^{-18}$ m^2/s, allows for a good accounting of the continuous heating primary crystallization peak (figure 31). To illustrate further the importance of impingement, the diffusion fields of two adjacent particles were each calculated by assuming growth into an infinite matrix (figure 34). Note that with conditions similar to those found to fit the exotherm in figure 31, ($D \approx 6x10^{-18}$ m^2/s and a particle spacing of 50 nm, which corresponds to $N_v \approx 8x10^{21}$ m^{-3}), diffusion field impingement begins at about 10 seconds and becomes significant at 20 seconds. Similar behavior is expected for the first crystallization peak for Al-Sm, although additional kinetic measurements are required for modeling the exotherm for the AlSm trace.

The analysis has been based on the assumption that the diffusion coefficient does not change with composition. Some reports have suggested that the inhibited growth of the nanocrystals is due to solute buildup. While composition gradient effects may indeed be important, especially for intermetallic formation [95YAV], the analysis presented in this work shows that with typical D values for amorphous alloys [93GRE], diffusion field impingement alone can account for the observed primary crystallization behavior. Thus, the key feature in the kinetic stabilization of nanocrystals developed during devitrification is a high initial nucleation density.

The origin and control of the nucleation process involved in the development of Al nanocrystals is an important basic issue in understanding the undercooling and crystallization kinetics in amorphous Al alloys. In this regard there have been several structural studies which indicate the existence of local short range ordering that may enhance glass forming ability [90HSI, 91HSI]. Indeed, it appears that this effect may be a consequence of the relatively large atomic size difference between Al and the rare-earth and transition metal components. For example, the observations suggest that Fe atoms associate with Al to form $FeAl_6$ octahedra in the melt [90HSI]. From these observations Egami has developed a useful model of glass formation based upon atomic size misfit which has a wide application [84EGA, 93EGA]. If preferential grouping of certain components does occur in the undercooled melt and glass then an influence of this association on diffusivity, heat capacity and other properties should be observable. There is some suggestion of anomalous volume behavior for Al-Fe solutions [90TUR] , but further work is needed to examine this feature and whether the proposed local structure has a significant influence on the nucleation of Al nanocrystals.

It is now possible to identify the events that contribute to the development of primary

nanocrystalline Al in Al-TM-RE alloys (Fig. 35). In the as-solidified samples both x-ray diffraction and TEM observation indicate an amorphous structure. However, this evidence does not exclude the possibility of quenched-in nuclei with sizes below the resolution limit of observation. After 30 seconds at low temperature, (200°C< Temperature < T1=276°C for Al-7Y-5Fe) there is no observable change in the as-solidified microstructure, but there may be a small change in size of possible quenched-in nuclei that is not detectable by TEM. After 30 seconds at higher temperatures, (T1=276°C < Temperature < T2=375°C for Al-7Y-5Fe) a dispersion of 10^{22} - 10^{23} m^{-3} approximately 20 nm particles with a narrow size distribution develops. Based on our kinetics analysis diffusion field impingement between neighboring Al nanocrystals has occurred at this point. After 10 minutes at low temperature, (200°C< Temperature < T1=276°C for Al-7Y-5Fe) a dispersion of 10^{21} m^{-3} particles with diameters of about 20-25 nm and a narrow size distribution develops. For the sample that was held for 10 minutes at higher temperatures, (T1=276°C < Temperature < T2=375°C for Al-7Y-5Fe) there is little change in the microstructure due to the kinetic stabilization associated with diffusion field impingement. Finally, after longer times (100 minutes) at low temperatures the dispersion of 10^{21} m^{-3} particles grows to 40-60 nm in diameter. Based upon our kinetics analysis diffusion field impingement develops at this stage. For the sample held at higher temperatures (276°C < Temperature < T2=375°C) for long times there is little change in the microstructure as before. However, for temperatures close to T2 the onset of intermediate phase nucleation is more likely.

The issue of diffusion field impingement will affect the current understanding of alloy design in that the modification of the nucleant density should be the primary focus in limiting nanocrystal growth. For very high particle densities, diffusion field impingement will occur rapidly due to reduced length scales, and the growth of the Al phase will be rapidly arrested. The thermodynamic model has shown that the liquid is more exothermic than the solid phase; the stabilization of the liquid phase enhances glass formation, but also diminishes the driving force for primary fcc formation (while increasing the driving force for intermetallic formation). Therefore a minimum level of transition metal additions is necessary to promote easy glass formation, but excess levels will prevent fcc formation in favor of intermetallic phases. A further examination of these alloy design concepts and the associated undercooling and kinetic behavior are clearly important and is intended for study in the proposed program.

II.C Analysis of Kinetic Competition

An examination of solidification reactions and undercooled liquids can provide a basis for the prediction of microstructural transitions that can be applied to guide alloy design and processing to yield an optimization of the preferred microstructure. In order to illustrate some of

the aspects of this developing area a few selected highlights will be presented from the current work to indicate some of the numerous possible pathways for microstructural development and the opportunities for the analysis of the kinetic competition.

II.C.1 Microstructural Transitions in Undercooled Powders

There been a number of previous studies of rapid solidification processing of alloy steel samples where the expectations of accelerated solidification in terms of refinement of microstructural scale, the suppression of segregation and the absence of carbon participates have been demonstrated [78RAY, 82FIS]. An analysis has not developed to quantify the observed trends in microstructural morphology, size scale and phase evolution during solidification. In the current work a more detailed examination of the dendrite-cell transition and the role of powder size as a controlling process parameter and the phase selection have been conducted [94SRI].

The trend and dendrite arm spacing and cell size with powder diameter in Fig. 36 was similar for the two alloy tool steel compositions examined and clearly demonstrates that microstructural homogeneity can be enhanced significantly by particle size refinement. Over the range of powder size that was examined, a dendritic morphology dominated the larger particles and was superseded by a cellular structure in the finer powders. It is also of interest that within the range where both dendritic and cellular structures were observed in separate particles the cellular morphology revealed a consistently finer spacing.

Powder size refinement has been shown to yield enhanced undercooling due to isolation of active nucleants [87PERc]. For a random distribution of nucleants and monodisperse powders, the fraction of powders without nucleants x can often be described by a Poisson distribution as: $\exp[-(d/d_o)^n]$ where d is the powder diameter, d_o is a constant related to the nucleant size and n is related to the controlling nucleation mechanism. The results of Fig. 36 with x given by the cellular fraction yield n values near 2 which can be modeled by a heterogeneous nucleation process [87PERc]. From this analysis it is likely that the operation of nucleant isolation during atomization provides for an increased undercooling with powder size refinement. Moreover, a refined cellular morphology is promoted by increasing undercooling.

The analysis of microstructural refinement during rapid solidification is an area of continuing interest [86KUR, 90BIL]. The morphological transition from dendrites to cells with decreasing powder size does reveal some important features of solidification kinetics. In the usual solidification treatment where external heat flow controls the solidification front movement and morphology, the first stage of planar interface instability is manifested by a cellular pattern which

then evolves into a dendritic array with increasing velocity and undercooling [93ALL]. During high undercooling solidification as the interface velocity approaches the limit of absolute stability, the dendritic array is expected to become refined and to develop into a fine cellular pattern which in turn develops into a planar front [86KUR, 90BIL]. The observations of this reverse dendrite to cell transition with a refinement of microstructural size scale as the powder size decreases is consistent with an increase in interface velocity or undercooling as indicated by the analysis of microstructural abundance. The features of the morphological transition have been observed in a model transparent material system and have been analyzed theoretically [90BIL] where it has been shown that across the transition the resultant cell spacings will be finer than the dendrite spacings. However, there do not appear to be comparable observations reported in previous powder solidification studies. Of course, the quantification of microstructural size and morphology as presented is necessary to identify the transition and such measurements are not yet reported usually.

II.C.2 Phase Selection Competition

Both metallographic and x-ray diffraction analysis of the tool steel powders as a function of size indicated that the samples consist of primarily bcc and fcc phases. It was observed that the relative x-ray peak intensities and areas under the peak of the fcc (111) and bcc (110) reflections change with powder size. From this consideration the parameter p defined as

$$P = \frac{I_{FCC(111)}}{I_{BCC(110)} + I_{FCC(111)}} x100 \qquad (9)$$

provides a measure to judge the fcc phase content as a function of particle size as shown in Fig. 37. Parameter P is seen to increase initially with powder size, but then decrease above a critical particle size which is approximately 40 μm. This trend suggests that in the larger particle sizes austenite may be transforming to bcc martensite. In addition, the intermediate and finer size ranges exhibited either a dual phase microstructure consisting of both bcc and fcc phases or single phase bcc or fcc occurring separately in different particles.

In order to address the origin of austenite and ferrite in the solidified powders a set of schematic temperature transformation curves occurs can be examined as shown in Fig. 38 which depict the possible reaction pathways immediately prior and after solidification. Large particles, P_1 cool slowly at $\dot{T}_1$ and exhibit a relatively low undercooling level so that nucleation and growth of austenite occurs from the melt giving rise to a single phase austenite microstructure with a segregated microstructural morphology. The fine powder particles, P_3 at less than approximately

40 μm exhibit a large undercooling and a relatively high cooling rate $\dot{T}_3$ that may yield nucleation of ferrite from the liquid in at least some fraction of the powder population. In the intermediate particles size range P_2 or P_2' with the cooling rate $\dot{T}_2$, the thermal path could intersect the austenite or ferrite curve. In this restricted size range nucleation of the austenite phase or ferrite phase could occur in one region of the droplet while the other region, still liquid, can develop the ferrite or austenite phase during the kinetic competition that ensues between the two phases. In other words, following nucleation of the first phase, the recalescence that occurs decreases the driving force for growth of that initial nucleated phase which allows for the possibility of the development of another phase in the remaining liquid portion of the droplet. Alternatively, the bcc phase may nucleate from the melt and transform to austenite in the solid state. Therefore, depending on recalescence effects, external cooling rate and solid state reactions, fine particles may solidify either as a mixture of ferrite and austenite phases or as single phase. The observed room temperature microstructure can be understood on the basis of a conceptional diagram as shown in Fig. 39. In the absence of a martensite transformation the amount of austenite would have steadily increased with powder size as indicated by the dotted line and the amount of ferrite would have decreased correspondingly as reported in previous studies. However, the intervention of an austenite/martensite transformation above a certain particle size leads to a decrease in the austenite content in larger particles, thus the small particles exhibited of ferrite structure. The austenite content increases at the expense of ferrite up to a critical particle size above which the microstructure develops which can contain all three constituents namely ferrite, austenite and martensitic phases. With the main points of the phase evolution identified, further work can be pursued to quantify the respective kinetics in specific particle size ranges in order to optimize the and preferred microstructural yield.

II.C.3 Growth Rate Limitations

An important result of kinetic competition is the development of kinetic transitions which are represented by the appearance of altered microstructural morphologies as well as the change from one product structure to another. They can develop as the result of competitive kinetics between different morphologies, the competitive nucleation between different product structures and even with a competition involving an initial growth and subsequent nucleation reaction. The first two cases are commonly known with many examples, but the last type has not received an extensive study.

One example where the conditions can be controlled carefully occurs during the surface melting. Usually because of epitaxial regrowth that develops from an unmelted substrate, a

growth kinetic analysis can be used to interpret the resolidification microstructure due to surface melting. However, for rapid beam scan velocities the solidification due to regrowth may lag behind the liquidus isotherm and allow for the nucleation of new grains within the undercooled liquid. A clear example is shown in Fig. 10 for an Al-26 wt%Si alloy [92PIE]. At slow regrowth velocities below 8 mm/sec a coupled eutectic growth structure develops within the regrowth microstructure. However, the eutectic morphology has a maximum regrowth velocity. As this limit is exceeded the liquid in front of the advancing solidification front develops increasing undercooling that allows for the nucleation of Si crystals. As the regrowth velocity increases the volume density of Si crystals increases substantially (Fig. 40) which is a signature of the onset of a nucleation controlled reaction. The volume density shown in Fig. 40 has been determined by a stereological analysis of the measured aerial particle density. The continuous nature of the variation of Si particle density with solidification rate suggests the continuous activation of internal nucleation sites, N_v, with increasing undercooling. The formulation of a nucleation kinetic model to analyze the observations on Al-Si alloys provides a useful illustration on the advances in analysis capability during the current program [96GRE]. The usual approach in nucleation calculations is to assign the mechanism (i.e. either homogeneous or heterogeneous) based on somewhat indirect evidence and then to carry out the evaluation of nucleation temperatures or rates based upon reasonable assignments for the various unknown kinetic parameters. While the results of this approach usually provide for a good accounting of the observed behavior, the uniqueness of the calculation solution is unclear. For example, how many different but also reasonable sets of kinetic parameter values may be used to obtain solutions? In order to address this issue a new approach to nucleation kinetics analysis has been developed in which a sensitivity analysis is incorporated in the calculation in order to provide some measure of the reliability of the solution.

For the case of Al-Si alloys, the nucleation kinetics model is based on a number of clearly established conditions. First, since the nucleation onset developed as a result of a growth rate limitation, a growth rate analysis provided for the initial nucleation temperature [92PIE]. From the well controlled laser processing conditions and the known growth behavior, steady state nucleation could be used for analysis. Also, from observations of the particle density of 4.5×10^{16} m^{-3}, it is evident that heterogeneous nucleation is operational. Moreover, from the continuous variation in Si particle density with laser scan velocity or nucleation time it was possible to define a nucleant site density function as given by [96GRE]

$$N_v = N_v^o \, exp(\beta \Delta T) \qquad (10)$$

where N_v^o is obtained as a base line nucleant level from droplet nucleation oscillation observations to be of the order of 10^{13} m^{-3} and β is a constant. The main calculation is based on the heterogeneous nucleation frequency as given by Eq. 2 where the prefactor term for a volume dependent heterogeneous nucleation can be expressed as

$$\Omega_v = \left[\frac{2D_L}{V_L}\left(\frac{\sigma}{kT}\right)^{1/2}[f(\theta)]^{1/6}\right]\left[A_p N_v\right] z(1-f_s) \qquad (11)$$

where V_L is the atomic volume in the liquid, A_p is a surface area per nucleant, Z is the Zeldovich non-equilibrium factor and f_s is the local volume fraction in a solid. For the conditions of interest Z is approximately .02 and for the early transformation period the term (1-f_s) is small.

To complete the calculation, the particle density and growth velocity provide an estimate of the time available for nucleation, the existing thermodynamic models for the Al-Si system allow for the evaluation of driving free energy [84MUR] and in this particle system separate measurements of the interfacial energy were available for use [85GUN]. For continuous cooling conditions the condition

$$Jvt > k(T_n) \qquad (12)$$

where $K(T_n)$ is about 50 for Al-Si alloys is used to establish the onset of nucleation [87PERc]. Knowing the parameter values based on the initial onset nucleation temperature allows the remaining nucleation conditions to be evaluated through the kinetics model.

The experimental data available did not allow for a unique solution to the nucleation kinetics problem. There are four unknown parameters A_p N_v^o β and $f(\theta)$ which can only be estimated. Of the four parameters the two involving β and $f(\theta)$ are most important since these appear in an exponential term. Estimates of β and $f(\theta)$ were based on several conditions. For example they must be large enough to be consistent with the observed number of silicon particles. Also these parameters must not be so large that their values predict the number of catalytic particles larger than that allowed by the total number of impurity atoms in the system. These bounds are illustrated in Fig. 41 as 1 and 2. There are other bounding limits as shown in Fig. 42 that may be established based on growth rate behavior for the eutectic so that a domain may be determined for the possible values of β and $f(\theta)$. The value of $f(\theta)$ is bounded by the bounds established on β and these in turn establish limits on the prefactor and the nucleation barrier as shown in Fig. 42. Conservative estimates of a number of other parameters including particle density and diffusivity values provide a domain of allowed values for the nucleation barrier and

prefactor. With this conservative approach it is possible to extend the analysis to other compositions as shown in Fig. 42 where there is good agreement between the established bounds and the observed nucleation behavior at other alloy compositions. While the full analysis [96GRE] includes a more detailed consideration of the assessments used to establish each of the bounds, the highlights presented here allow for a reasonable appreciation of the type of approach developed and its value in terms of making conservative evaluations of nucleation kinetics behavior which have some reliability. With this analysis method one can extend the conclusions to develop a process map to allow for some prediction of the phase selection and microstructural morphology under various processing conditions. The analysis based on the nucleation kinetics model allows for the development of a process map including the eutectic to primary silicon transition as shown in Fig. 43. The line corresponding to this transition has been shown with a negative slope since it is expected that the eutectic mode of solidification will be favored at slow scan speeds. A line separating primary silicon and primary α-Al phase regions must also be present. This line has been included on the process map for illustration purposes only, since no information is available at present regarding the slope of this line. Different experimental conditions will shift the transition line shown in plot somewhat, however the basic form of the map should remain constant for surface melting conditions.

II.D Dispersed Phase Catalysis of Liquid Droplets

The nucleation of a solid on an energetically favorable surface present within a liquid can ultimately control the solidification microstructure and interrelated physical and mechanical properties of many materials. By examining the solidification responses generated from liquids containing a variety of identifiable catalytic sites such as primary phases or secondary dispersed particle additions it is possible to modify and control the solidification microstructure by altering the heterogeneous nucleation response. In order to promote a given solidification pathway by nucleation on an intended catalyst in addition to conducting a meaningful assessment concerning actual catalytic potency of a specified agent, it is essential that all background nucleation sites more potent than the intended agent be removed or isolated from the sample. Based upon past and current experience, the DET is well suited for this purpose and can be used effectively to study heterogeneous nucleation responses generated through primary phase catalysis as illustrated by the current work involving cast iron alloy compositions.

In current research concerning nucleation catalysis this background is being used as a basis for the examination of systems in which nucleation of a solid is produced through particle agents that are introduced into a melt. The addition of dispersed particle catalysis has wide commercial application as grain refining agents and as strengthening agents in composite materials. In order

to examine the factors that influence effective nucleation in systems which rely upon the use of dispersed particle additions, the DET was modified to accommodate for the production of droplets containing dispersed particles. To accomplish dispersed particle droplet production, a bulk sample which contains dispersed particles in a mechanically mixed state with aluminum is placed in a molten eutectic salt which acts as a carrier fluid. Upon emulsification, the dispersed particle nucleants are incorporated into many droplets in contact with the Al liquid phase. A high speed rotating agitator generates a fine dispersion of droplets containing dispersed particles within the carrier fluid. Following emulsification and freezing of the droplets, the solidified salt mixture is dissolved in distilled water and the emulsified powder is prepared by filtration and sorted according to size.

The successful application of the DET to study the influence of incorporated particles on a nucleation catalysis and solidification microstructure development has been extended to establish a new capability to examine a variety of dispersed particle types in Al-based matrices such as those of interest in metal-matrix composites. For the purpose of studying how refractory reinforcement particles affect the solidification, particulate such as nitrides (i.e. AlN, Si_3N_4, TiN) has been incorporated it into aluminum by cold rolling a sandwich of aluminum of a thin layer of compound particles spread inside the sandwich. The sandwich is rolled and folded several times to promote intimate contact between the particles and fresh aluminum surface. Rolled material is then processed by the droplet emulsion technique to obtain droplets with incorporated particulate. The incorporation of particulate has been confirmed by both x-ray diffraction and metallographic (BSI-SEM) examination. The differential thermal analysis system used for this work was improved to allow for more sensitive measurements. Analysis of individual Al droplets with sizes below 100 microns is now possible. With this system the thermal history of individual droplets can be obtained and used to study the catalytic effects of incorporated particulates on solidification; especially for particles that may react with the melt. For example, metallographic evidence for particle incorporation is shown in Fig. 44 for Si_3N_4 and Al. The associated DTA thermograms as shown in Fig. 45a and b reveal a major nucleation onset, at about 585°C which is related to uncatalyzed Al droplets and a broad exotherm at higher temperatures related to the catalyzed droplet population. The effect of droplet size on the uncatalyzed exotherm is evident in Fig. 45b, but the catalyzed nucleation exotherm is influenced by particle size in only a minor way as would be expected due to internal catalysis. In this case the particulate and the Al melt do not appear to undergo extensive reaction although there is some evidence for the development of an AlN phase in the preliminary examination. A more reactive system is that of Al and TiN. As shown in Fig. 46a and b, successful incorporation is possible for TiN, but often extensive reaction to yield Al_3Ti based on x-ray diffraction study is observed. As shown in Fig. 46a in some cases

little or no reactivity with the melt is observed for incorporated particles. Again the DTA evidence from such a droplet population shows both catalyzed and uncatalyzed exotherms. For the TiN reaction, nucleation initiates very close to the melting point for aluminum as expected for the Al_3Ti reaction product, but the uncatalyzed exotherm is unaffected.

The initial efforts on composite Al droplets are continuing, but the current capability provides the essential experimental background to pursue a systematic investigation of particle/melt interaction and solidification microstructure evolution in Al alloy metal-matrix composite systems. Indeed, the preliminary work has shown that there is some variation in the degree reactivity between reinforcement particles and the melt. For Al/TiN with identical histories large differences in reactivity have been observed. With the averaging behavior of the usual droplet population sample further information on the details of the undercooling response for reactive and unreactive droplets is obscured. With the newly developed single droplet method, a further understanding of this behavior should be possible and is intended to be one focal point for future work in this area.

III. PUBLICATIONS OF THE CURRENT PROGRAM

During a research program, substantial time intervals often elapse between the completion of a research study, submission of a manuscript, and the final appearance of a paper in print. As a result, the following list gives publications in preparation as well as those in print or in press.

1. "Fundamentals of Solidification at High Rates", W. J. Boettinger and J. H. Perepezko in "Rapidly Solidifying Alloys", ed. HLiebermann (Marcel Dekker, NY) 17 (1993).

2. "Nucleation Kinetics in Undercooled Liquid Metals and Alloys", J. S. Paik and J. H. Perepezko in "Fourth International Symposium on Nucleation and Crystallization in Liquids and Glasses", Ceramic Trans vol. 30, ed. M. C. Weinberg (Amer. Ceramic Soc., Westerville, OH) 13 (1993). (invited)

3. "Solidification of Highly Supercooled Liquid Metals and Alloys", J. H. Perepezko, Jnl. Non-Cryst. Solids 156-158 463 (1993). (invited)

4. "Interface Reactions and Microstructure Control in Composite Processing", J. H. Perepezko, Composite Interfaces 1 463 (1993). (invited)

5. "Solidification Reactions in Undercooled Alloys", J. H. Perepezko, Mat. Sci. and Engr. A179/A180 52 (1994) (invited).

6. "Formation of Metastable $L1_2Al_3Y$ Through Rapid Solidification Processing", J. C. Foley, J. H. Perepezko and D. J. Skinner, Mat. Sci. and Engr. A179/A180 205 (1994).

7. "Nucleation Reactions in Undercooled Liquids", J. H. Perepezko, Mat. Sci. and Engr. A178 105 (1994) (invited).

8. "Supersaturation of the AL_2Y Laves Phase by Rapid Solidification", J. C. Foley, D. J. Thoma and J. H. Perepezko, Met. Trans. 25A 229 (1994).

9. "Microstructure Control in Alloy Steel Powders", K. Sridharan and J. H. Perepezko, Int. Jnl. of Powd. Met. 30 301 (1994).

10. "Rapid Solidification: Metastable Phase Formation", J. H. Perepezko, "Encyclopedia of Advanced Materials", D. Bloor, R. J. Brook, M. C. Flemings and S. Mahajan, eds. (Pergamon Press, NY) 2194 (1994). (invited)

11. "Undercooling and Nucleation During Solidification", J. H. Perepezko and M. J. Uttormark, ISIJ International 35 580 (1995) (invited).

12. "Kinetic Competition in Undercooled Liquid Metals", J. H. Perepezko, Mats. Sci. Forum, 179-181, 701 (1995). (invited)

13. "Formation of Nanocrystalline Al in Al-Y-Fe Amorphous Alloys", J. C. Foley and J. H. Perepezko, Mats. Sci. Forum, 225-227, 323 (1996).

14. "The Devitrification of Al-Y-Fe Amorphous Alloys", J. C. Foley and J. H. Perepezko, J. Non-Cryst. Solids, 205-207, 559 (1996) .

15. "Kinetic Competition in Undercooled Liquid Alloys", J. H. Perepezko and D. R. Allen, Mat. Res. Soc. Symp. Proc., 398, 3 (1996) (invited).

16. "The Development of Nucleation Controlled Microstructures During Laser Treatment of Al-Si Alloys", M. Gremand, D. R. Allen, M. Rappaz and J. H. Perepezko, Acta Mat., 44, 2669 (1996).

17. "Nucleation Controlled Solidification Kinetics", J. H. Perepezko and M. J. Uttormark, Met. and Mat. Trans. A, 27A, 553 (1996) (invited).

18. "Grain Refinement in Melt Spun Ribbons", R. Matsuki and J. H. Perepezko, ISIJ International, 37, 668 (1997).

19. "Heterogeneous Nucleation in Cast Iron", T. Mizoguchi and J. H. Perepezko (in preparation for Met. and Mat. Trans.).

20. "Repeated Nucleation of an Undercooled Al Droplet", M. J. Uttormark, J. W. Zanter and J. H. Perepezko, Jnl. Crystal Growth, 177.

21. "Analysis of Nanocrystal Development in Al-Y-Fe and Al-Sm Glasses", J.C. Foley, D.R. Allen and J.H. Perepezko, Scripta Mat. 35, 655 (1996)

IV. PARTICIPATING SCIENTIFIC PERSONNEL

1. Professor John H. Perepezko, Principal Investigator
2. J.C. Foley, Graduate Student, PhD Metallurgical Engineering May 1997
3. R. Matsuki, Graduate Student, M.S. Metallurgical Engineering May 1994
4. J.W. Zanter, Graduate Student, M.S. Metallurgical Engineering December 1995
5. T. Mizoguchi, Graduate Student, M.S. Metallurgical Engineering May 1996

V. REFERENCES

[50FRA] F.C. Frank, *Proc. Royal Soc.* A, 201, 586, (1950).

[50TUR] D. Turnbull, *J. Appl Phys.*, 21, 804, 1022, (1950).

[50WAN] C.C. Wang and C.S. Smith, *Trans. AIME*, 188, 136 (1950).

[51CIB] A. Cibula, *J. Inst. Met.*, 76, 321 (1950), 80, 11, (1951-1952).

[51CRO] F.A. Crossley and L.F. Mondolfo, *Trans. AIME*, 141, 1143, (1951).

[52CIB] A. Cibula, *Foundry Trade Jnl.*, 93, 695, (1952).

[52TUR] D. Turnbull and B. Vonnegut, *Ind. Eng. Chem.*, 44, 1292, (1952).

[54HUM] M. Humenik Jr. and W.D. Kingery, *J. Amer. Ceram Soc.*, 37, [1], 18, (1954).

[56CEC] R.E. Cech and D. Turnbull, *Trans. AIME*, 206, 124, (1956).

[58HAM] F.S. Ham, *J. Phys. Chem. Solids*, 6, 335, (1958).

[58PIW] E. Piwowarsky, Hochwertiges Gusseisen, 2nd ed., Springer-Verlag, Berlin, (1958).

[61LIF] I.M. Lifshitz and V.V. Slyozov, *J. Phys. Chem. Solids*, 19, 35, (1961).

[61SUN] B.E. Sundquist and L.F. Mondolfo, *Trans. AIME*, 221, 607, (1961).

[61WAG] C. Wagner, *Z. Elektrochem*, 65, 581, (1961).

[64CHA] B, Chalmers, "Principles of Solidification",Wiley, NY (1964).

[64SHI] S.Y Shirashi and R.G. Ward, *Canadian Met. Quarterly*, 3, 117, (1964).

[66BRO] H.D. Brody and M.C. Flemings, *Trans. AIME*, 236, 615, (1966).

[66KAT] T.Z. Kattamis and M.C. Flemings, *Trans. AIME*, 236, 1523, (1966).

[66YAS] G.A. Yasinskaya, *Poroshkovaya Met.*, 7, [43], 53, (1966).

[67KAT] T.Z. Kattamis and M.C. Flemmings, *Trans. AFS*, 75, 191, (1967).

[68CRO] P.B. Crosley, A.W. Douglas, and L.F. Mondolfo, "The Solidification of Metals", Iron and Steel Inst., 10, (1968).

[68HIL] M. Hillert and Subba Rao V.V., "The Solidification of Metals", p. 204, The Iron and Steel Institute, London, (1968).

[68LUX] B. Lux and W. Kurz, in "The Solidification of Metals", The Iron and Steel Institute, London, 193, (1968).

[68NAI] Y.U. Naidich and G.A. Koleschenko, *Poroshkovaya Met.*, 2, 76, (1968).

[68SAM] G.V. Samsonov, A.D. Pansasyuk, and G.K. Kozina, *Sov. Powder Met. and Met. Ceram.*, 11, 874, (1968).

[69TIL] W.A. Tiller and T. Takahashi, *Acta Met.*, 17, 483, (1969).

[69TUR] D. Turnbull, *Contemp. Phys.*, 10, 473, (1969).

[70KAU] L. Kaufman and H. Bernsein, "Computer Calculation of Phase Diagrams", Academic Press, NY, (1970).

[70DAV] I.G. Davies, J.M. Dennis, and A. Hellawell, *Met. Trans.*, 1, 275, (1970).

[70MAR] J.A. Marcantonio and L.F. Mondolfo, *J. Inst. Met.*, 98, 23, (1970).

[70RHE] S.K. Rhee, *J. Amer. Ceram. Soc.*, 53, [7], 386, (1970).

[72ASH] M.F. Ashby, *Acta Met.*, 20, 887, (1972).

[72CIS] J. Cisse, G.F. Bolling, and H.W. Kerr, *J. Cryst. Growth*, B-14, 777, (1972).

[73WOO] D.P. Woodruff, "The Solid-Liquid Interface", Cambridge Univ. Press, London, 25 (1973).

[74BUR] M.H. Burden and J.D. Hunt, *J. of Crystal Growth*, 22, 328, (1974).

[74FLE] M.C. Flemings, "Solidification Processing", McGraw-Hill, NY, 141, (1974).

[75COR] A.J. Cornish, *Met. Sci.*, 9, 477, (1975).

[75MAX] I. Maxwell and A. Hellawell, *Acta Met.*, 23, 895, (1975).

[75MAR] J.A. Marcantonio and L.F. Mondolfo, *Met. Trans.*, 2, 465, (1975).

[75MEY] E. Meyer and L. Rinderer, *J. Crystal Growth*, 28, 199, (1975).

[76JON] G.P. Jones and J.Pearson, *Met. Trans.*, 7B, 223, (1976).

[76MON] L.F. Mondolfo, "Aluminum Alloys: Structure and Properties", TheButterworth Group, Butterworth publishers, Boston Mass., (1976).

[76PAU] J. Paull, J. Ryall and G.W. Delamore, *Scripta Met.*, 10, 845, (1976).

[77JAC] K.A. Jackson and C.E. Miller, *J. Cryst. Growth*, 40, 169, (1977).

[78RAY] J.H. Rayment and B. Cantor, *Metal Science*, 12 156, (1978).

[79HEL] A. Hellawell, "Solidification and Casting of Metals", The Metals Society, 161 (1979).

[79PER] J.H. Perepezko, D.H. Rasmussen, I.E. Anderson and C.R. Loper Jr, "Sheffield Int. Conf. on Solidification and Casting of Metals", Metals Soc., London,169, (1979).

[80CYN] T.W. Cyne and M.H. Robert, *Met. Tech.*, 177 (1980).

[80JON] G.P. Jones, "New Ideas on the Mechanism of Heterogeneous Nucleation in Liquid Aluminum", NPL Report DMA(A) 19, Oct. (1980).

[80GEI] G.H. Geiger and D.R. Poirier, "Transport Phenomena in Metallurgy", ed. M.Cohen, Addison-Wesley Publishing Company, Inc., Reading, MA, (1980).

[80LAC] L.L. Lacy, M.B. Robinson and T.J. Rathz, *J. Crystal Growth*, 51, 47, (1980).

[80PERa] J.H. Perepezko, "Rapid Solidification Processing: Principles and Technologies II", eds. R. Mehrabian, B.H. Kear, and M. Cohen, Claitors Publishing Division, Baton Rouge, LA, 56, (1980).

[80PERb] J.H. Perepezko and I.E. Anderson, "Synthesis and Properties of Metastable Phase", Eds. T.J. Rowland and E.S. Machlin, The Metallurgical Society of the American Institure of Mining, Metallurgical, and Petroleum Engineers,Warrendale, PA, 31, (1980).

[81SAU] R.E. Sanders, Jr., G.J. Hildeman, Air Force Wright Aeronautical Laboratories Technical Report, AFWAL-TR-81-4076 (1981).

[82ARN] L. Arnberg, L. Backerud, and H. Klang, *Met. Tech.*, 9, 1 (1982), 9, 7, (1982).

[82ASH] M.F. Ashby and K.E. Easterling, *Acta Met.*, 30, 1969, (1982).

[82BOE] W.J. Boettinger, "Rapidly Solidified Amorphous and Crystalline Alloys", B.H. Kear, B.C. Giessen and M. Cohen, eds. Elsevier, Amsterdam, 15, (1982).

[82COO] K.P. Cooper, I.E. Anderson and J.H. Perepezko, "Proc. 4th Int. Conf. on Rapidly Quenched Metals", Eds. T Masumoto and K. Suzuki, Japan Inst. Metals, Sendai, 107, (1982).

[82FIS] H.F. Fischmeister, A.D. Ozerskii and L. Olsson, *Powder Met.*, 25, 1, (1982).

[82JON] H. Jones, "Rapid Solidification of Metals and Alloys", Inst. of Metallurgists, London, (1982).

[82LEV] C.G. Levi and R. Mehrabian, *Metall. Trans. A*, 13A, 221, (1982).

[82PERa] J.H. Perepezko and J.S. Paik, "Rapidly Solidified Amorphous and Crystalline Alloys", eds., B. Kear, B.C. Giessen, and M. Cohen, North Holland, NY, 49, (1982).

[82PERb] J.H. Perepezko, and S.E. LeBeau, "Aluminum Transformation Technology and Its Applications", C.A. Pampillow, H. Biloni, and L.F. Mondolfo, Eds., ASM, Metala Park, OH, 309, (1982).

[83KEL] K.F. Kelton, A.L. Greer, and C.V. Thompson, *J. Chem. Phys.*, 79, 6261, (1983).

[83KOB] K.F. Kobayashi, S. Hashimoto, and P. Shingu, *Z. Metallkde.*, 74, 751, (1983).

[83RIC] J.J. Richmond, J.H. Perepezko, S.E. LeBeau and K.P. Cooper, "Rapid Solidification Processing: Principles and Technologies III', Ed. R. Mehrabian, NBS, Washington, DC, 90, (1983).

[83MON] L.F. Mondolfo, "Grain Refinement in Castings and Welds", G.J.Abbaschian and S.A. David, Eds., TMS, 3, (1983).

[83NAI] Y.U. Naidich and Y.N. Chuvashov, *J. Mat. Sci.*, 18, 2071, (1983).

[83NAG] V.K. Nagesh, A.P. Tomisia, and J.A. Pask, *J. Mat. Sci.*, 18, 2173, (1983).

[83PER] J.H. Perepezko and W.J. Boettinger, *Proc. Mat. Res. Soc. Symp.*, 19, 223, (1983).

[84EGA] T. Egami and Y. Waseda, *J. Non-Cryst. Solids*, 64, 113, (1984).

[84MUR] J.L. Murray and A.J. McAlister, *Bull. of Alloy Phase Diagrams*, 5, 74, (1984).

[84KRI] B.P. Krishnan and P.K. Rohatgi, *Met. Tech.*, 11, 41, (1984).

[84PERa] J.H. Perepezko and J.S. Paik, *J. Non-Cryst. Solids*, 61, 113, (1984).

[84PERb] J.H. Perepezko, *Mat. Sci. Eng.*, 65, 125, (1984).

[85ANG] L. Angers, Y. Chen, M.E. Fine, J.R. Weertman and M.S. Zedalis, "AluminumAlloys - Physical and Mechanical Properties",S.K. Das, TMS-AIME, Warrendale PA, 320, (1985).

[85BLA] N. Blake and M.A. Hopkins, *J. Mat. Sci.*, 20, 2861, (1985).

[85BOE] W.J.Boettinger and J.H. Perepezko, in "Rapidly Solidified Crystalline Alloys", S. K. Das, B. H. Kear, and C. M. Adams, Eds., TMS-AIME, Warrendale, PA, 21, (1985).

[85GRA] D.A. Granger, "Practical Aspects of Grain Refining Aluminum Alloy Melt", Laboratory Report 11-1985-01, Aluminum Company of America, (1985).

[85GUN] M. Gündüz and J.O. Hunt, *Acta. Metall.*, 33, 1651, (1985).

[85HEL] A.S. Helle, K.E. Easterling and M.F. Ashby, *Acta Met.*, 33, 2136, (1985).

[85PER] J.H. Perepezko, S.E. LeBeau, B.A. Mueller and G.J. Hildeman, "Rapidly Solidified Powder Al Alloys", Eds. E.A. Starke and M.E. Fine, ASTM-STP 890, Philadelphia, PA, 118, (1985).

[85HOF] M.K. Hoffmeyer, M.S. Thesis, University of Wisconsin-Madison (1985).

[86ELI] D. Eliezer, S.J. Savage, Y.R. Mahajan, and F.H. Froes, *Mat. Res. Soc. Symp. Proc.*, 58, 293, (1986).

[85HEL] A.S. Helle, K.E. Easterling and M.F. Ashby, *Acta Met.*, 33, 2136, (1985).

[86KIR] J.L. Kirby, "Aluminum Alloys-Physical and Mechanical Properties", E.AStarke and T.H. Sanders, Eds., 1, EMAS, West Midlands, U.K., 61, (1986).

[86KUR] W. Kurz, B. Giovanola and R. Trivedi, *Acta Met.*, 34, 823, (1986).

[86LAN] S.L. Langenbeck, R.A. Rainen, et al., Air Force Wright Aeronautical Laboratories Technical Report, AFWAL-TR-86-4027, (May 1986).

[86PER] J. H. Perepezko and W. J. Boettinger, "Surface Alloying by Ion, Electron, and Laser Beams", L.E. Rehn, S.T. Picraux, and H. Wiedersich, Eds., ASM, Metals Park, OH, (1986).

[86SKI] D.J. Skinner, R.L. Rye, D. Raybould, and A.M. Brown, *Scripta Metal.*, 20, 867,

(1986).

[86ZEN] M.S. Zendalis and M.E. Fine, *Met. Trans. A.*, 17A, 2187, (1986).

[87GUZ] M.M. Guzowski, G.K. Sigworth, and D.A. Sentner, *Met. Trans.*, 18A, 603, (1987).

[87LAU] V. Laurent, D. Chatain and N. Eustathopoulos, *J. Mater. Sci.*, 22, 244, (1987).

[87PERa] J.H. Perepezko, D.M. Follstaedt and P.S. Peercy, *Mat. Res. Soc. Sym. Proc.*, 74, 161, (1987).

[87PERb] J.H. Perepezko, J.A. Graves, and B.A. Mueller, "Processing of Structural Metals by Rapid Solidification", F. H.Froes and S. J. Savage, Eds., ASM, Metals Park, OH, 13, (1987).

[87PERc] J.H. Perepezko, B.A. Mueller, and K.O. Ohsaka, "Undercooled Alloy Phases", eds. E.W. Collings and C.C. Koch, TMS-AIME, Warrendale, PA, 289, (1987).

[88ANG] L.M. Angers, D.G. Konitzer, J.L. Murray and W.G. Truckner, "Dispersion Strengthened Aluminum Alloys", eds. Y-W Kim and W.M. Griffith, TMS-AIME, Warrendale, PA, 355, (1988).

[88FOL] D.M. Follstaedt, P.S. Peercy and J.H. Perepezko, *Mat. Res. Soc. Sym. Proc.*, 100, 573, (1988).

[88HE] Y. He, S.J. Poon and G.J. Shiflet, *Science*, 241, 1640, (1988).

[88HOFa] M.K. Hoffmeyer and J.H. Perepezko, *Scripta Met.*, 22, 1143, (1988).

[88HOFb] M.K. Hoffmeyer and J.H. Perepezko, "Light Metals 1989", P.G. Campbell, Ed., TMS, 913, (1988).

[88INO] Akihisa Inoue, Katsumasa Ohtera, An-Pang Tsai and Tsuyoshi Masumoto, *Japenese J. of Appl. Phys.*, 27, L479, (1988).

[88PERa] J. H. Perepezko and D. U. Furrer, in "Dispersion Strengthened Aluminum Alloys", Y-W. Kim and W.M. Griggith, Eds., TMS, Warrendale, PA, 77, (1988).

[88PERb] J.H. Perepezko, "Metals Handbook" 9th Edition, 15, 101, (1988).

[88SAW] R.R. Sawtell and J.W. Morris, Jr., "Exploratory Alloy Development in the System Al-Sc-X", Dispersion Strengthened Aluminum Alloys, p. 409-420 Eds. Y-W. Kim and W.M. Griffith, (1988).

[88SHI] G.J. Shiflet, Y. He and S.J. Poon, *J. Appl. Phys.*, 64, 6863, (1988).

[89HOF] M.K. Hoffmeyer and J.H. Perepezko, *Scripta Met.*, 23, 315, (1989).

[89KUR] W. Kurz and D.J. Fisher, in "Fundamentals of Solidification",Trans Tech, Aedermannsdorf, Switzerland, (1989).

[89PER] J. H. Perepezko and W. P. Allen, "Proc. of the Third International Colloqium on Drops and Bubbles", T. Wang, Ed., Amer. Inst. of Phys., (1989).

[90BIL] B. Billia, H. Jamgotchian and R. Trivedi, *Jnl. Crystal Growth*, 106, 410, (1990).

[90FEC] H. J. Fecht, J. H. Perepezko, M. C. Lee and W. L. Johnson, *J. Appl. Phys.*, 68, 4494,

(1990).

[90HSI] H.Y. Hsieh, B.H. Toby, T. Egami, Y. He, S.H. Poon and G.J. Shiflet, *J. Mater. Res.* 5, 2807, (1990)

[90KIM] Yeong-Hwan Kim, Akihisa Inoue and Tsuyoshi Masumoto, *Materials Trans. JIM*, 31, 747, (1990).

[90TUR] D. Turnbull, *Acta Metall. Mater.*, 38, 243, (1990).

[91BEC] D. Bechet and G. Regazzoni, *Materials Science and Engineering*, A134, 1120, (1991).

[91HSI] H.Y. Hsieh, T. Egami, Y. He, S. J. Poon and G.J. Shiflet, *J. Non-Cryst. Solids*, 135, 248, (1991).

[91KIM] Yeong-Hwan Kim, Akihisa Inoue and Tsuyoshi Masumoto, *Materials Trans. JIM*, 32, 331, (1991).

[92LAV] E.J. Lavernia, J.D. Ayers and T.S. Srivatsan, *Int. Mats. Rev.*, 37, 1, (1992).

[92MOR] A. Mortensen and I. Jin, *Int. Mater. Rev.*, 37 (3), 101, (1992).

[92PER] J.H. Perepezko, in "Thermal Analysis in Metallurgy", ed. by DShull and A. Joshi, Minerals Metals and Materials Society,Warrendale, PA, 121, (1992).

[92PIE] M. Pierantoni, M. Gremaud, P. Magnin, D. Stoll and W. Kurz, *Acta Metall. Mater.*, 40, 1637, (1993).

[92THO] D.J. Thoma and J.H. Perepezko, J. Appl. Phys., 71, 676, (1992).

[93ALL] D.R. Allen, S. Das and J.H. Perepezko, in "Nucleation and Crystallization in Liquids and Glasses", M.C. Weinberg, ed. American Ceramic Society, Westerville, OH, vol 30, 343, (1993).

[93BOE] W.J. Boettinger and J.H. Perepezko, in "Rapidly Solidified Alloys", H.H. Liebermann, ed., Marcel Dekker, NY, 17, (1993).

[93EGA] T. Egami, "Rapidly Solidified Alloys: Processes, Structures, Properties, Applications", ed. H.H. Liebermann, Marcel Dekker, NY, 231, (1993).

[93GRE] A.L. Greer, "Rapidly Solidified Alloys: Processes, Structures, Properties, and Applications", ed. by H.H. Liebermann, Marcel Dekker, NY, 2269, (1993).

[93NAK] K. Nakazato, Y. Kawamura, A.P. Tsai, A. Inoue, *Appl. Phys. Lett.*, 63, 2644, (1993).

[94BAT] L. Battezzati, M. Baricco, P. Schumacher, W.C. Shih, and A.L. Greer, *Mat. Sci. and Eng.*, A179/180, 600, (1994).

[94GRE] A.L. Greer, *Mat. Sci. Eng.*, A179/A180, 41, (1994).

[94KIM] Y.H. Kim, K. Hiraga, A. Inoue and T. Masumoto, and H.H. Jo, *Materials Trans. JIM*, 35, 293, (1991).

[94PER] J.H. Perepezko, "Encyclopedia of Advanced Materials", eds. D. Bloor, R.J. Brook, M.C. Flemings and S. Mahajan, Pergamon Press, NY, 2194, (1994).

[94SRI] K. Sriharan and J.H. Perepezko, *Int. Jnl. Powder Met.*, (1994).

[95HON] K. Hono, Y. Zhang, A. Inoue, and T. Sakurai, *Mat. Trans. JIM*, 36, 909, (1995).

[95YAV] A.R. Yavari and O. Drbohlav, *Mat. Trans. JIM* 36, 896, (1995).

[96ALL] D.R. Allen, J.C. Foley, and J.H. Perepezko, in preparation, (1996).

[96FOLa] J.C. Foley and J.H. Perepezko, *Journal of Non-Crystalline Solids*, 205-207, 559 (1996).

[96FOLb] J.C. Foley, D.R. Allen and J.H. Perepezko, Scripta Mat., 35, 655, (1996).

[96GRE] M. Gremand, D. R. Allen, M. Rappaz and J. H. Perepezko, *Acta Mat.*, in press, (1996).

[96INO] A. Inoue and H. Kimura, "Synthesis and Processing ofNanocrystalline Powder", ed. David L. Bourell, Warrendale, Pennsylvania, 91, (1996).

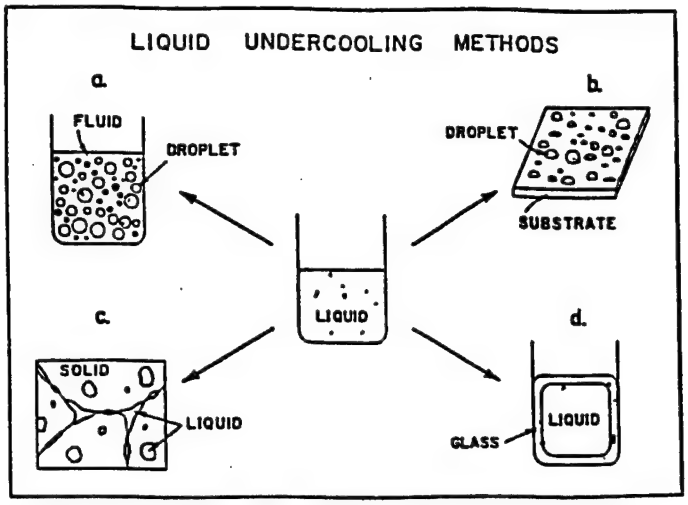

Figure 1. Schematic illustration of different undercooling methods.

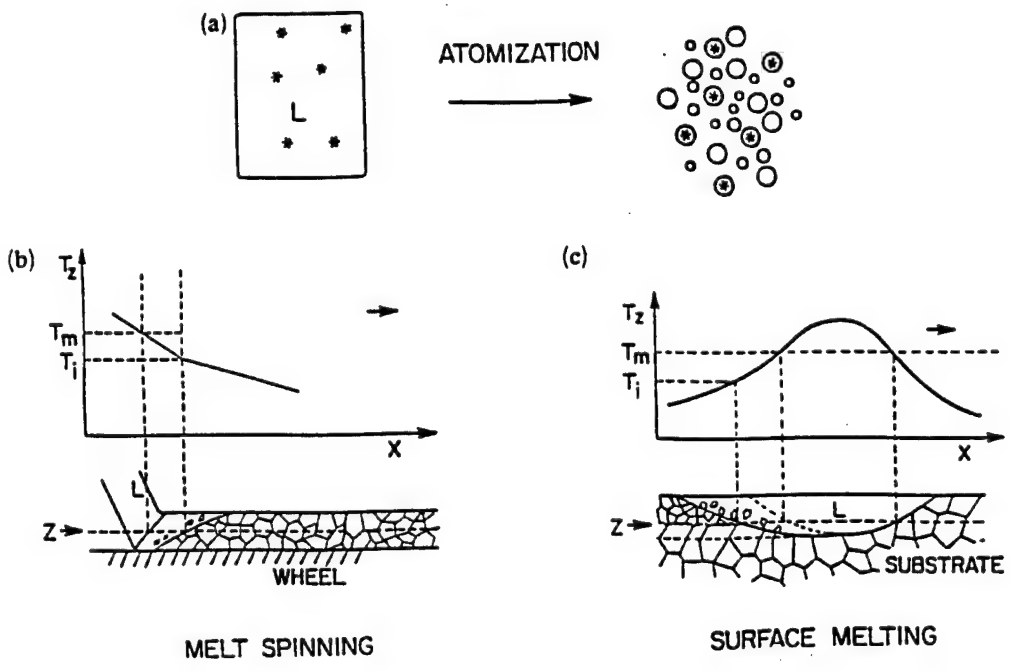

Figure 2. Schematic representation of three common methods of rapid solidification processing involving: (a) powder atomization; (b) melt-spinning; and (c) surface melting of thin layers. In b and c the position of the liquid-solid interface is shown relative to the alloy liquidus for conditions that yield liquid undercooling. Some of the vertical (Z) distances are exaggerated for clarity.

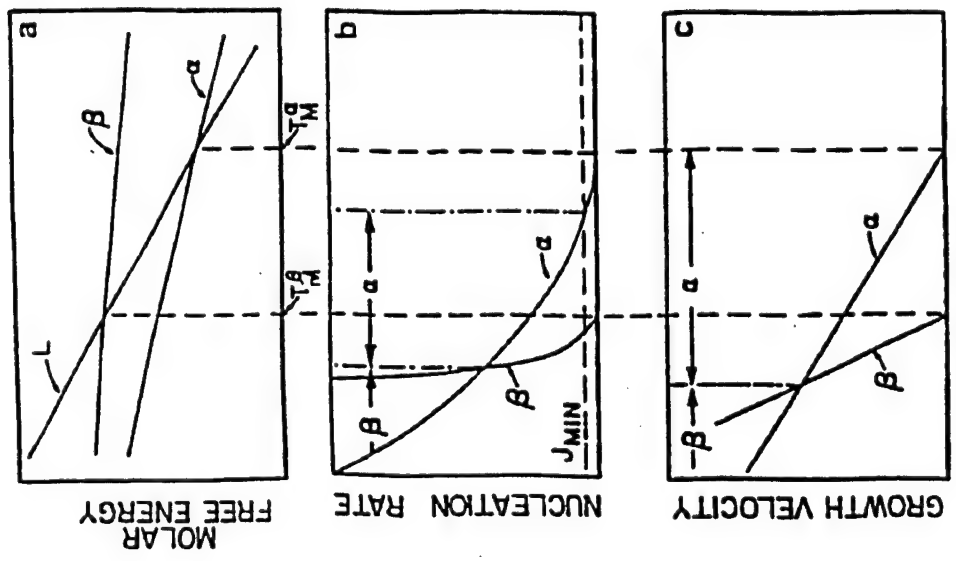

Figure 3. Schematic of competitive phase selection kinetics that favors L → β reaction at low temperature in spite of (a) thermodynamic stability of α. (b) Temperature range for faster nucleation of β. (c) Temperature range for faster growth of β.

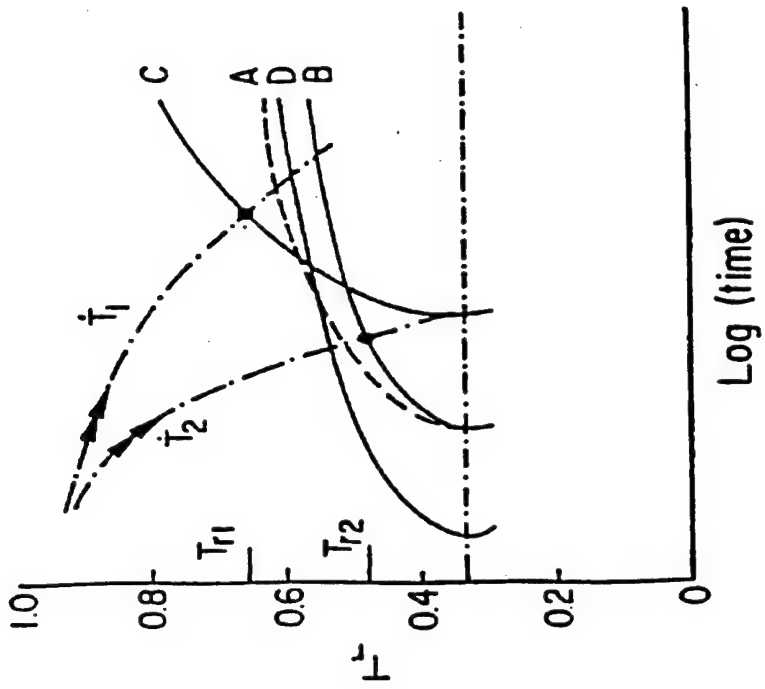

Figure 4. Time-temperature-transformation diagram representing different nucleation kinetics that may occur during continuous cooling of undercooled liquids.

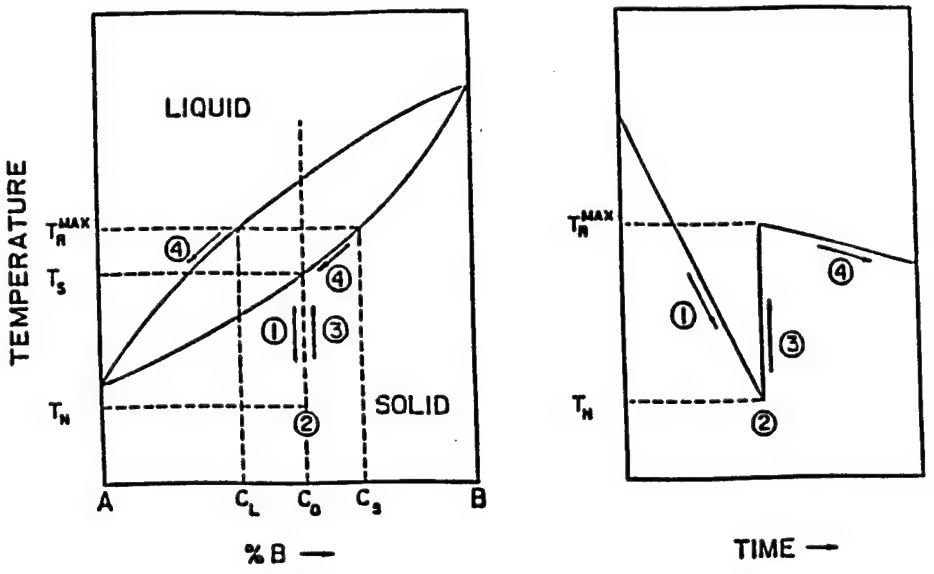

Figure 5. Schematic representation of the recalescence for an isomorphous alloy of composition C_0.

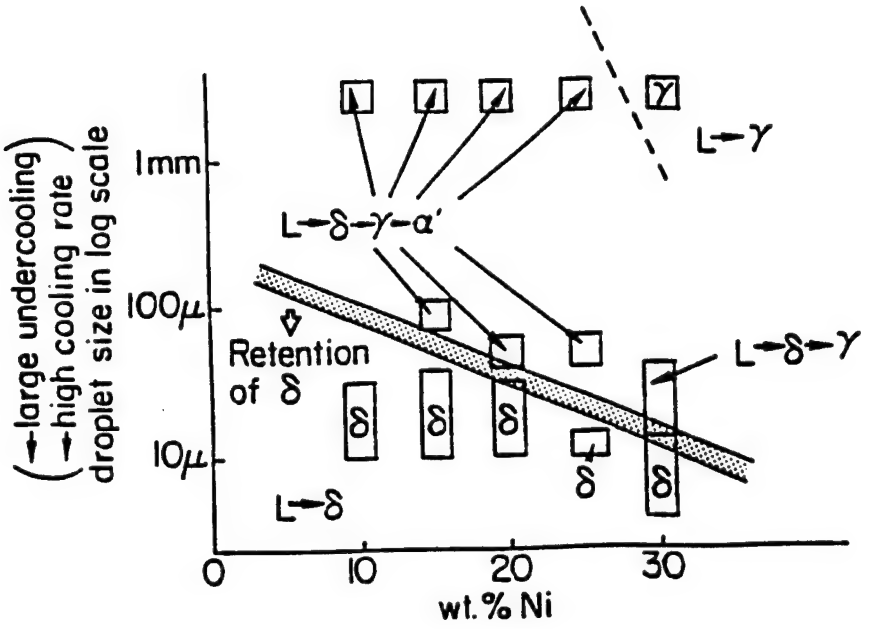

Figure 6. Summary of the structural evolution in the drop tube processing of Fe-Ni alloy processed in a He-2% H_2 environment.

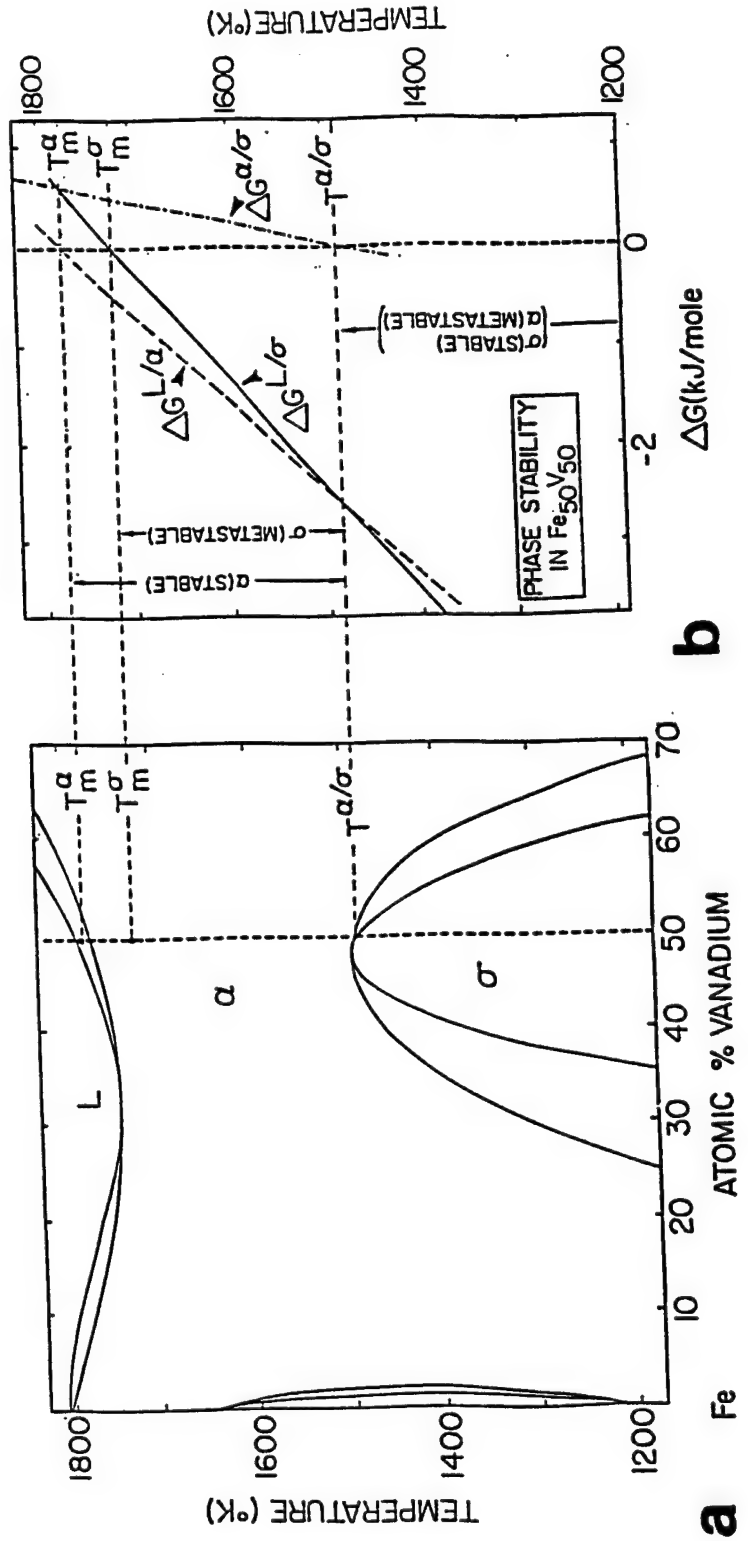

Figure 7. (a) Portion of the Fe-V phase diagram; (b) Calculated thermodynamic phase stabilities for the liquid, α and σ phases in $Fe_{50}V_{50}$.

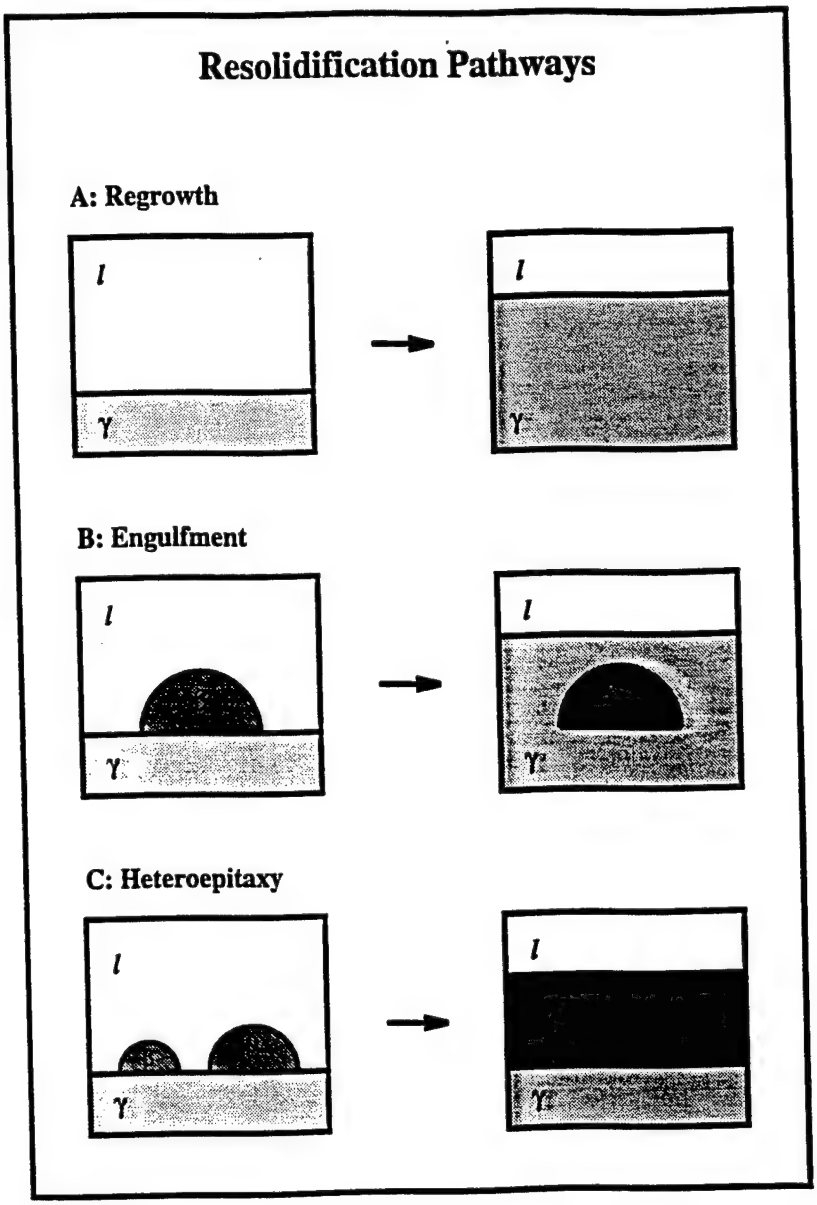

Figure 8. Schematic illustration of different resolidification pathways following rapid surface melting. (a) Regrowth of the original γ substrate. (b) Nucleation of β at the regrowing γ interface which subsequently engulfs β. (c) Nucleation of β at the regrowing γ interface and rapid growth of β over the γ substrate.

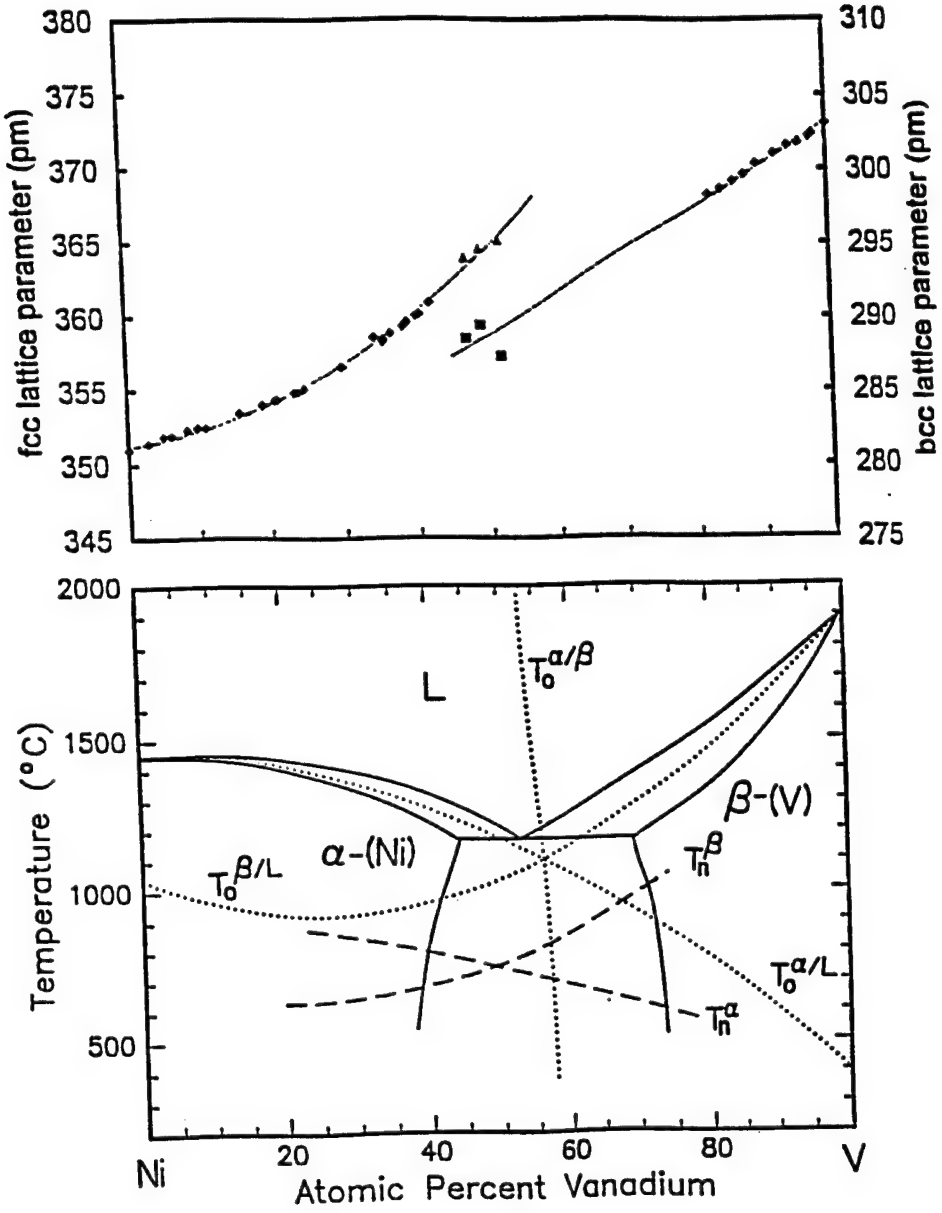

Figure 9. Lattice parameter measurements for FCC, α, and BCC, β, phases in the Ni-V system (top) and calibrated metastable Ni-V phase diagram together with T_0 curves and nucleation temperatures, T_N, for the α and β phases.

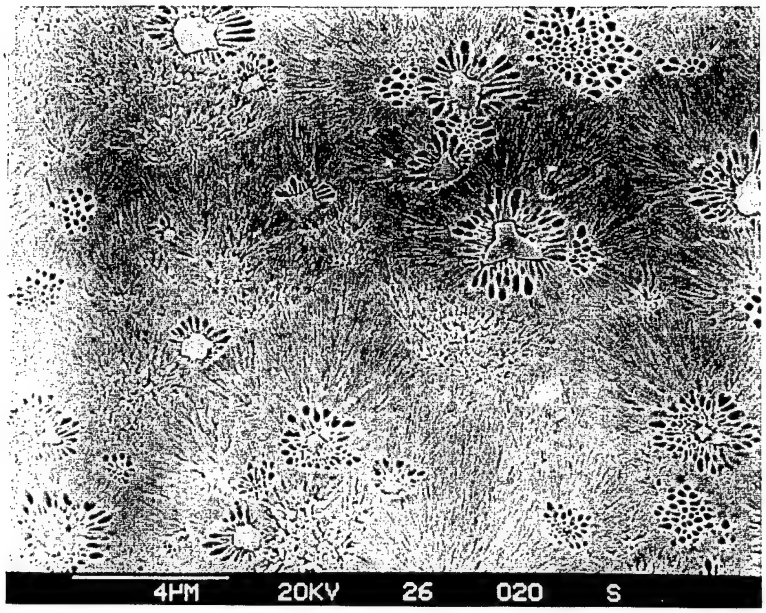

Figure 10. Microstructure of laser treated Al-26wt. % Si alloy melted at a beam speed of 0.1 m/s showing fine Si crystals surrounded by α-Al cells and distributed in an equiaxed eutectic matrix.

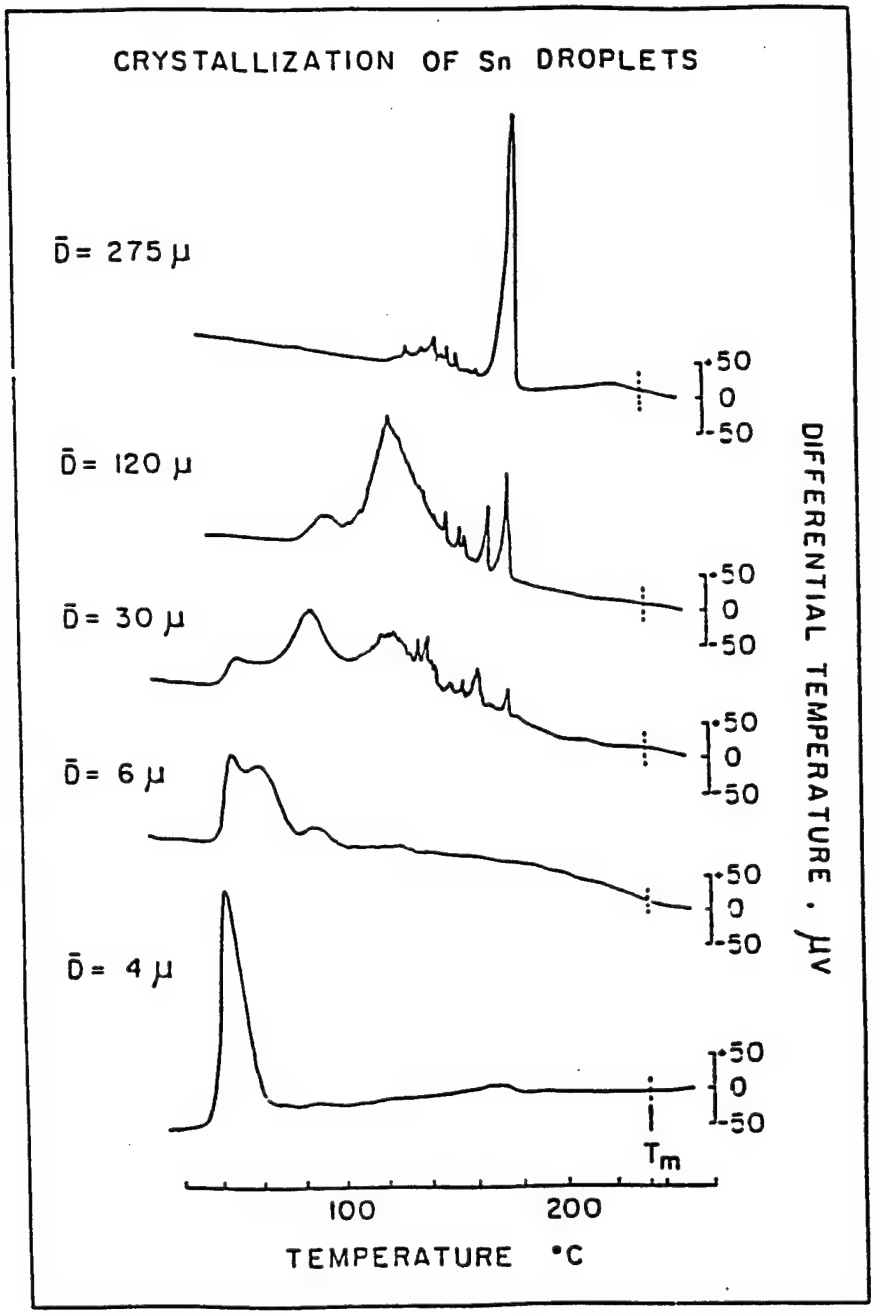

Figure 11. Crystallization of pure Sn droplets at different levels of size refinement.

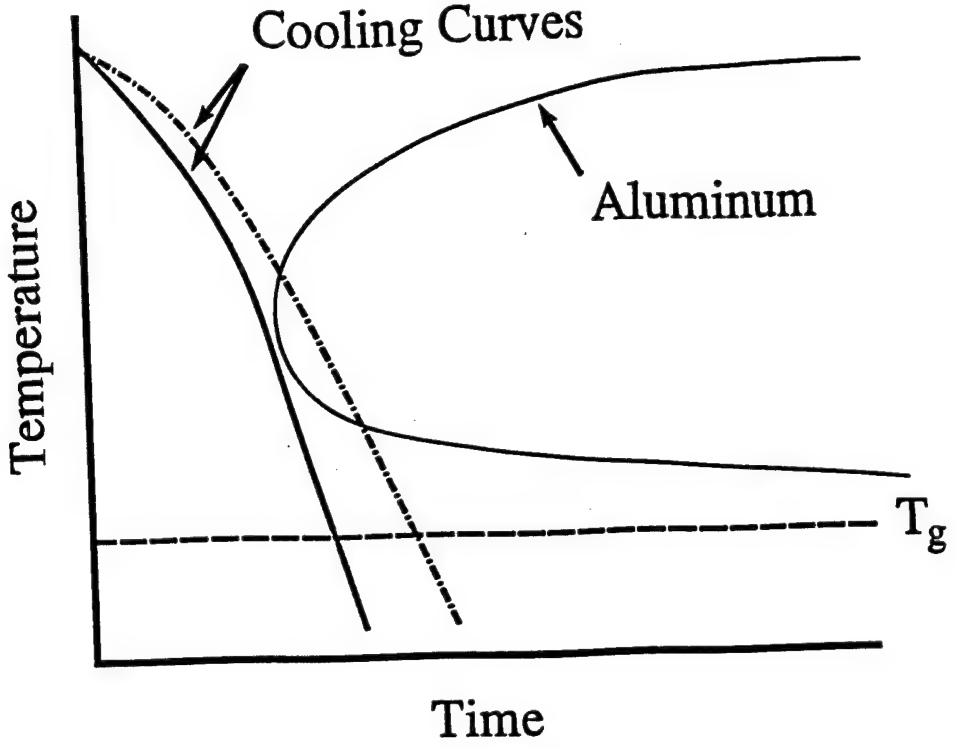

Figure 12. Schematic TTT curve illustrating kinetic competition between glass formation and crystallization for Al-rich glass forming alloys.

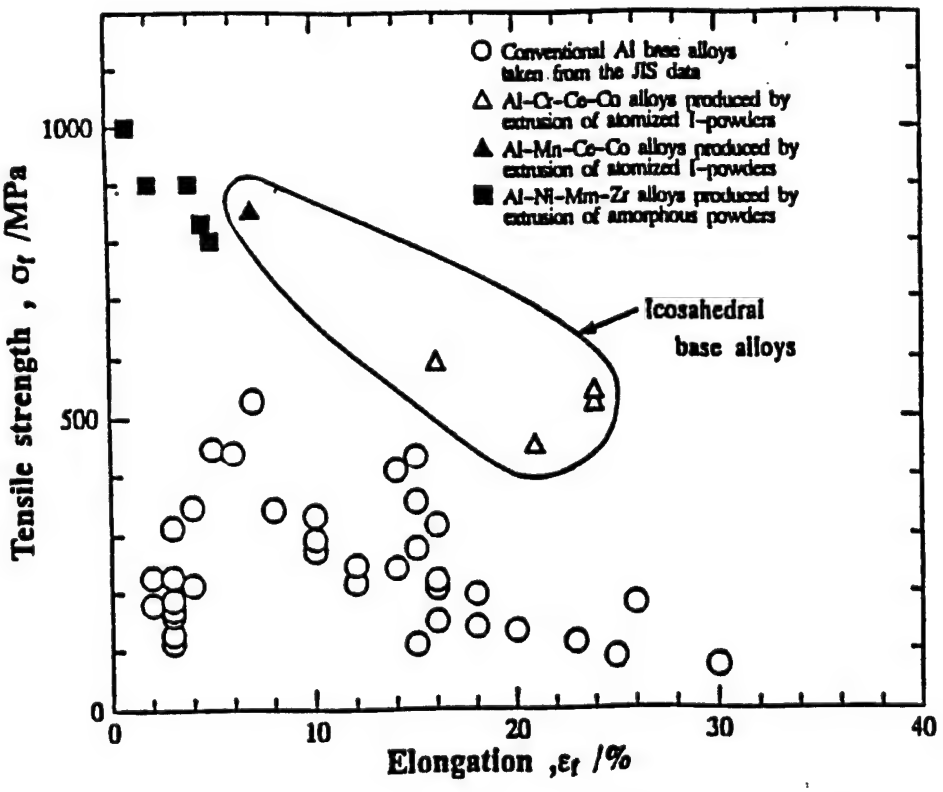

Figure 13. Comparison of σ_f and ε_f for icosahedral based alloys and conventional Al alloys [96INO].

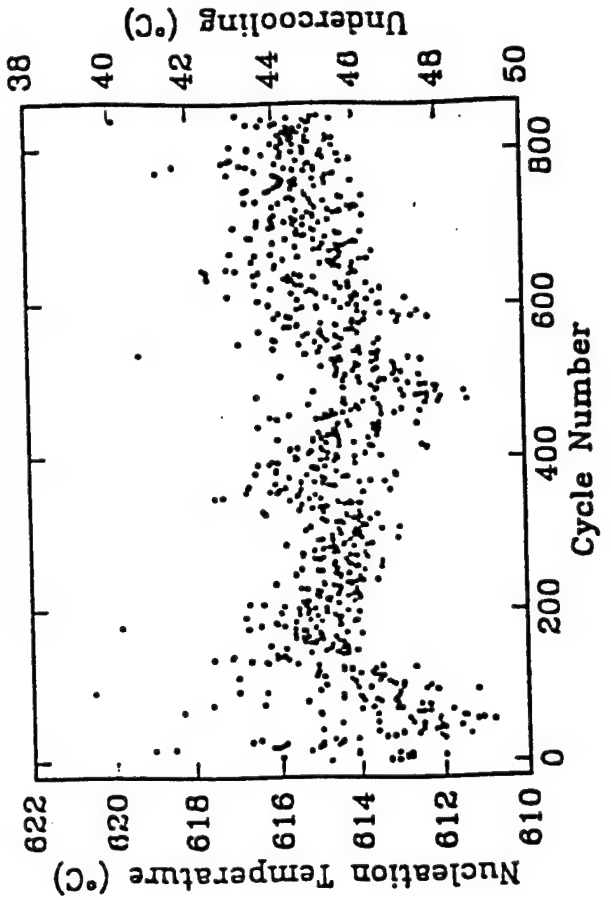

Figure 15. Nucleation temperatures and undercoolings measured for 845 nucleation events.

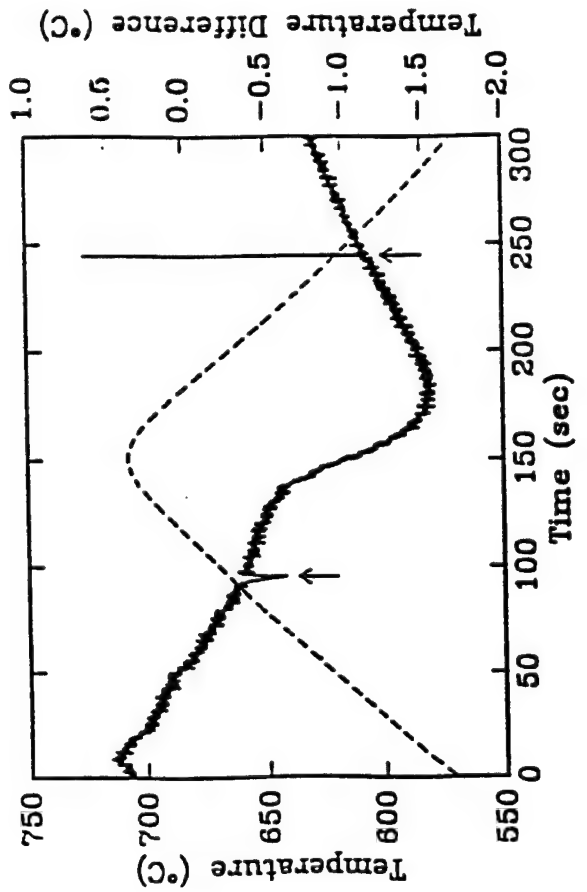

Figure 14. Temeperature measurement of a single nucleation event. Dashed curve indicates reference temperature, solid curve is temperature difference between sample and reference. Arrows indicate melting and freezing transitions.

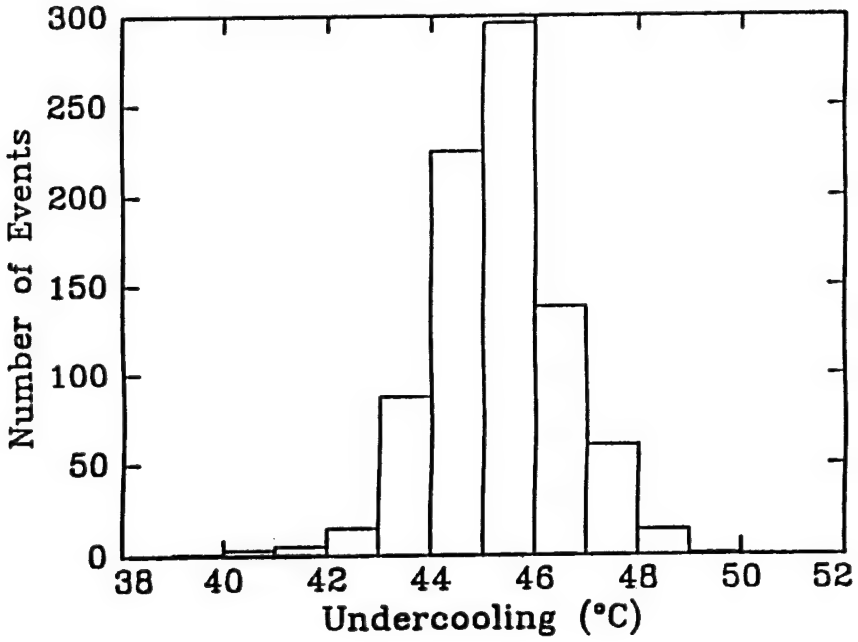

Figure 16. Distribution of nucleation events versus undercooling.

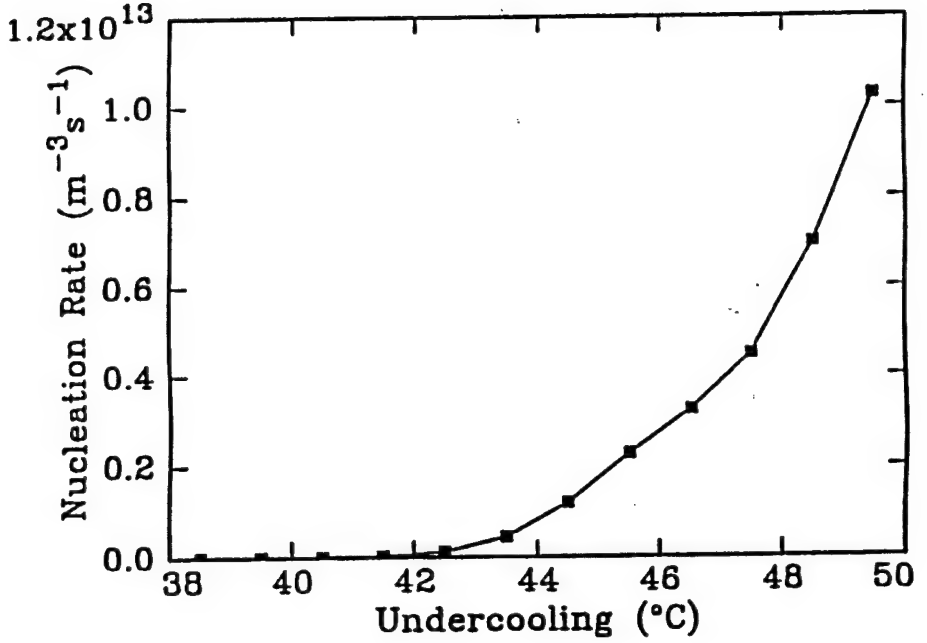

Figure 17. Nucleation rate as a function of undercooling.

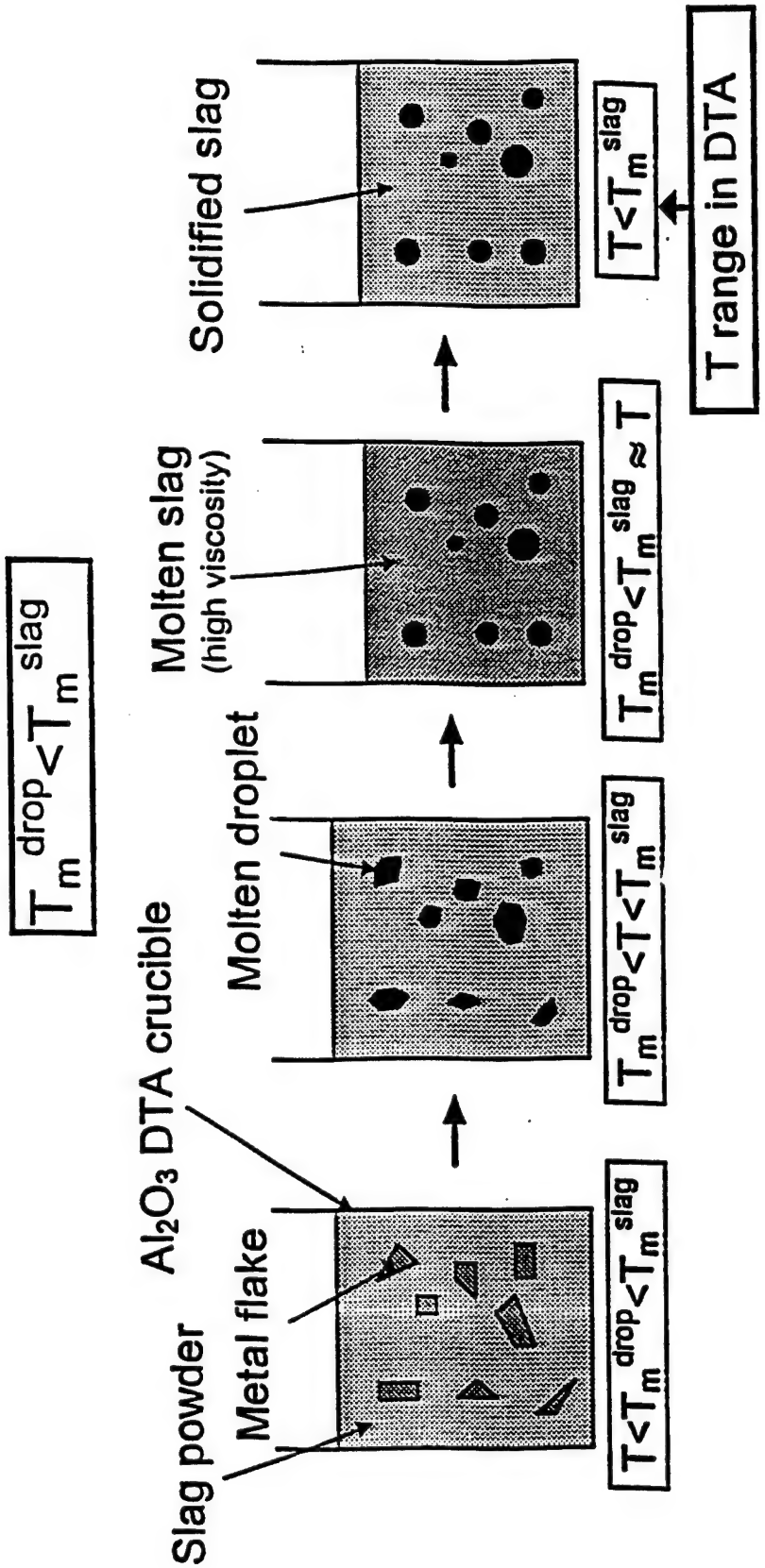

Figure 18. Schematic of droplet/slag emulsion technique.

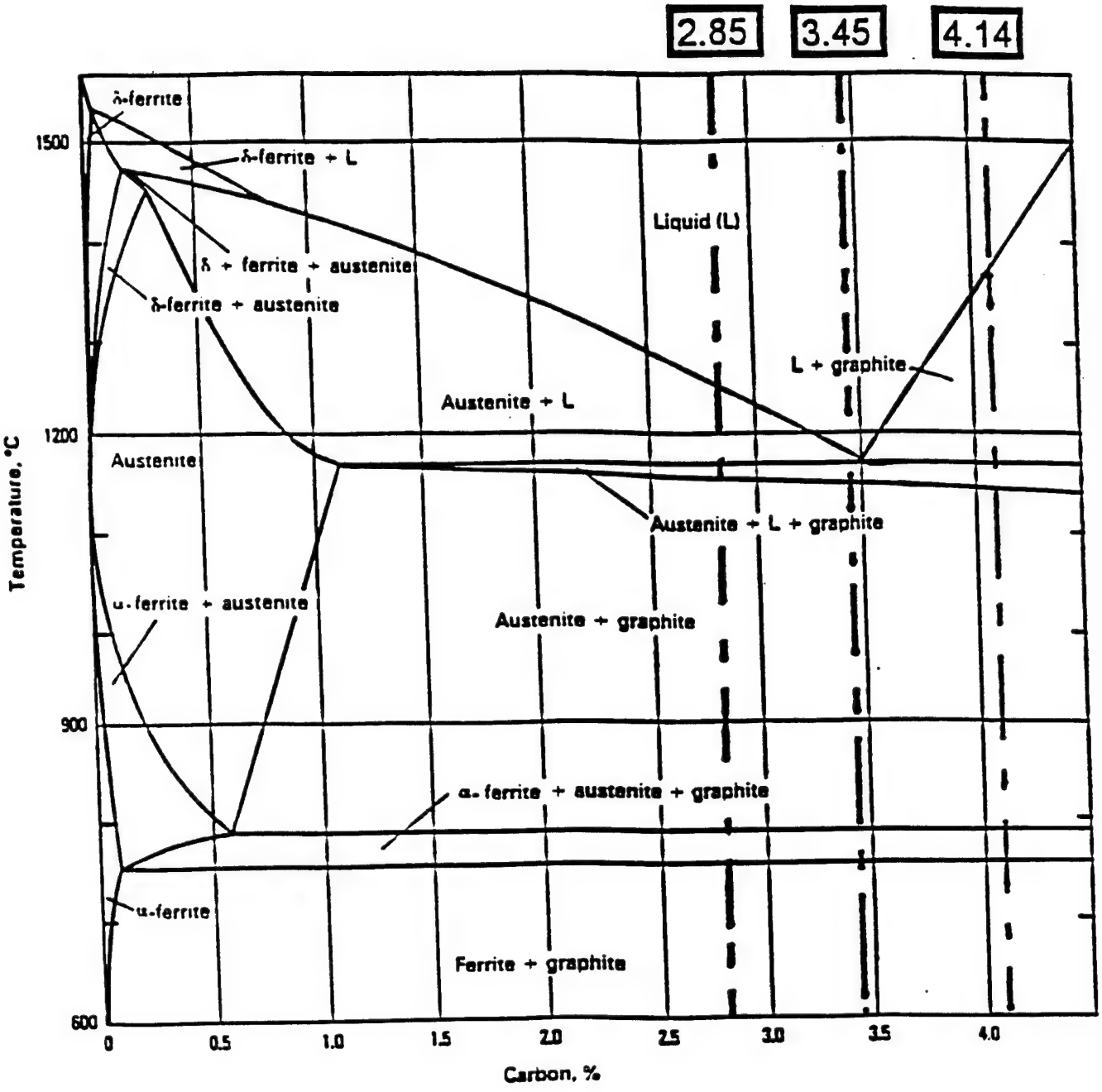

Figure 19. Stable Fe-C phase diagram [58PIW]

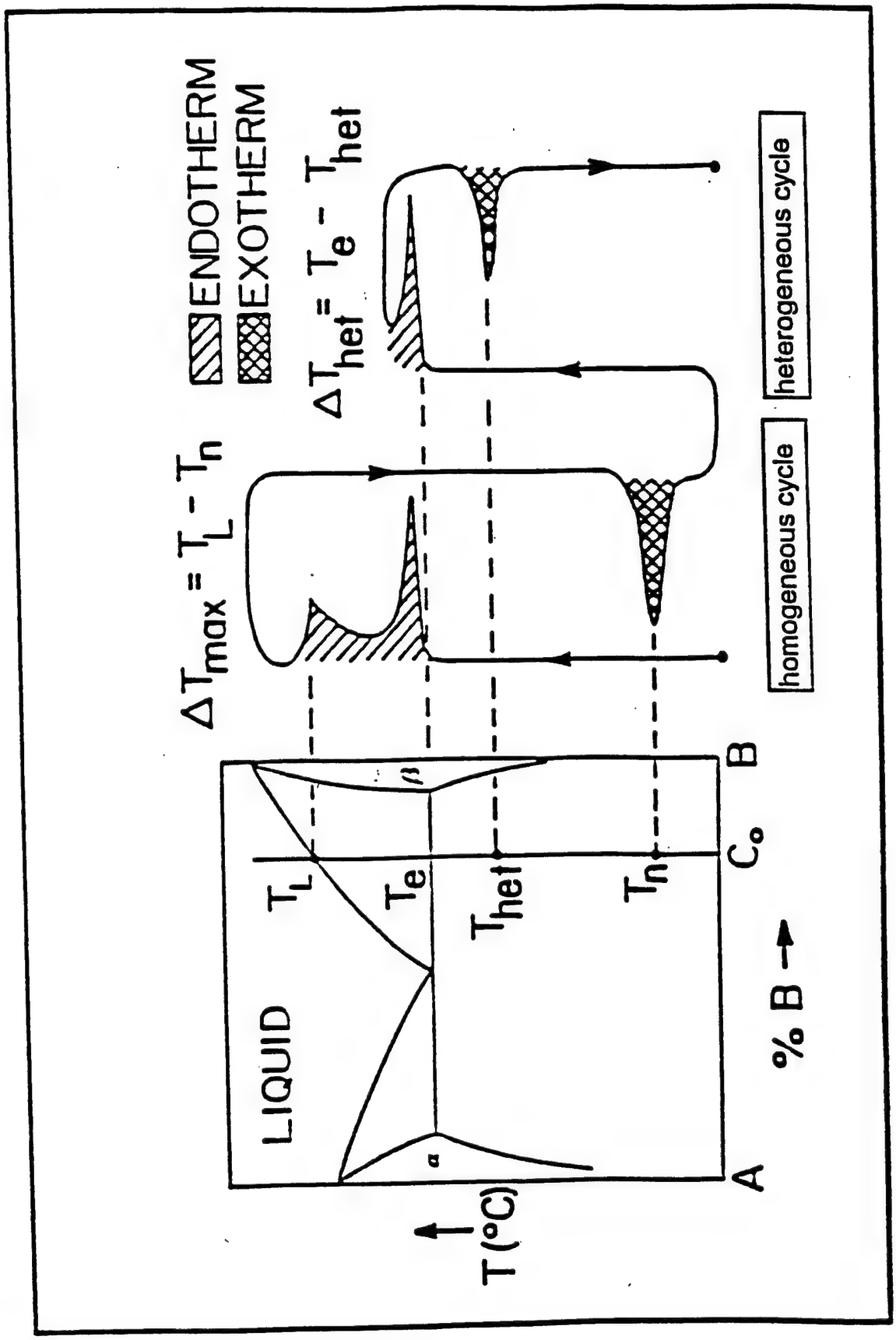

Figure 20. General thermal schedule for solidification catalysis experiments with alloy droplets.

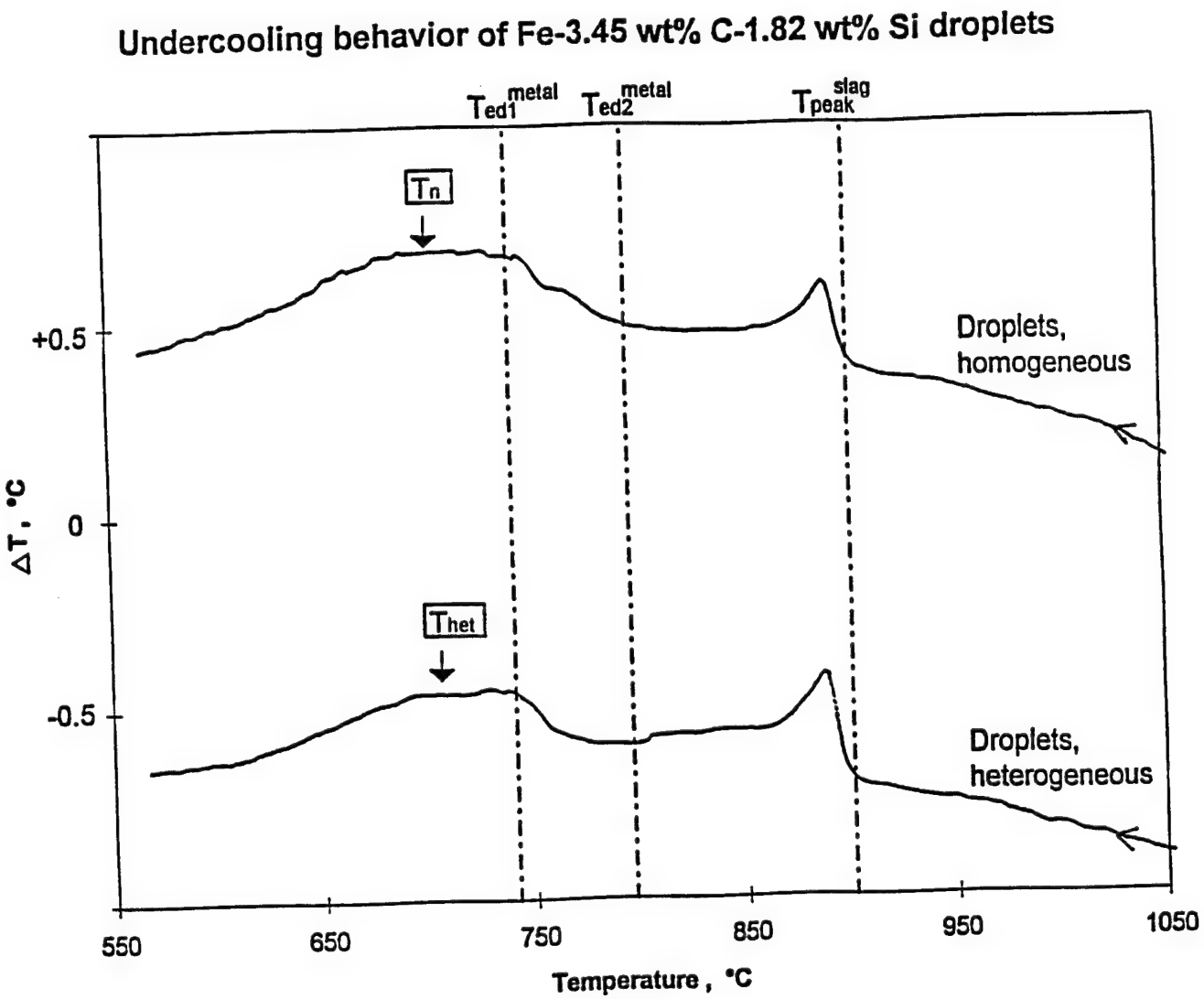

Figure 21. Undercooling behavior of Fe-C-Si droplets.

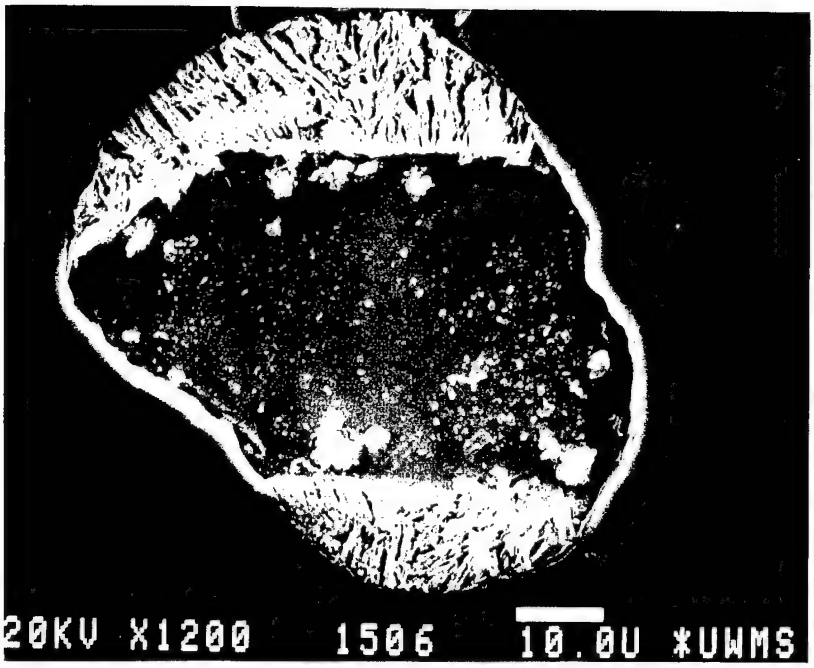

Figure 22. Microstructure of hypoeutectic droplet showing primary austenite.

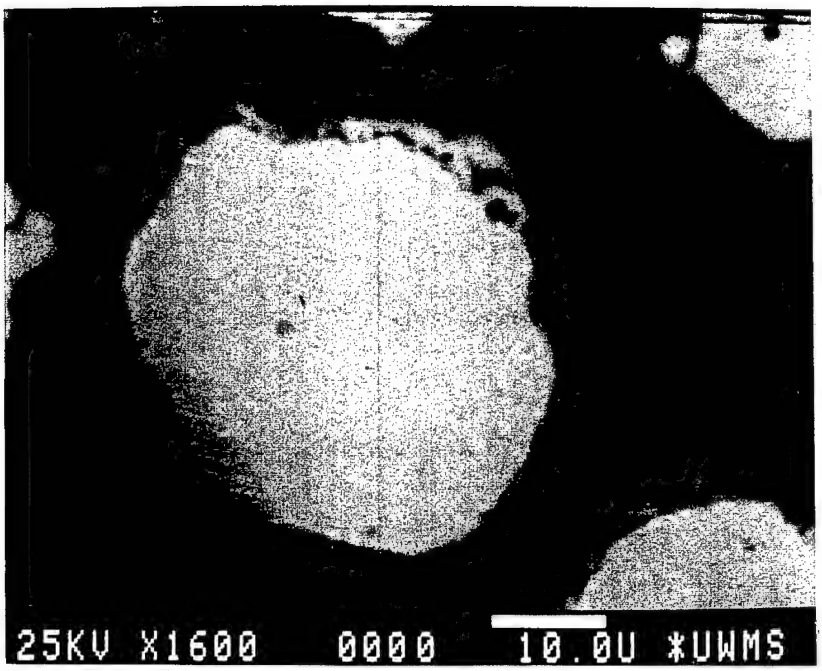

Figure 23. Interior section of Cu alloy droplet.

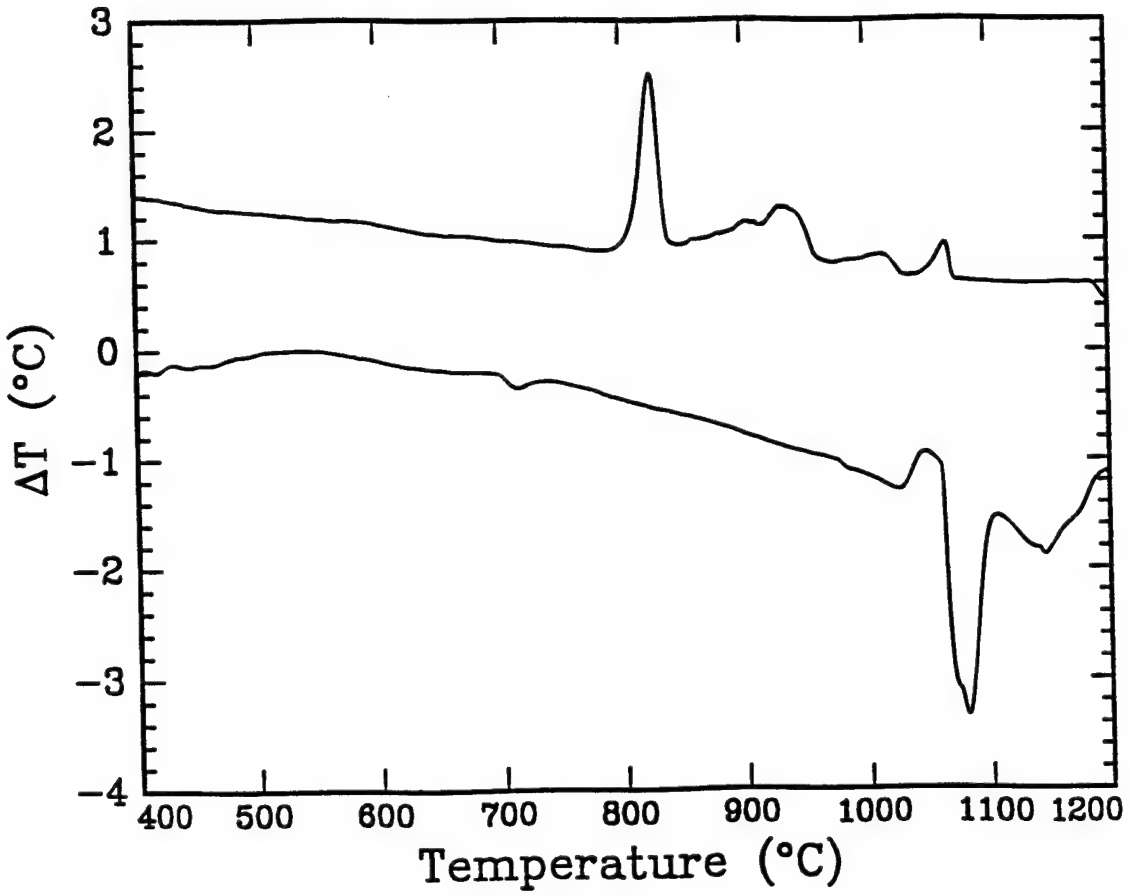

Figure 24. Cu alloy droplet DTA trace showing large undercooling and multiple phase reactions.

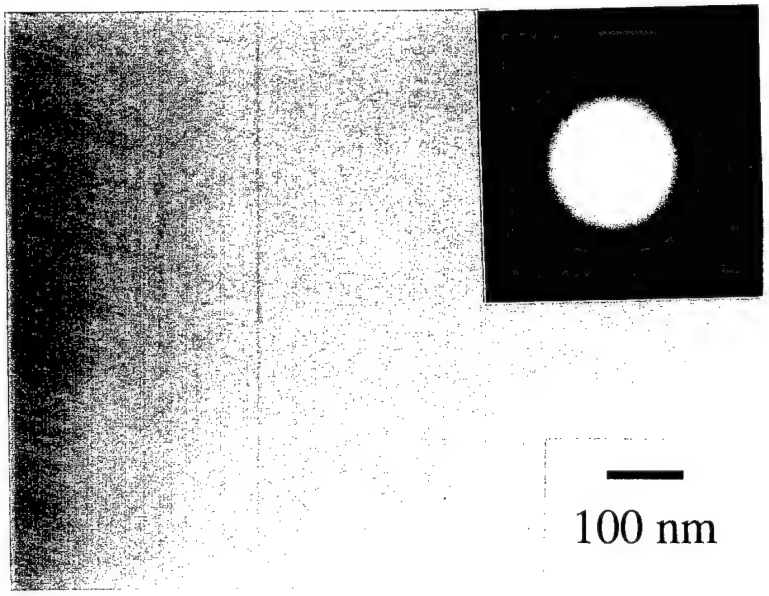

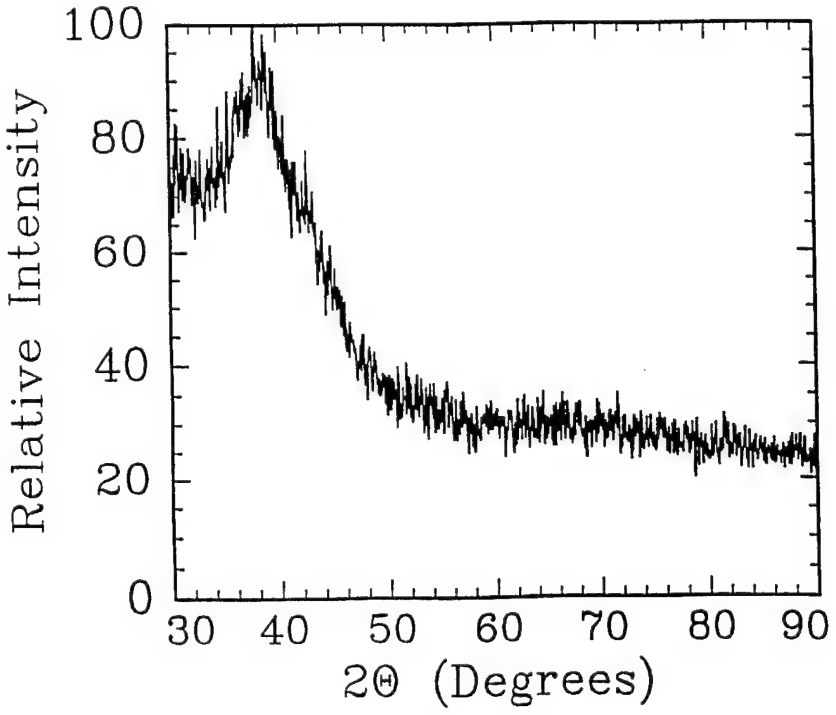

Figure 25. TEM and XRD of Al-7Y-5Fe as-solidified ribbon showing amorphous nature.

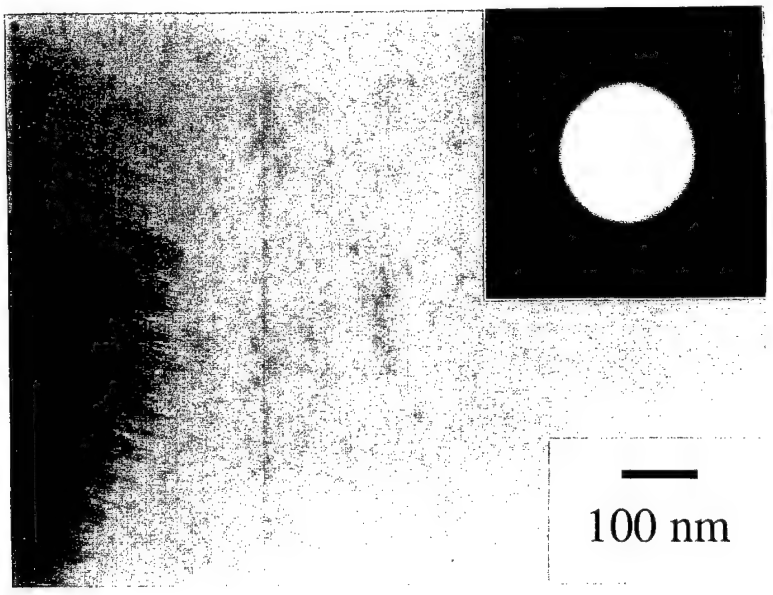

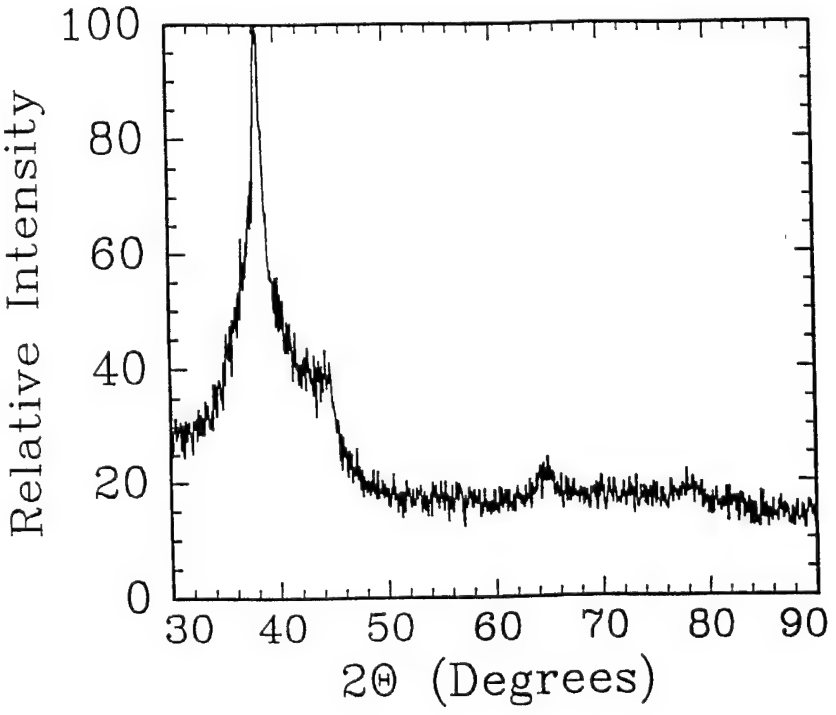

Figure 26. TEM and XRD of Al-5Y-5Fe as-solidified ribbon showing amorphous plus aluminum nanocrystals.

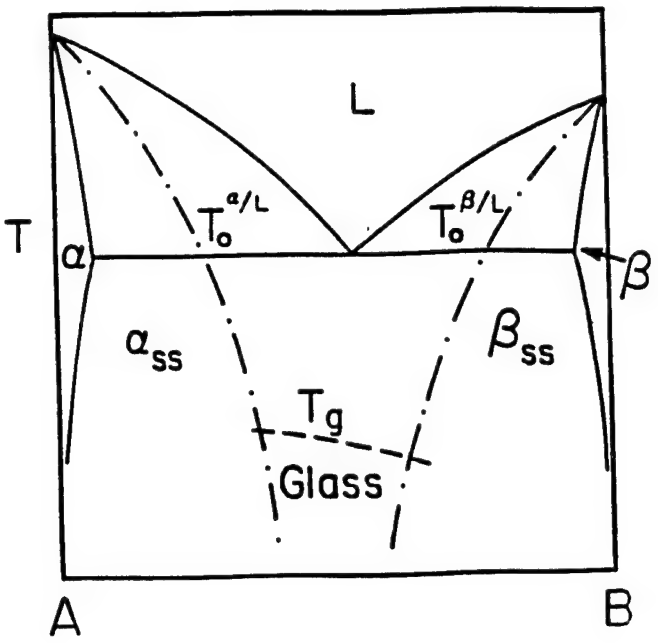

Figure 27. Eutectic system with plunging T_0 curves [93BOE].

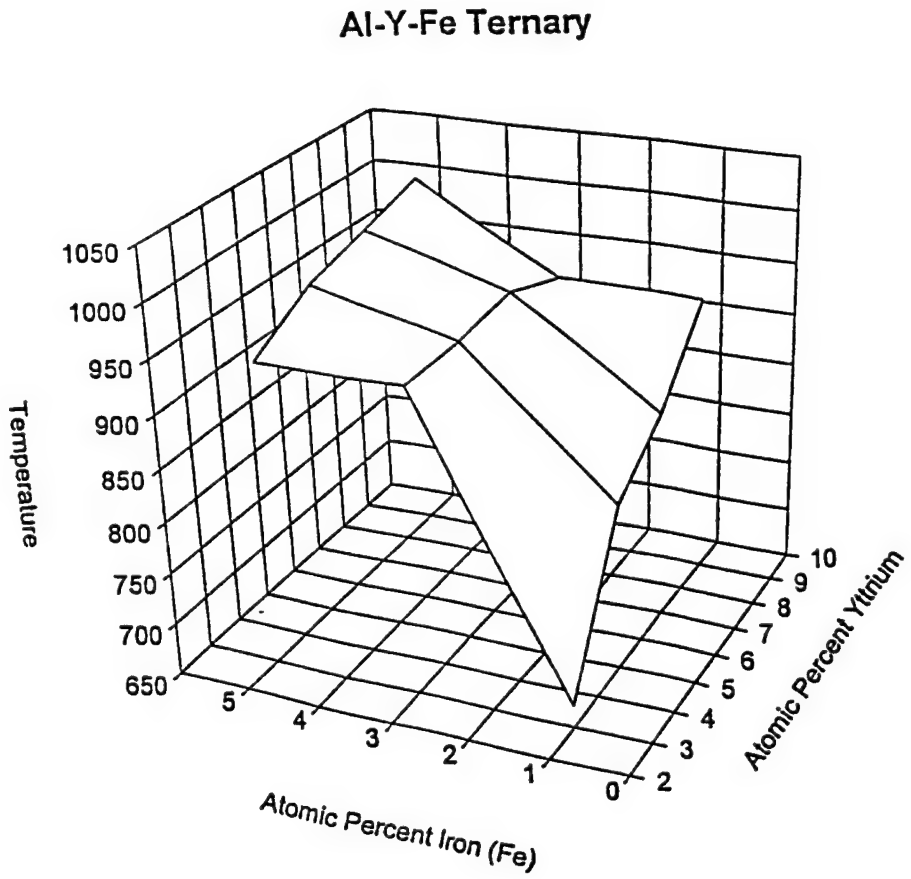

Figure 28. Liquidus surface of the Al-rich portion of the Al-Y-Fe phase diagram.

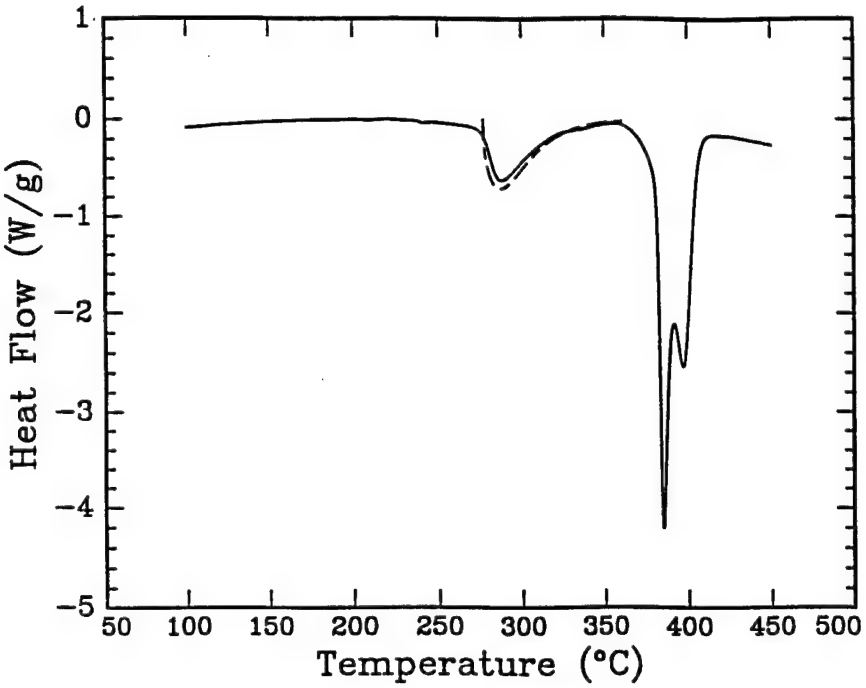

Figure 29. DSC continuous heating trace at 40°C/min of Al-7 Y-5 Fe showing primary crystallization reaction at 276°C as well as crystallization reactions at higher temperatures. . The dashed line shows the fit of the first peak of Al-Y-Fe sample with the model by Ham

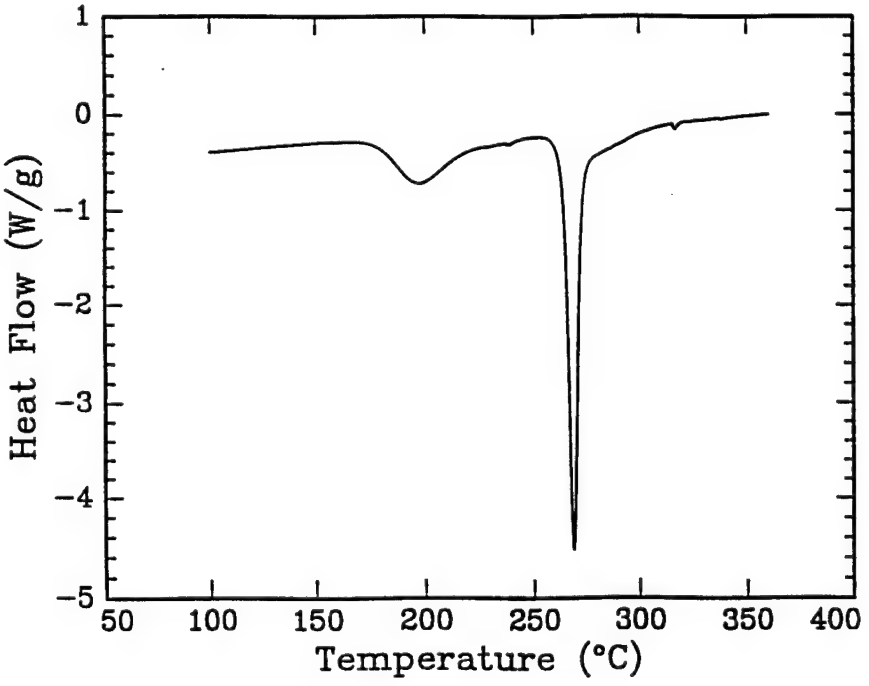

Figure 30. DSC continuous heating trace at 40°C/min of Al-8 Sm.

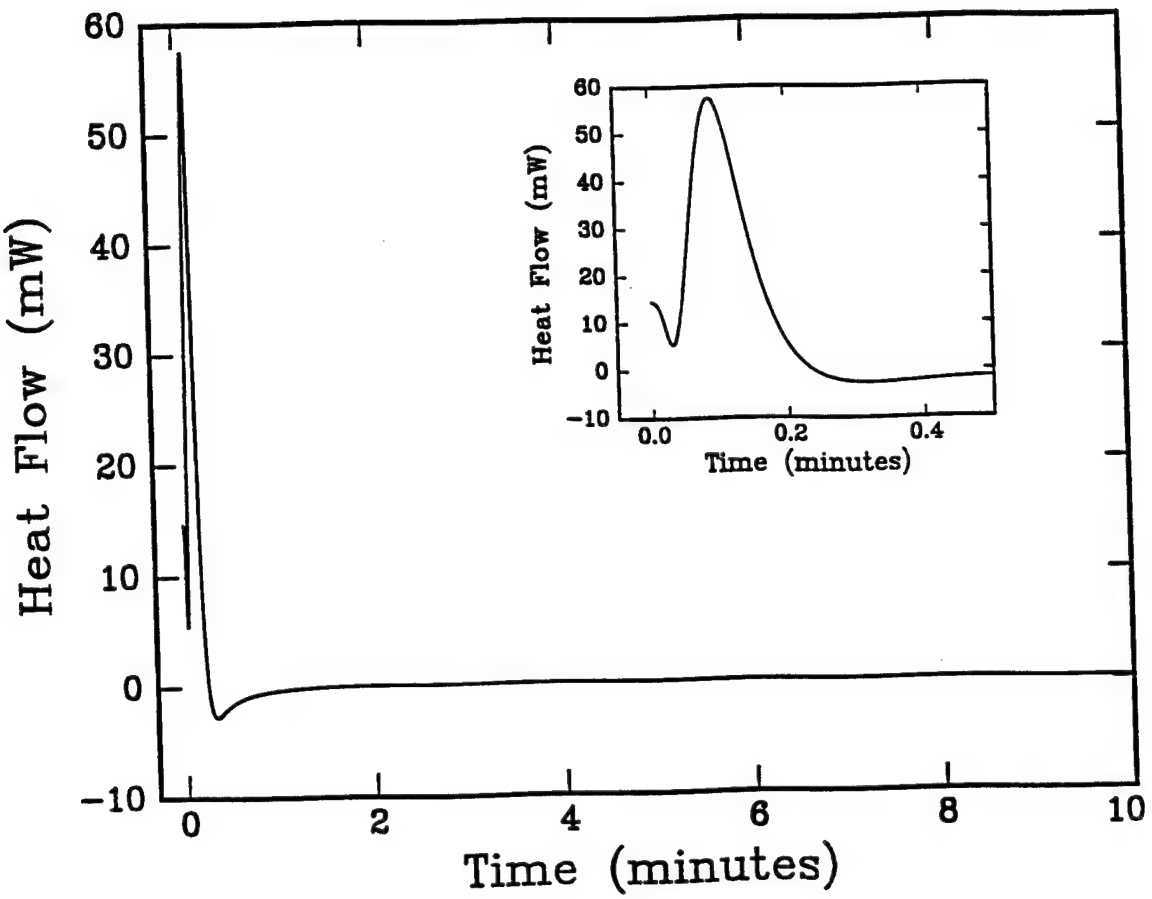

Figure 31. Isothermal DSC trace of Al-7 Y- 5 Fe sample at 245°C with initial instrument transient (shown in detail in inset) and return to baseline.

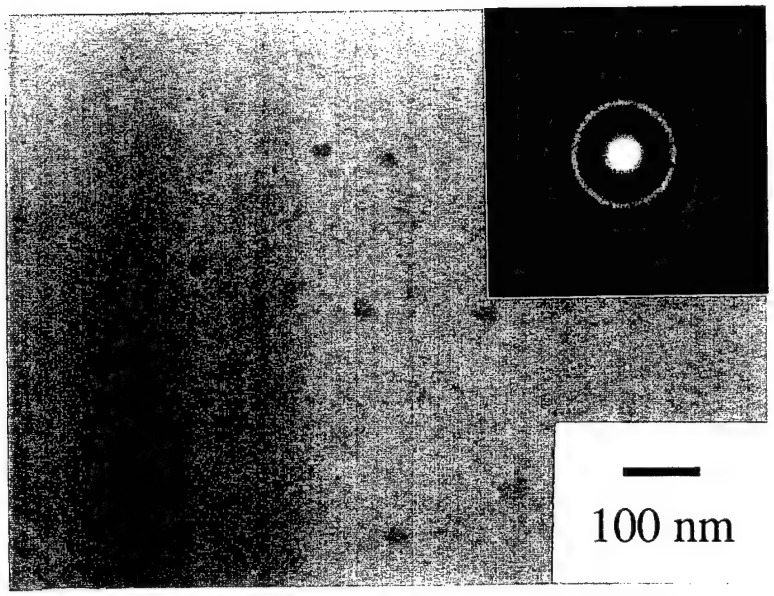

a

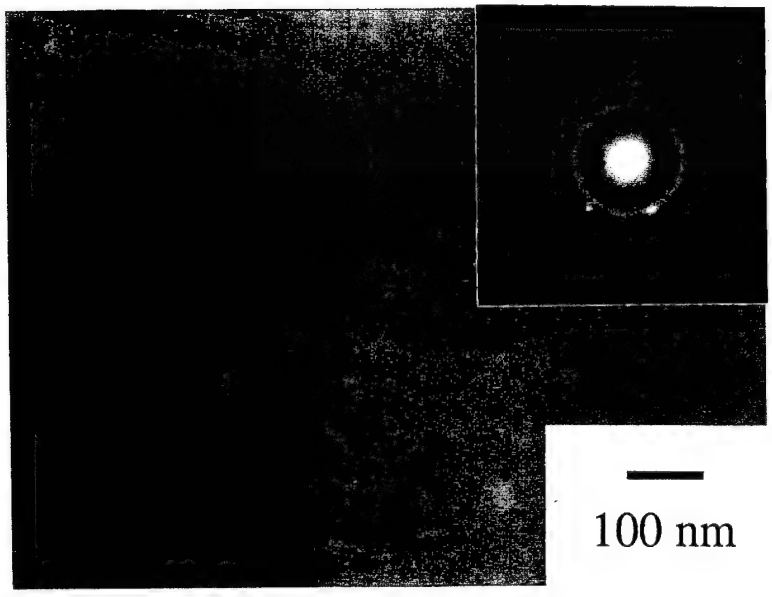

b

Figure 32. (a) TEM of Al-7Y-5Fe isothermal for 10 minutes, (b) TEM of Al-7Y-5Fe isothermal for 100 minutes.

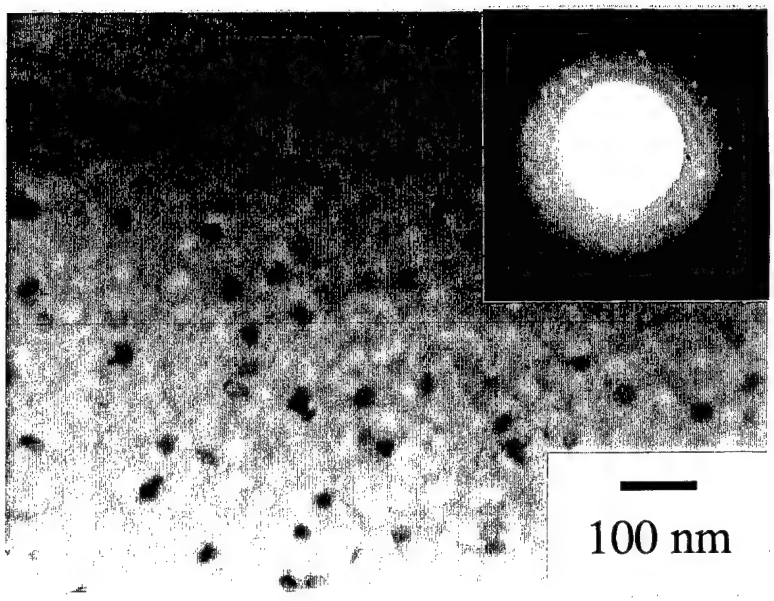

Figure 33. TEM bright-field micrograph of Al-7 Y-5 Fe sample held at 275°C for 10 minutes.

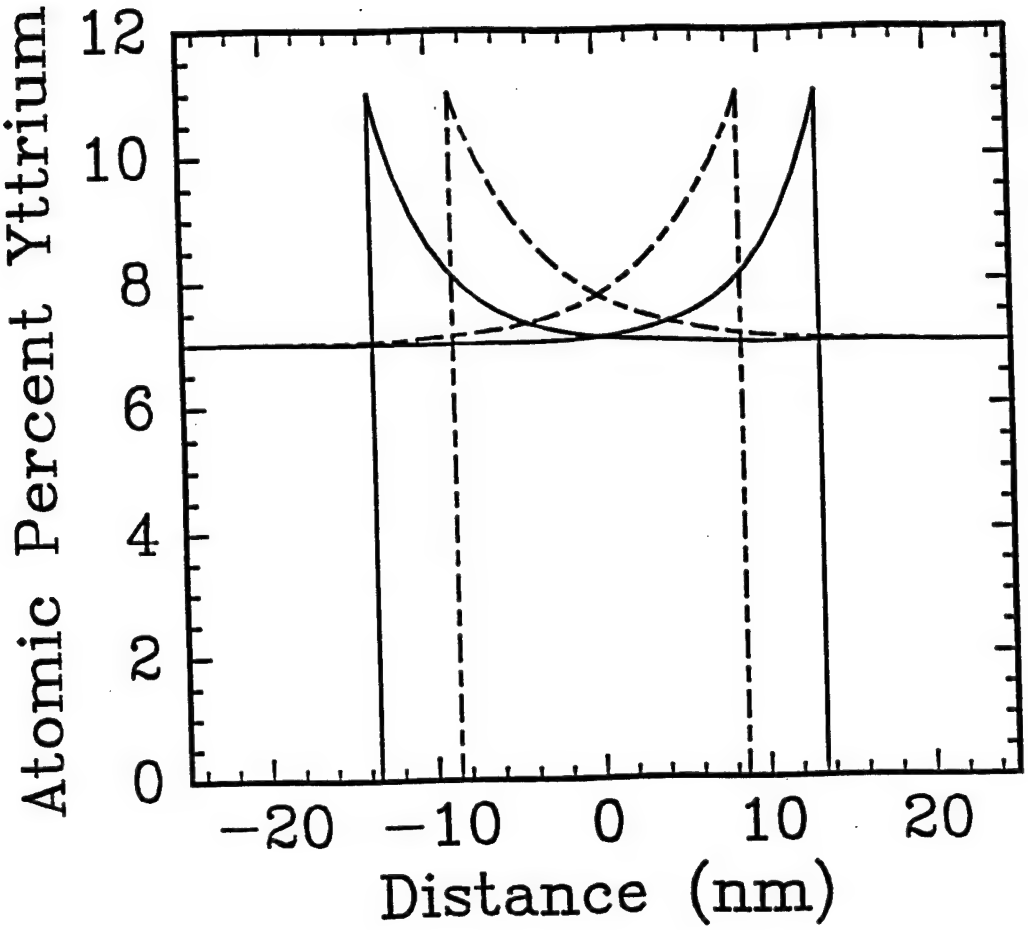

Figure 34. Calculated diffusion fields for yttrium for particles 50 nm apart with midpoint at zero at 10 seconds (solid lines) and 20 seconds (dashed lines). Vertical lines represent the interfaces between Al and the amorphous matrix.

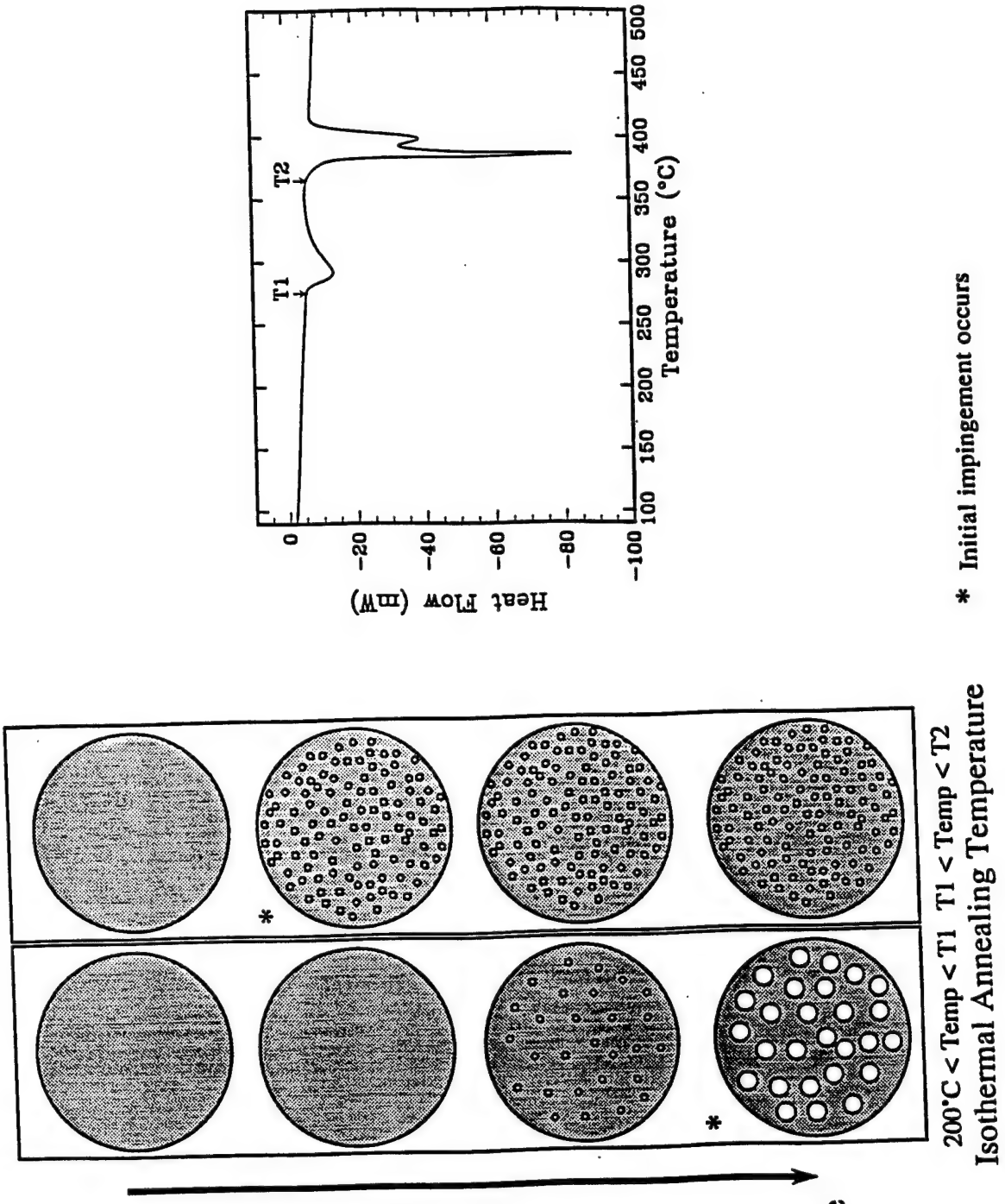

Figure 35. Schematic of Al nanocrystal formation during low temperature annealing and primary crystallization for Al-7Y-5Fe with associated DSC heating trace.

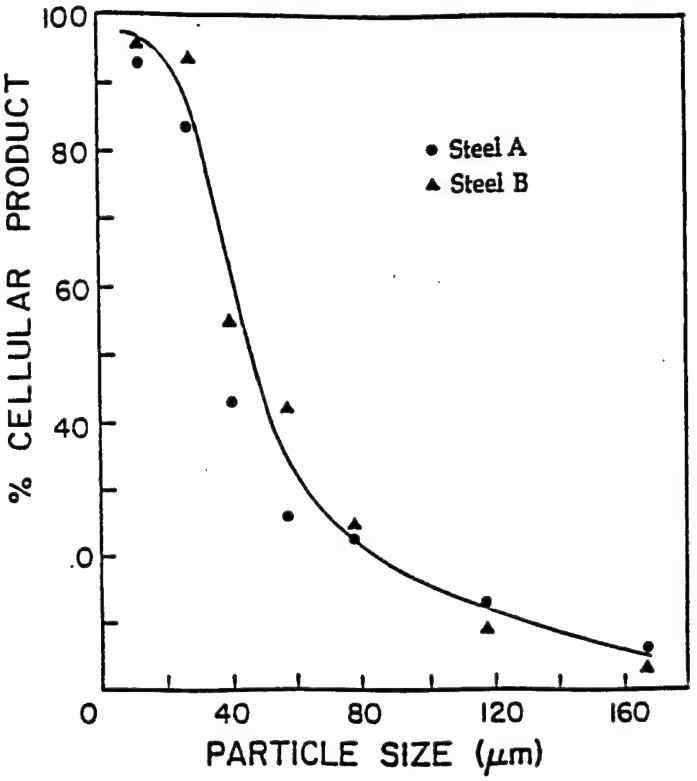

Figure 36. Percentage cellular particles in various size ranges obtained by random sampling of particles in two alloy tool steel powders.

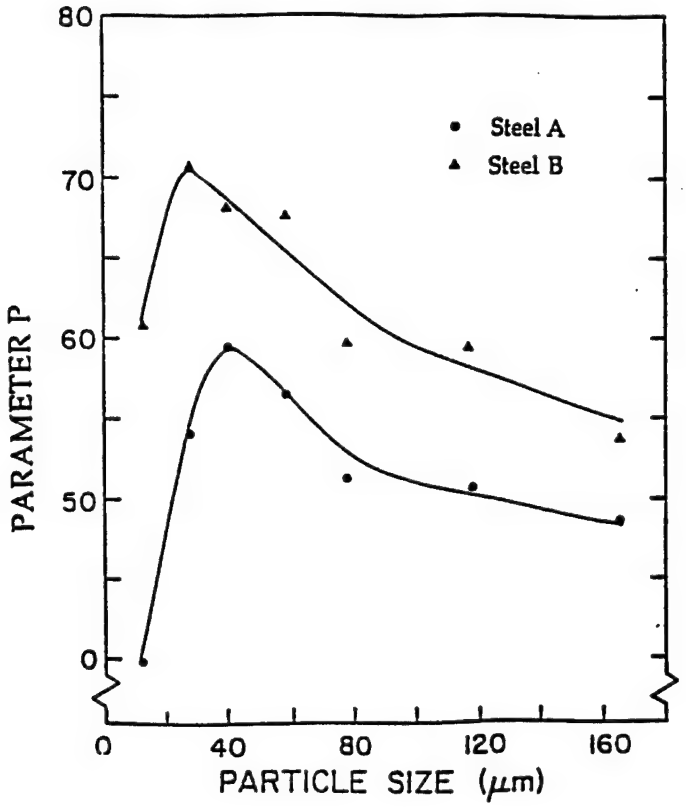

Figure 37. Variation in the relative intensity of the FCC (111) peak with particle size for the two steels.

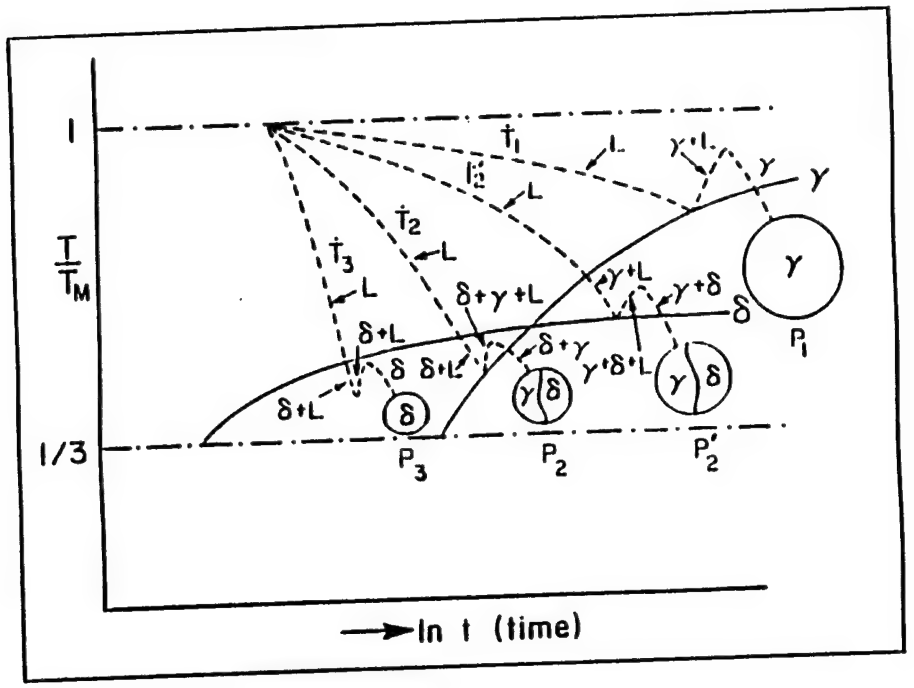

Figure 38. Schematic illustration of a possible mechanism for phase selection during solidification of different particle sizes. The vertical axis represents the homologous temeprature and the horizontal axis represents time for transformation. P1, P2, P'2, and P3 denote preogressively larger powder particles.

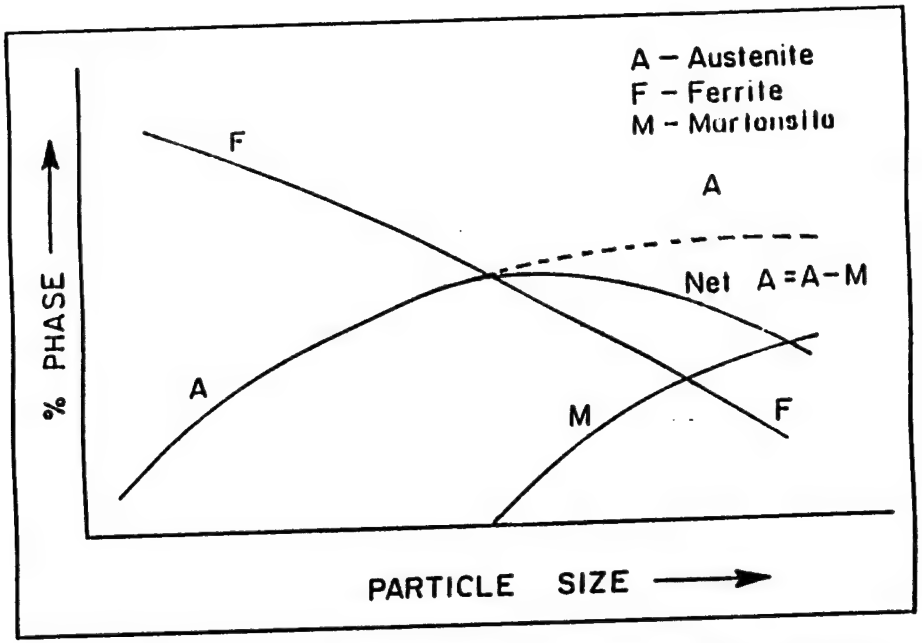

FIGURE 13. Schematic diagram showing the probable distribution

Figure 39. Schematic diagram showing the probable distribution of phases immediately after solidification and at room temperature.

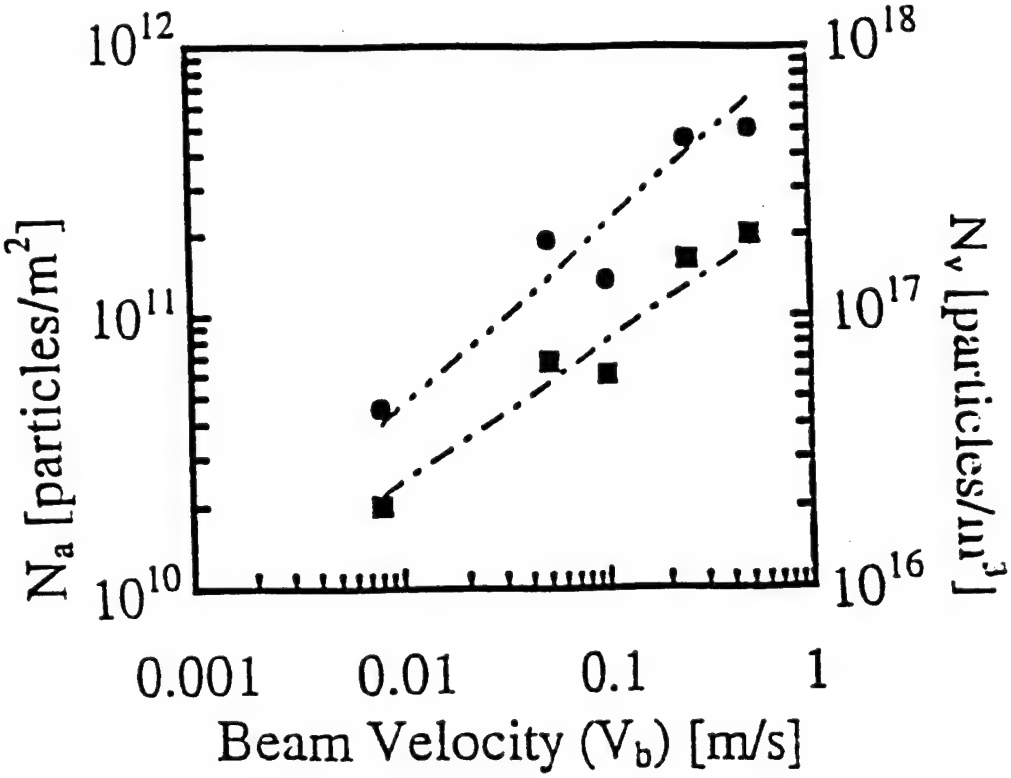

Figure 40. Number of primary Si crystals per unit area as a function of beam rate in the Al-26 wt% Si alloy (square symbols). The calculated volume density is given by the circle symbols.

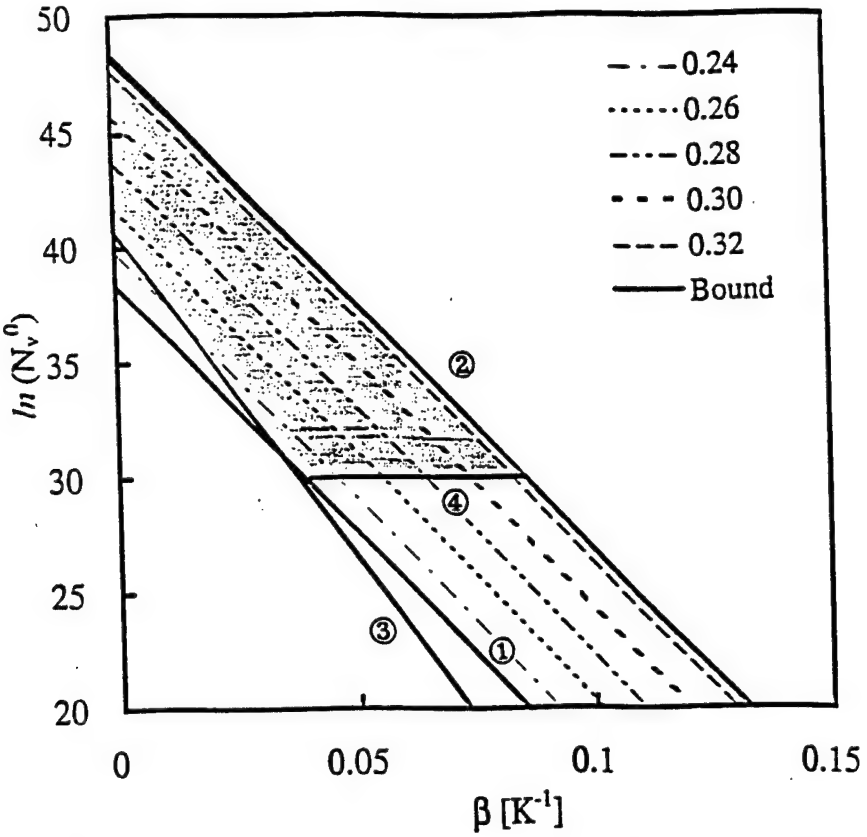

Figure 41. Plot of N_v^0 and β with associated values of $f(\theta)$. Darkened region represents possible range of values based on parameter bound analysis.

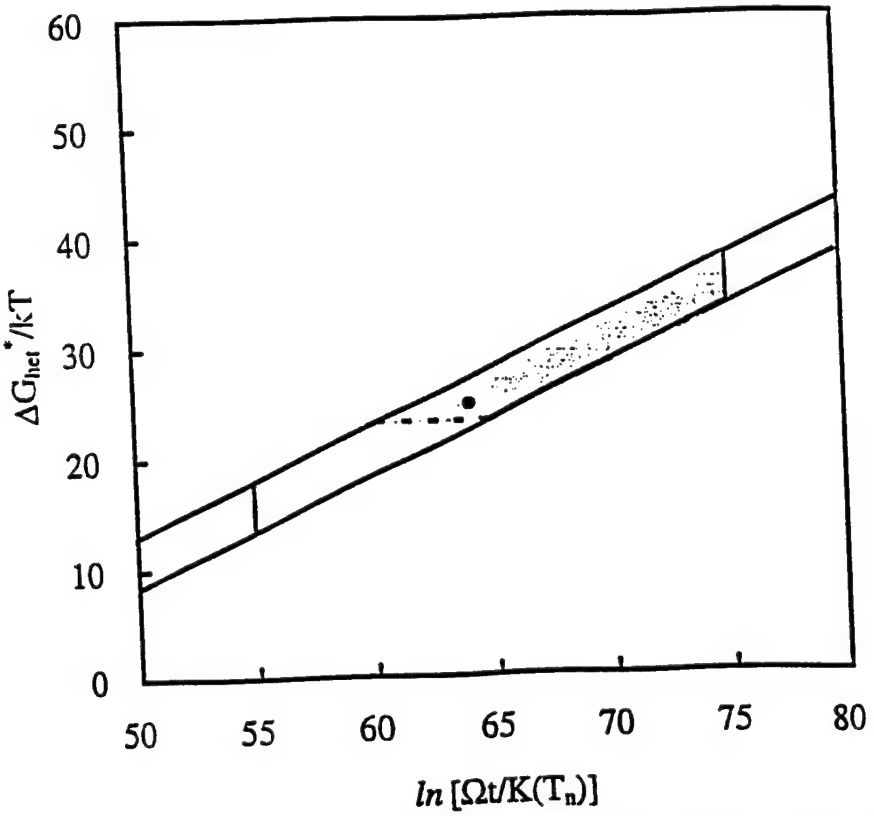

Figure 42. Estimated bounds (solid lines) on $\Delta G^*_{het}/kT$ and $\Omega_v t/K(T_n)$ from kinetics analysis for Al-26 wt % Si alloys.

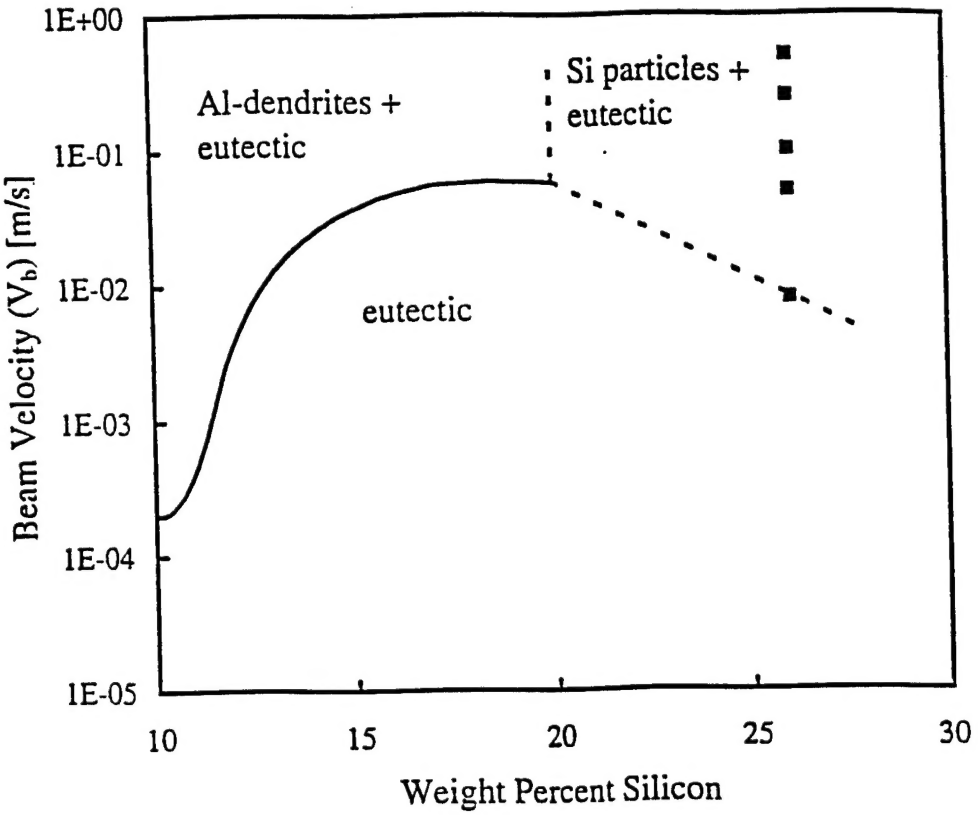

Figure 43. Microstructure map for laser-processed Al-Si alloys. The domain labels indicate the microstructure that develops for the given processing conditions. The data points represent the experiment conditions that resulted in primary silicon nucleation.

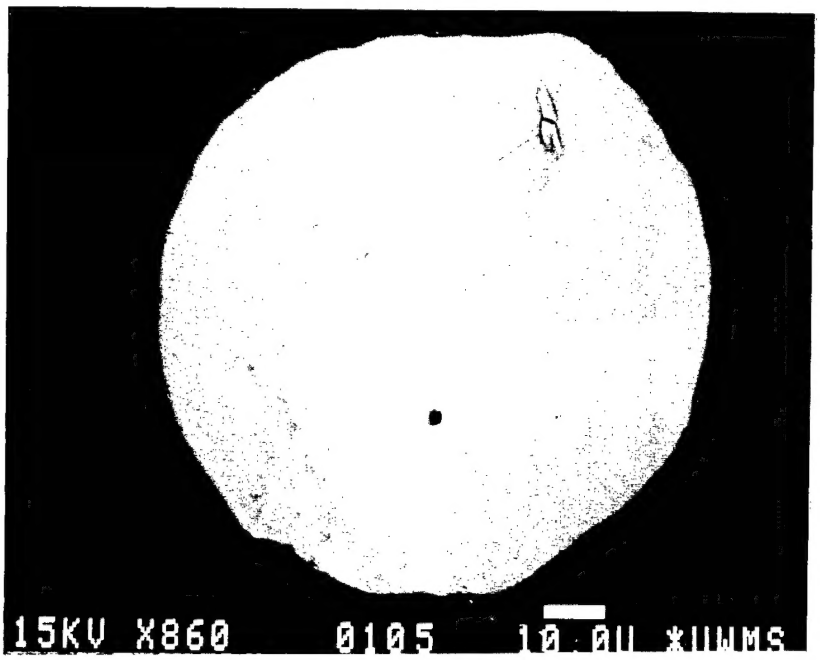

Figure 44. SEM micrograph of Si_3N_4 particle incorporated into an Al droplet.

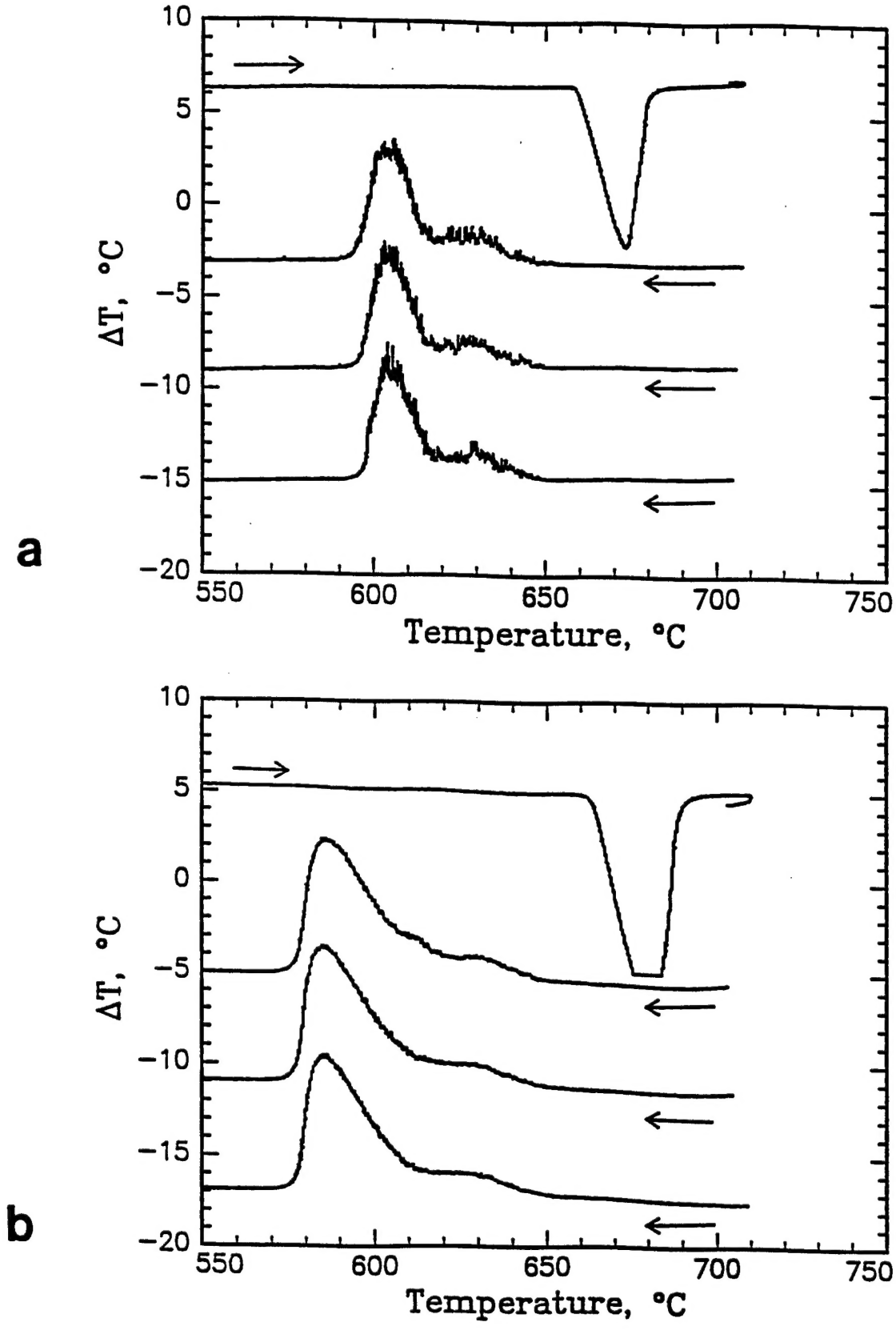

Figure 45. Three consecutive DTA thermograms of 106-125 μm Al-Si_3N_4 powder (a), and < 53 μm Al-Si_3N_4 powder (b).

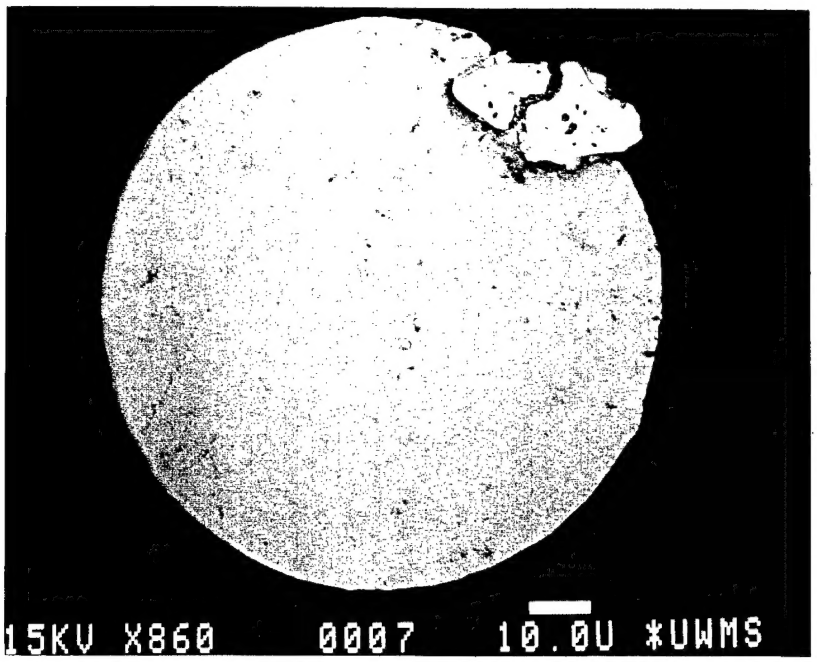

a

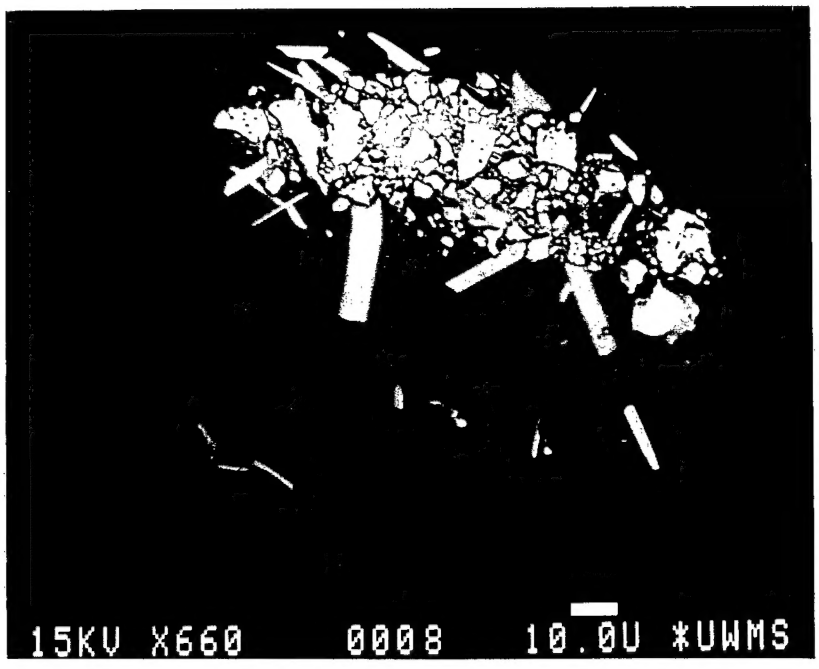

b

Figure 46. SEM micrographs of particle incorporation of TiN in Al.